



unesp

UNIVERSIDADE ESTADUAL PAULISTA

“JÚLIO DE MESQUITA FILHO”

FACULDADE DE ENGENHARIA DE ILHA SOLTEIRA

Camila Gianini Gonsalez Bueno

*AN INVESTIGATION INTO THE WAY IN WHICH
LONGITUDINAL AND FLEXURAL WAVES
INTERACT WITH CORROSION-LIKE DAMAGE*

**Ilha Solteira
2019**

PROGRAMA DE PÓS-GRADUAÇÃO EM ENGENHARIA MECÂNICA

CAMILA GIANINI GONSALEZ BUENO

**AN INVESTIGATION INTO THE WAY IN WHICH LONGITUDINAL
AND FLEXURAL WAVES INTERACT WITH CORROSION-LIKE
DAMAGE**

Dissertação apresentada à Faculdade de Engenharia - UNESP – Campus de Ilha Solteira, para obtenção do título de Doutor em Engenharia Mecânica.

Área de Conhecimento: Mecânica dos Sólidos

Orientador: Prof. Dr. Michael John Brennan

FICHA CATALOGRÁFICA

Desenvolvido pelo Serviço Técnico de Biblioteca e Documentação

G639i Gonzalez Bueno, Camila Gianini.
An investigation into the way in which Longitudinal and Flexural waves interact with corrosion-like damage / Camila Gianini Gonzalez Bueno. -- Ilha Solteira: [s.n.], 2019
166 f. : il.

Tese (doutorado) - Universidade Estadual Paulista. Faculdade de Engenharia de Ilha Solteira. Área de conhecimento: Mecânica dos Sólidos, 2019

Orientador: Michael John Brennan
Inclui bibliografia

1. Longitudinal waves. 2. Flexural waves. 3. Piezoelectric elements. 4. Structural Health Monitoring. 5. Corrosion.


Raiane da Silva Santos

Supervisora Técnica de Seção
Seção Técnica de Referência, Atendimento ao usuário e Documentação
Divisão Técnica de Biblioteca e Documentação
CRB/8 - 9999



UNIVERSIDADE ESTADUAL PAULISTA

Câmpus de Ilha Solteira

CERTIFICADO DE APROVAÇÃO

TÍTULO DA TESE: An investigation into the way in which Longitudinal and Flexural waves interact with corrosion-like damage

AUTORA: CAMILA GIANINI GONSALEZ BUENO

ORIENTADOR: MICHAEL JOHN BRENNAN

Aprovada como parte das exigências para obtenção do Título de Doutora em ENGENHARIA MECÂNICA, área: Mecânica dos Sólidos pela Comissão Examinadora:

Prof. Dr. MICHAEL JOHN BRENNAN 
Departamento de Engenharia Mecânica / Faculdade de Engenharia de Ilha Solteira

Prof. Dr. MARCIO ANTONIO BAZANI 
Departamento de Engenharia Mecânica / Faculdade de Engenharia de Ilha Solteira

Prof. Dr. RICARDO TOKIO HIGUTI 
Departamento de Engenharia Elétrica / Faculdade de Engenharia de Ilha Solteira

Prof. Dr. PAULO JOSÉ PAUPITZ GONÇALVES 
Departamento de Engenharia Mecânica / Faculdade de Engenharia de Bauru

Prof. Dr. DOMINGOS ALVES RADE 
Divisão de Engenharia Mecânica / Instituto Tecnológico de Aeronáutica

Ilha Solteira, 31 de janeiro de 2019

To Douglas and Clara.

ACKNOWLEDGMENTS

I would first like to thank God for all.

I would like to my sincere gratitude to my advisor Professor Mike Brennan. He expanded my horizon in the research and teaching. Prof Mike was always ready to help me when I ran into a trouble spot or had a question about my research or writing. He steered me in the right the direction and I will be eternally grateful to him.

I would also like to acknowledge the exam committee for participating and contributing to this work with very valuable comments.

I would also like to thank the support of Carlos José Santana e Diego de Alcântara. Without their participation the experimental tests could not have been successfully conducted.

I would also like to thank the inputs of Professor Eurípedes Guilherme de Oliveira Nóbrega and Paulo Henrique de Oliveira Lopes about the experimental setup. Their comments were very important.

I am very grateful to the GMSINT group to provide me facilities to carry out this research, in special to Professor Vicente Lopes Junior, to his open door policy. I would like also to thank my group colleagues Pedro Christian Ayala Castillo and Rodrigo Borges Santos for uncountable productive discussions about wave propagation in structures.

My special thanks for my husband Douglas Domingues Bueno for providing me continuous support and encouragement throughout these years. Always patient and helpful. I must express my very profound gratitude to my mother and my mother in law for providing to my family with support during my years of study.

Finally, I would like to thank the Department of Mechanical Engineering and the Post Graduation to readiness to help me.

This study was financed in part by the Coordenação de Aperfeiçoamento de Pessoal de Nível Superior - Brasil (CAPES) - Finance Code 001.

*The scientific search is infinite.
Just try to see with the eyes of a child.*

ABSTRACT

The guarantee of security in transport vehicles, buildings, bridges and critical structures is extremely important for people and the environment. Therefore, in the last decades, several Structural Health Monitoring (SHM) techniques have been proposed and developed for many areas. One technique to detect corrosion could be the use of guided waves. Considering one wave travelling in a structure and impinging on a discontinuity (damage), this wave will interact with this discontinuity and will be scattered. Thus wave motion in structures may be a powerful way to indicate the presence of damage in a structure. This work aims to investigate wave propagation in a thin Euler-Bernoulli infinite beam, and the way in which these waves interact with simulated corrosion damage (symmetric and asymmetric). The studies show the importance to know the behavior of waves before chose main frequencies to used for a SHM system. Piezoelectric elements are used to excite and sense the waves. The behavior of the systems studied are widely discussed in frequency and time domains. In order to detect and quantify the damage, reflected waves showed better sensitivity and proportionality with damage severity for all configuration studied. The longitudinal wave incident in the damage is easier to be used in a SHM system than flexural waves because longitudinal waves present simplicity compared to flexural. However, is important to choose appropriate frequency range in order to generate good levels of the longitudinal waves.

Keywords: Longitudinal Waves, Flexural Waves, Structural Health Monitoring, Piezoelectric elements, Corrosion

RESUMO

A garantia de segurança em veículos de transporte, edifícios, pontes e estruturas críticas é extremamente importante para as pessoas e o meio ambiente. Portanto, nas últimas décadas, várias técnicas de Monitoramento da Integridade Estrutural (SHM) foram propostas e desenvolvidas para diversas áreas. Uma técnica para detectar corrosão pode ser o uso de ondas guiadas. Considerando uma onda propaganda em uma estrutura e se chocando a uma descontinuidade (dano), esta onda irá interagir com esta descontinuidade e será transformada (parte é refletida e parte transmitida). Assim, o movimento de ondas em estruturas pode ser uma maneira poderosa de indicar a presença de dano em estruturas. Este trabalho tem como objetivo investigar a propagação de ondas em uma viga de Euler-Bernoulli e a forma como estas ondas interagem com danos simulados de corrosão (simétricos e assimétricos). Os estudos mostram a importância de conhecer o comportamento das ondas antes de escolher as frequências principais a serem usadas em um sistema SHM. Elementos piezelétricos são usados para gerar sensoriar as ondas. O comportamento dos sistemas estudados é amplamente discutido nos domínios de frequência e tempo. Para detectar e quantificar os danos, as ondas refletidas apresentaram melhor sensibilidade e proporcionalidade com a severidade do dano para todas as configurações estudadas. As ondas longitudinais incidentes no dano são mais recomendadas pelo sistema SHM por apresentarem maior simplicidade em relação às ondas de flexural. No entanto, é importante escolher a faixa de frequência apropriada para gerar bons níveis das ondas longitudinais.

Palavras-chave: Ondas Longitudinais, Ondas Flexurais, Monitoramento da Integridade Estrutural, Elementos Piezoelétricos, Corrosão

LIST OF FIGURES

Figure 1: Aloha Airlines flight 243 accident.....	19
Figure 2: Symmetric and Asymmetric corrosion damage.....	20
Figure 3: Case 1 – Infinite beam with piezoelectric bimorphs and symmetric damage.	23
Figure 4: Case 2 - Infinite beam with asymmetric actuator and symmetric damage.	23
Figure 5: Case 3 - Infinite beam with symmetric actuator and symmetric damage.	24
Figure 6: Case 4 - Infinite beam with asymmetric actuator and damage.....	24
Figure 7: Illustration of the most basic waves types on elastic structures; (a) Longitudinal waves; (b) Bending waves and; (c) Shear waves.	31
Figure 8: Segment of a beam (or rod) with loads.	36
Figure 9: Segment of an Euler-Bernoulli beam with flexural loads.	39
Figure 10: First study case divided in segments.....	42
Figure 11: Sign convention used with state vector.	43
Figure 12: Waves that can exist at each cross section of an Euler-Bernoulli beam.	45
Figure 13: Piezoelectric actuator; (a) longitudinal waves generated by a pair of forces on symmetric configuration; (b) flexural waves generated by a pair of moments on symmetric configuration and (c) longitudinal and flexural waves generated by an asymmetric actuation.	47
Figure 14: Simplified model of a piezoelectric actuator.....	49
Figure 15: Amplitude of longitudinal right going wave from symmetric actuator of length $l_A = 0.0127m$	52
Figure 16: Amplitude of flexural right going wave from symmetric actuator of length $l_A = 0.0127m$	53
Figure 17: Piezoelectric sensor; (a) symmetric configuration and; (b) asymmetric configuration.	55
Figure 18: Waves presented in the segments extremities of a symmetric damage.	60
Figure 19: Scattering waves by a symmetric damage for an incident longitudinal wave.....	64
Figure 20: Relation of scattering waves in a symmetric damage with $l_D = 0.025m$ and a longitudinal incident wave.	65
Figure 21: Maximum of wave amplitude ratios (reflected and transmitted) for different damage depth considering incident longitudinal wave and $l_D = 0.025m$	66

Figure 22: Scattering waves by a symmetric damage for an incident flexural propagating wave.	67
Figure 23: Relation of scattering waves in a symmetric damage with $l_D = 0.025m$ and an incident flexural propagating wave.....	68
Figure 24: Maximum of wave amplitude ratios (reflected and transmitted) for different damage depth considering incident flexural wave and $l_D = 0.025m$	69
Figure 25: Efforts on junctions of asymmetric damage section with adjacent beams.....	70
Figure 26: Scattering waves by an asymmetric damage for an incident longitudinal wave. ...	72
Figure 27: Relation of longitudinal scattering waves in an asymmetric damage with $l_D = 0.025m$ and a longitudinal incident wave.	73
Figure 28: Relation of flexural scattering waves in an asymmetric damage with $l_D = 0.025m$ and a longitudinal incident wave.	74
Figure 29: Scattering waves by an asymmetric damage for an incident flexural propagating wave.	75
Figure 30: Relation of longitudinal scattering waves in asymmetric damage ($l_D = 0.025m$ and 50% de thickness reduction) and incident flexural wave.....	76
Figure 31: Relation of flexural scattering waves in asymmetric damage ($l_D = 0.025m$ and 50% de thickness reduction) and incident flexural wave.....	77
Figure 32: Waves behaviors for; (a) Case 1; (b) Case 2; (c) Case 3 and (d) Case 4.	80
Figure 33: Input burst signals for main frequency of 10kHz (blue solid line) and 50kHz (red dot-dot line): (a) time domain; (b) frequency domain.	83
Figure 34: Reflection and Transmission coefficients (symmetric damage) in frequency domain with the highlighted excitation frequency range for input burst signals for main frequency of 10kHz (blue box) and 50kHz (red box): (a) longitudinal and; (b) flexural waves.....	84
Figure 35: Reflection and Transmission coefficients (asymmetric damage, longitudinal incident wave) in frequency domain with the highlighted excitation frequency range for input burst signals for main frequencies of 10kHz (blue box) and 50kHz (red box): (a) longitudinal and; (b) flexural waves.	85
Figure 36: Reflection and Transmission coefficients (asymmetric damage, flexural incident wave) in frequency domain with the highlighted excitation frequency range for input burst signals for main frequencies of 10kHz (blue box) and 50kHz (red box): (a) longitudinal and; (b) flexural waves.	86

Figure 37: Case 1 - Waves interaction in symmetric damage (longitudinal or flexural incident).	87
Figure 38: Electrical voltage signal generated by longitudinal scattered waves (at 50kHz) by symmetric damage of 5% (black dash-dot line), 30% (cyan dashed line), 50% (blue dot-dot line) compared to baseline (green solid line): (a) transmitted and; (b) reflected.	88
Figure 39: Electrical voltage signal generated by flexural scattered waves (at 10kHz) by symmetric damage of 5% (magenta dash-dot line), 30% (black dashed line), 50% (red dot-dot line) compared to baseline (yellow solid line): (a) transmitted and; (b) reflected.	90
Figure 40: Case 2 - Waves interaction in symmetric damage (longitudinal and flexural incident).	91
Figure 41: Electrical voltage generated by scattered waves (at 10kHz) considering an asymmetric actuator and symmetric damage of 5% (black dash-dot line), 30% (cyan dashed line), 50% (blue dot-dot line) compared to baseline (green solid line): (a) transmitted and; (b) reflected.....	93
Figure 42: Electrical voltage signals generated by scattered waves (at 50kHz) considering an asymmetric actuator and symmetric damage of 5% (black dash-dot line), 30% (cyan dashed line), 50% (blue dot-dot line) compared to baseline (green solid line): (a) transmitted and; (b) reflected.....	94
Figure 43: Case 3 - Waves interaction in asymmetric damage (longitudinal or flexural incident).	95
Figure 44: Electrical voltage signals generated by scattered waves (at 10kHz) considering a symmetric actuator and asymmetric damage of 5% (black dash-dot line), 30% (cyan dashed line), 50% (blue dot-dot line) compared to baseline (green solid line): (a) transmitted and; (b) reflected.....	96
Figure 45: Electrical voltage signals generated by scattered waves (at 50kHz) considering a symmetric actuator and asymmetric damage of 5% (black dash-dot line), 30% (cyan dashed line), 50% (blue dot-dot line) compared to baseline (green solid line): (a) transmitted and; (b) reflected.....	97
Figure 46: Electrical voltage signals generated by scattered waves (at 10kHz) considering an asymmetric actuator and asymmetric damage of 5% (magenta dash-dot line), 30% (black dashed line), 50% (red dot-dot line) compared to baseline (yellow solid line): (a) transmitted and; (b) reflected.....	100

Figure 47: Electrical voltage signals generated by scattered waves (at 50kHz) considering an symmetric actuator and asymmetric damage of 5% (magenta dash-dot line), 30% (black dashed line), 50% (red dot-dot line) compared to baseline (yellow solid line): (a) transmitted and; (b) reflected.....	101
Figure 48: Case 4 - Waves interaction in an asymmetric damage (longitudinal and flexural incident).....	102
Figure 49: Electrical voltage signals generated by scattered waves (at 10kHz) considering a symmetric actuator and asymmetric damage of 5% (black dash-dot line), 30% (cyan dashed line), 50% (blue dot-dot line) compared to baseline (green solid line): (a) transmitted and; (b) reflected.....	103
Figure 50: Longitudinal and flexural wave packets of transmitted waves (at 10kHz) considering a asymmetric actuator and asymmetric damage of 5% (black dash-dot line), 30% (cyan dashed line), 50% (blue dot-dot line) compared to baseline (green solid line)	104
Figure 51: Longitudinal and flexural wave packets of reflected waves (at 10kHz) considering a asymmetric actuator and asymmetric damage of 5% (black dash-dot line), 30% (cyan dashed line), 50% (blue dot-dot line) compared to baseline (green solid line)	105
Figure 52: Electrical voltage signals generated by scattered waves (at 50kHz) considering a symmetric actuator and asymmetric damage of 5% (black dash-dot line), 30% (cyan dashed line), 50% (blue dot-dot line) compared to baseline (green solid line): (a) transmitted; (b) reflected.....	106
Figure 53: Longitudinal and flexural wave packets of transmitted waves (at 50kHz) considering a asymmetric actuator and asymmetric damage of 5% (black dash-dot line), 30% (cyan dashed line), 50% (blue dot-dot line) compared to baseline (green solid line).	107
Figure 54: Longitudinal and flexural wave packets of reflected waves (at 50kHz) considering a asymmetric actuator and asymmetric damage of 5% (black dash-dot line), 30% (cyan dashed line), 50% (blue dot-dot line) compared to baseline (green solid line)	108
Figure 55: Experimental and simulated beams.	111
Figure 56: Illustration of the experimental setup.....	112
Figure 57 Photographic of the experimental setup.....	113
Figure 58: Input burst signals for main frequency of 25kHz (blue solid line), 35kHz (black dot-dot line) and 45kHz (red dashed-dot line): (a) time domain; (b) frequency domain.....	114
Figure 59: Comparison between simulated and experimental transmitted waves (25kHz) for baseline (blue solid line) and damage (red dot-dot line) conditions.....	115

Figure 60: Comparison between simulated and experimental reflected waves (25kHz) for baseline (blue solid line) and damage (red dot-dot line) conditions.....	117
Figure 61: Comparison between simulated and experimental transmitted waves (35kHz) for baseline (blue solid line) and damage (red dot-dot line) conditions.....	118
Figure 62: Comparison between simulated and experimental reflected waves (35kHz) for baseline (blue solid line) and damage (red dot-dot line) conditions.....	119
Figure 63: Comparison between simulated and experimental transmitted waves (45kHz of central frequency).	120
Figure 64: Comparison between simulated and experimental reflected waves (45kHz) for baseline (blue solid line) and damage (red dot-dot line) conditions.....	121
Figure 65: Division of a symmetric damage section.	132
Figure 66: Scattering waves by symmetric change of cross sectional area considering a longitudinal incident wave; (a) Reducing and; (b) Amplifying.	133
Figure 67: Scattering waves by symmetric change of cross sectional area considering an incident flexural propagating wave; (a) Reducing and; (b) Amplifying.....	133
Figure 68: Waves presented on the area change.....	134
Figure 69: Efforts on the asymmetric change of cross-sectional area.	138
Figure 70: Scattering waves by an asymmetric change of cross sectional area considering a longitudinal incident wave; (a) Reducing and; (b) Amplifying.	140
Figure 71: Amplitude of longitudinal scattering waves by asymmetric change of cross sectional area considering an incident longitudinal wave; (a) Reducing 50% and; (b) Amplifying 50%.	141
Figure 72: Amplitude of flexural scattering waves by asymmetric change of cross sectional area considering an incident longitudinal wave; (a) Reducing 50% and; (b) Amplifying 50%....	143
Figure 73: Scattering waves by an asymmetric change of cross sectional area considering an incident flexural propagating wave; (a) Reducing and; (b) Amplifying.....	144
Figure 74: Amplitude of longitudinal scattering waves by asymmetric change of cross sectional area considering an incident flexural wave; (a) Reducing 50% and; (b) Amplifying 50%. ..	145
Figure 75: Amplitude of flexural scattering waves by asymmetric change of cross sectional area considering an incident flexural wave; (a) Reducing 50% and; (b) Amplifying 50%.	146
Figure 76: Scattering waves by a symmetric damage for an incident longitudinal wave.....	149
Figure 77: Illustration of reflection and transmission coefficient.	149
Figure 78: Illustration of the waves behavior considering a vertical time line.	151

Figure 79: Reflection coefficient in symmetric discontinuity for a damage deep of 10%; (a) Amplitude and (b) Phase.....	155
Figure 80: Reflection coefficient in symmetric discontinuity for a damage deep of 30%; (a) Amplitude and (b) Phase.....	156
Figure 81: Reflection coefficient in symmetric discontinuity for a damage deep of 50%; (a) Amplitude and (b) Phase.....	157
Figure 82: Transmission coefficient in symmetric discontinuity for a damage deep of 10%; (a) Amplitude and (b) Phase.....	161
Figure 83: Transmission coefficient in symmetric discontinuity for a damage deep of 30%; (a) Amplitude and (b) Phase.....	162
Figure 84: Transmission coefficient in symmetric discontinuity for a damage deep of 50%; (a) Amplitude and (b) Phase.....	163
Figure 85: Minimum transmission coefficient and maximum reflection coefficient for a symmetric discontinuities varying with the damage deep.	165

LIST OF TABLE

Table 1: Geometrical and material properties of infinite beam and piezoelectric elements....	51
Table 2: Lengths of each beam segment	81
Table 3: Lengths of each experimental and simulated beams.....	112

CONTENTS

1	INTRODUCTION.....	18
1.1	Background	20
1.2	Literature Review.....	24
1.3	Objectives	27
1.4	Contributions to Knowledge	28
1.5	Thesis Outline.....	28
2	BRIEF OVERVIEW OF WAVE MOTION ON ELASTIC STRUCTURES	30
2.1	Basic Waves types on Elastic Structures	30
2.2	Some Basic Aspects of Harmonic Wave Motion	31
2.2.1	<i>Phase velocity (c).....</i>	31
2.2.2	<i>Wavelength (λ).....</i>	32
2.2.3	<i>Wavenumber (k).....</i>	33
2.2.4	<i>Group Velocity (c_g)</i>	33
2.2.5	<i>Dispersive and Non-Dispersive waves</i>	33
2.3	Guided Waves.....	34
2.3.1	<i>Waves on Beams.....</i>	34
2.3.1.1	<i>Longitudinal Waves</i>	35
2.3.1.2	<i>Flexural Waves.....</i>	38
2.4	Conclusions.....	41

3	WAVE MODELS IN THE FREQUENCY DOMAIN.....	42
3.1	Introduction.....	42
3.2	Wave Model.....	43
3.3	Piezoelectric Actuator	46
3.3.1	<i>Symmetric Actuator.....</i>	<i>47</i>
3.3.2	<i>Asymmetric Actuator.....</i>	<i>54</i>
3.4	Piezoelectric Sensor.....	54
3.4.1	<i>Symmetric Sensor.....</i>	<i>55</i>
3.4.1	<i>Asymmetric Sensor.....</i>	<i>58</i>
3.5	Discontinuities (damage).....	59
3.5.1	<i>Symmetric Damage.....</i>	<i>59</i>
3.5.1.1	<i>Longitudinal Incident Wave</i>	<i>63</i>
3.5.1.2	<i>Flexural Incident Wave.....</i>	<i>67</i>
3.5.2	<i>Asymmetric damage</i>	<i>70</i>
3.5.2.1	<i>Longitudinal Incident Wave</i>	<i>72</i>
3.5.2.2	<i>Flexural Incident Wave.....</i>	<i>74</i>
3.6	Conclusions.....	77
4	CASE STUDIES.....	79
4.1	Introduction.....	79
4.2	Overall Aspects of Simulations	81
4.3	Case 1: Symmetric Actuation and Symmetric Damage.....	87
4.3.1	<i>Longitudinal Incident Wave.....</i>	<i>87</i>
4.3.2	<i>Flexural Incident Wave.....</i>	<i>89</i>
4.4	Case 2: Asymmetric Actuation and Symmetric Damage.....	91

4.5	Case 3: Symmetric Actuation and Asymmetric Damage.....	95
4.5.1	<i>Longitudinal Incident Wave</i>.....	95
4.5.2	<i>Flexural Incident Wave</i>.....	99
4.6	Case 4: Asymmetric Actuation and Asymmetric Damage.....	102
4.7	Conclusions.....	108
5	PARTIAL VALIDATION	110
5.1	Introduction.....	110
5.2	Experimental Beam.....	110
5.3	Experimental Setup.....	112
5.4	Comparison	113
5.5	Conclusions.....	121
6	FINAL CONSIDERATIONS.....	123
6.1	Further works.....	124
	REFERENCES.....	126
	A.1 WAVE MODELS OF SINGLE DISCONTINUITES	132
	A.1.1 Symmetric Change of Cross-Sectional Area.....	132
	A.1.1.1 Longitudinal Incident Wave	136
	A.1.1.2 Flexural Incident Wave	137
	A.1.2 Asymmetric Change of Cross-Sectional Area.....	138
	A.1.2.1 Longitudinal Incident Wave	140
	A.1.2.1 Flexural Incident Wave	144
	A.1.3 Conclusions	147

A.2 PHYSICAL ASPECTS OF A LONGITUDINAL WAVE INTERACTING WITH SYMMETRIC DAMAGE.....	148
A.2.1 Objectives.....	148
A.2.2 Methodology.....	148
A.2.2.1 Reflected Wave.....	151
A.2.2.2 Transmitted Wave.....	158
A.2.3In the Optimum Frequency.....	164
A.2.4 Conclusions.....	166

1 INTRODUCTION

The guarantee of security in transport vehicles, buildings, bridges and critical structures is extremely important for people and the environment. Therefore, in the last decades, several Structural Health Monitoring (SHM) techniques have been proposed and developed for many areas, such as civil (CHANG *et al.*, 2003), naval (SOLIMAN *et al.*, 2015), aerospace (BOLLER *et al.*, 2004) and aeronautical (GONSALEZ *et al.*, 2015) structures, pipes (DEMMA *et al.*, 2004), wind turbines (CIANG *et al.*, 2008) and others.

In the context of the aeronautical industry, the search for safety results in critical and conservative processes for design and conservation of product integrity (maintenance). However, the process of aircraft maintenance results in very high costs for aircraft operating companies. “[...] Maintenance and repairs represent about a quarter of commercial aircraft operating costs [...]” (GIURGIUTIU, 2007, p. 1).

Regarding the benefits of introducing Structural Health Monitoring (SHM) into commercial aviation, Kent and Murphy (2000) provided cost benefit analysis for three different structures (trailing edge, vertical stabilizer and engine mount) showing that a significant reduction in the life-cycle costs could result in a realistic return on investments. According to this study, considering a replacement of 30 to 40% of traditional maintenance requirements by SHM solutions, the time to recover the cost of the initial investment for both the engine mount and the trailing edge structure would be two to three years (Santos, 2013) (Rulli; Gonzalez Bueno; Dotta; Silva, 2016, p. 329).

Considering this scenario, systems for structural health monitoring are desirable; for safety, reducing operating costs (through an as-needed maintenance) and, additionally, automating complex processes of damage detection, for example, in regions of difficult access for maintainers.

In particular, an accident occurred in 1988 with an aircraft of Aloha Airlines, when part of the fuselage was ripped out due to corrosion. This attracted attention to the corrosion problem in aircraft and triggered a series of preventive and corrective actions for corrosion in airplanes (Technical Report NTSB/AAR-89/03, 1989). The corrosion problem requires complex maintenance processes as, in general, it occurs mainly in regions of restricted visual access.

Figure 1: Aloha Airlines flight 243 accident.

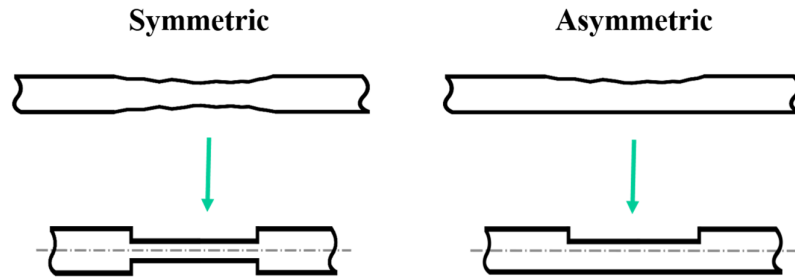


Source: ATSB Transport Safety Report - Aviation Research and Analysis Report – B20050505

One technique to detect corrosion could be the use of structural waves considering one wave travelling in a structure and impinging on a discontinuity (damage), this wave interacts with this discontinuity and is scattered. Thus, wave motion may be a powerful way to indicate the presence of damage in a structure.

Based on the context described above, this thesis aims to investigate wave propagation in a thin infinite beam, excited in such a way that these waves interact with simulated corrosion damage, symmetric and asymmetric by the neutral axis of the beam. Figure 2 presents an illustration of these damage and the simplification adopted here in order to model them.

Figure 2: Symmetric and Asymmetric corrosion damage.



Source: Elaborated by author

1.1 Background

Several types of SHM systems have been proposed and developed in the last decades and guided waves techniques have received great attention because some advantages inherent in such methods, as presented by Mitra and Gopalakrishnan (2016). They are:

- Ability to scan a large area with a relatively small number of transducers;
- High frequency excitation is involved hence small damage can be detected;
- Low frequency ambient vibration does not interfere with the guided wave;
- The transducers used are cheap, light-weight and can be relatively easily incorporated in the structure.

There are many studies showing the use of guided waves to detect hidden damage (CHAN *et al.*, 2015), corrosion (CHEW; FROMME, 2014) and fatigue cracks (MASSEREY; FROMME, 2013). As mentioned by Kolalowski (2007) high frequency wave methods are widely applied for aeronautic structures.

SHM using guided waves has been widely explored and several forms of guided waves have been studied to improve real applications. Some of them are summarized below:

- **Axial Waves** or **Longitudinal Waves** – are waves such that particles oscillate back and forth on an axis that is the same as the axis wave propagation. These waves are very common and occur for example in rods, beams and thin plates, hollow cylinders (pipes and tubes). Extensive work has been presented on one-dimensional wave propagation for damage detection in cables, truss structures, and concrete rebar (MITRA; GOPALAKRISHNAN, 2016).
- **Transversal Waves** or **Flexural Waves** – are waves such that particles oscillate back

and forth on an axis that is perpendicular to the axis of wave propagation. These waves are very common and occur, for example on strings, beams and thin plates, hollow cylinders (pipes and tubes).

- **Rayleigh-like Waves or Surface Acoustic Waves (SAW)** – are waves propagating on a free surface of thicker plates and are usually used to detect damage on free surfaces. Some work in this area are Masserey and Fromme (2009) and Guillaume and Vanlanduit (2008);
- **Lamb Waves** – propagate through parallel free surfaces (thin beam, plates and shells) and are usually used to detect surfaces or through-cracks, hole and hidden faults. Lamb Waves are the most common form of guided wave used for damage detection. Some works are Su *et al.* (2006), Higuti *et al.* (2010), Wilcox *et al.* (2010), Prado *et al.* (2013), Chan *et al.* (2015), Takiy *et al.* (2017), Masserey *et al.* (2014), Masserey and Fromme (2015, 2017), Roy *et al.* (2014), Roy *et al.* (2015), Giurgiutiu *et al.* (2015), Shen and Giurgiutiu (2015, 2016);
- **Sear-Horizontal (SH) Waves** – propagate through parallel free surfaces (thin beam, plates and shells) but are horizontally polarized. Some works are Su *et al.* (2007), Kamal and Giurgiutiu (2014);

Nowadays, SHM systems have come to the wider question of increasing the maturity of technology or the Technology Readiness Level (TRL), as defined by Mankins (1995). However, it is not easy to define robust strategies for damage detection. In some cases, to represent the behavior of SHM systems in real conditions it is necessary to evaluate an extensive amount of data and this can be impracticable. An example is the widely used process of POD (Probability of Detection). This is a SHM system adopted as a tool to certify a SHM system for aircraft, as can be seen in SAE ARP 6461 (2013). Software to simulate and analyze the behavior of the data could be useful to understand and design SHM systems. The prediction of POD curves appears to be a powerful tool for companies.

The use of representative models helps to understand the behavior of waves and their interaction with discontinuities, boundaries and contact interfaces. To develop this kind of model it is necessary to understand the physical phenomena involved, as are the propagation of elastic waves in structures and their interaction with discontinuities.

As presented by Mitra and Gopalakrishnan (2016), modeling and simulations form an important part of the understanding of the mechanics of damage, its interaction with diagnostic or ambient input, and participation in the response. Also, it is important to understand

transducer-structure interaction, their optimal placement, tuning of input parameters and to correlate the damage signature to the attributes of the damage.

In this context, there has been much work carried out by research. Some of which can be discussed in the next section.

There are some initiatives to develop software packages to model and simulate guided waves propagation and interaction with damage. Among them are:

- *WaveFromRevealer*: This is an analytical framework and predictive tool able to insert damage effects into an analytical framework. It is a predictive tool and is able to insert damage effects into the analytical model (wave transmission, reflection, mode conversion and nonlinear higher harmonics) in two-dimensional thin-walled structure composed of isotropic material (SHEN; GIURGIUTIU, 2014) and;
- *EWavePro*: This uses the Spectral Finite Element Method to model elastic wave propagation (*EWavePro*) in two and three-dimensional thin-walled structures (isotropic) (OSTACHOWICZ *et al.*, 2012);

In addition, there is a commercial software by Weidlinger Associates who developed *PZFlex*. It involves Finite Element Analysis (FEA) to solve two and three-dimensional problems about wave-propagation and piezoelectric applications. (pzflex.com).

To contribute to the understanding of elastic wave propagation and their interaction with damage, the work in this thesis uses a frequency domain model proposed by Brennan *et al.* (1997) to consider the interaction of waves with simulated corrosion faults. This model was proposed for the active control of waves, and here it is adapted to solve SHM problems.

This work implements and validates models that represent the physical phenomena of wave motion on primary structures with simulated corrosion damage. The waves are generated and sensed by piezoelectric transducers. Simulations are used to investigate the way in which longitudinal and flexural waves interact with damage in a beam, and the results are validated by experimental tests.

There are significant advantages in the use of piezoelectric transducers for SHM systems. They have low costs, light weight and high performance. Furthermore, they can generate purely longitudinal or flexural waves if they are bonded appropriately.

In the aeronautical context, to use piezoelectric transducers on aircraft some operational aspects need to be taken into account. Among them:

- Guaranteed safety during the aircraft operation;

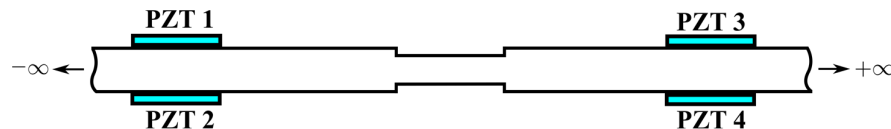
- Mechanical strength of the transducer submitted to operational conditions of aircraft;
- Transducer replacement;
- Practical viability of the installation process.

Considering this last item, for many structural configurations in aircraft it can be impracticable to use a pair of piezoelectric in a symmetric way (bimorphs). It seems to be more feasible to work with single piezoelectric (asymmetric) bonded to only one side of structure. Thus, to cover more applicability elements both transducer configurations are studied. The symmetric configuration is analyzed first and the asymmetric case, second.

To determine the behavior of waves travelling in a beam and their interaction with damage, three cases studies are defined in this work. The configurations consist of infinite beams and these cases are presented from Figure 3 to Figure 6.

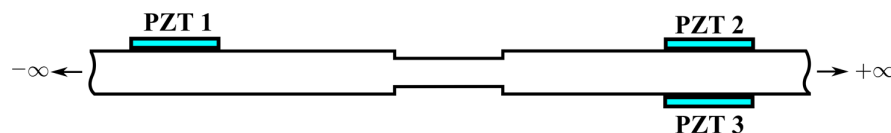
The first case (Figure 3) comprises a pair of actuator, symmetric damage and sensors. The second one (Figure 4) consists in a single actuator (an asymmetric excitation), a symmetric damage and sensor. The third case (Figure 5) involves symmetric actuator and sensors and an asymmetric damage. The last case (Figure 6) consists of asymmetric actuator and damage, and a symmetric sensor.

Figure 3: Case 1 – Infinite beam with piezoelectric bimorphs and symmetric damage.



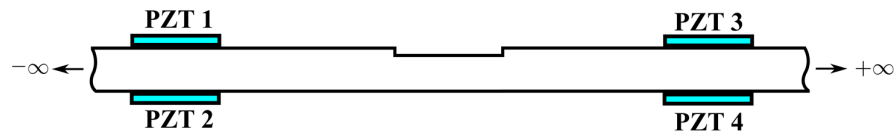
Source: Elaborated by author

Figure 4: Case 2 - Infinite beam with asymmetric actuator and symmetric damage.



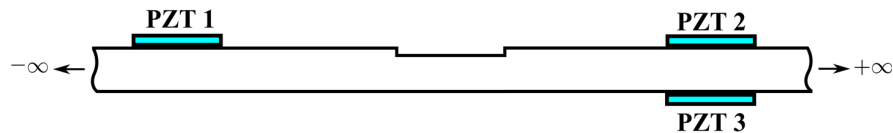
Source: Elaborated by author

Figure 5: Case 3 - Infinite beam with symmetric actuator and symmetric damage.



Source: Elaborated by author

Figure 6: Case 4 - Infinite beam with asymmetric actuator and damage.



Source: Elaborated by author

It is important to note that although this work is contextualized for the aeronautics area these developments and findings can be used for other similar applications since they are compatible with the primary structure studied here.

The approach used here to study the wave interaction with the damage in the frequency domain (BRENNAN, 1994; BRENNAN *et al.*, 1997). The behavior in the time domain is also studied using the Inverse Fast Fourier Transform (IFFT) (OPPENHEIM; WILLISKY, 2010).

1.2 Literature Review

Structural Health Monitoring (SHM) is a field of knowledge that has increased a lot in the last decades. It involves many universities, companies, research centers, committees and others.

It is possible to conclude that SHM is an advance of conventional NDT&E (nondestructive testing and evaluation) since SHM techniques also aim to monitor structures. Among the main differences, a SHM process can be made to work automatically, and it can provide real-time damage prognosis with minimal manual intervention (BOLLER *et al.*, 2009).

It is possible to find much information about SHM in the literature. Examples of some

books are: Inman *et al.* (2005), Balageas *et al.* (2006), Adams (2007), Giurgiutiu (2007), Stepinski *et al.* (2013), Boller *et al.* (2009).

According to Mitra and Gopalakrishnan (2016) the underlying concept of SHM is to record responses of a monitored structure and in then to analyze the response and to extract features resulting from the defect. These features are related to the attributes of the defect either through a physical model or data-driven statistical and machine learning techniques.

Following the classifications used by Rytter (1993) and Doebling *et al.* (1998), a SHM system can be classified on levels related of its capacity:

- **LEVEL 1** - SHM system is able to detect the damage;
- **LEVEL 2** - SHM system detects and gives the geometric location of the damage;
- **LEVEL 3** - SHM system can detect, localizes and quantify the severity of damage and;
- **LEVEL 4** - SHM system detects, localize, quantifies the damage and estimates the remaining service life of the structure.

All levels described are of high important for a SHM system. However, in practical cases, considering the influences of the operational environment (such as temperature and loading changes, joint backlash, aging and others) the guarantee of high reliability in a SHM system Level 1 is already quite labor intensive. In this context, there is the possibility of false alarm denoted as:

- **False positive** – when the system detects damage that does not exist;
- **False negative** – when the system does not detect damage that exists.

Nowadays, there are many techniques or technologies for a SHM system. Some of them are:

- **Comparative Vacuum Monitoring (CVM);**
- **Acoustic Emission (AE);**
- **Fiber Bragg Grating (FBG);**
- **Automated Eddy Current;**
- **Vibration-based techniques;**
- **Electromechanical Impedance-based techniques (EMI);**
- **Guided Waves (GW).**

Alleyne and Cawley (1992) studied the interaction of Lamb waves with defects. The authors used a finite element analysis to demonstrate experimental results obtained. Their study showed that the position of the maxima and minima transmitted amplitudes are a function of damage depth and because of this the monitoring the change in transmission ratio with frequency can allow to detect its sizing.

Diligent *et al.* (2002) studied the S0 Lamb wave in a nondispersive frequency range with a circular through-thickness hole in a plate. The hole diameters were limited in the range of 1 to 3 wavelengths and it was verified an agreement between simulated and experimental results. Finite Element method and analytical formulations allowed to investigate the reflection coefficient, which increases with the diameter of the hole and decreases with the distance with from the hole.

Moreau *et al.* (2011) investigated the three-dimensional scattering of guided waves by a through-thickness cavity in an isotropic plate. The scattering field was decomposed on propagating and non-propagating waves. The authors used a Finite Element based model to study two types of cavities (an elliptical and irregular one) and they comment that their approach can be extended to different cavities. In this sense, these researchers presented an additional study for the scattering of guided waves by a flat-bottomed cavity with irregular form (Moreau *et al.*, 2012). The proposed method was validated by comparison with the Finite Element method.

Chew and Fromme (2014) analysed the thickness reduction due to generalized corrosion in steel specimens. They worked in the frequency range around 5MHz and the corrosion damage was monitored based on the effect on wave propagation and interference of the different modes. The change in the wave interference was quantified based on an analysis in the frequency domain.

Farhidzadeh and Salamone (2015) worked with longitudinal waves in steel strands and proposed a reference-free algorithm to estimate the strand's cross-section loss by using dispersion curves, continuous wavelet transform, and wave velocity measurements.

Gao and Rose (2010) monitored the metal loss in an aluminum plate. The authors proposed new definitions of guided wave excitability and sensitivity dispersion curves in order to select appropriate guided wave modes for a particular application.

In the civil structures, Sharma and Mukherjee (2010) used longitudinal waves to monitoring corrosion of reinforcing steel in concrete. Ervin *et al.* (2009) presented a discussion about monitoring real corrosion of rebar embedded in Mortar using longitudinal waves mode at high frequency.

Terrien *et al.* (2007) investigated the interaction of hidden corrosion in aircraft structures to Lamb waves through a Finite Element (FE) based hybrid approach. The FE mesh was used to describe the region surrounding the corrosion pits while a modal decomposing method was employed to determine the waves reflected and transmitted by the damaged area. According to the authors, their methodology is able to detect corrosion pits down to 80 micro-meters depth.

Poddar and Giurgiutiu (2015) presented an analytical model for Lamb Wave interaction with the simplest of all geometric discontinuity – a step (or asymmetric reduction of cross-sectional area), since this fundamental understanding can be extended to corrosion or a crack. The authors developed an analytical approach using the method called complex mode expansion with vector projection (CMEP) to predict the scatter of Lamb Waves produced by the discontinuity. This model was validated with an FEM model (considering 27 wave modes).

Palacz (2018) shows recently a review of spectral methods to model wave propagation in structures in the field on detect damage. The paper compares Frequency Domain Spectral Finite element method with Time Domain Spectral Finite element method avoiding for numerical errors that can be obtained using reverse Fourier transforms in two-dimensional geometry.

Although there are many related works in the literature, the behavior of longitudinal and flexural transmitted and reflected waves is not completely described and this work aims to make a contribution in this context.

1.3 Objectives

Considering the monitoring of a primary aircraft structure like a beam, the main objectives of this thesis are to:

- Develop frequency domain models of a beam containing piezoelectric actuation and sensors, and a damaged section;
- Investigate the filtering effects of the actuators and sensors;
- Investigate the interaction of longitudinal and flexural waves with symmetric and asymmetric corrosion like damage;
- Transform the frequency domain models to the time domain to investigate the interaction of a wave packet with symmetric and asymmetric damages;
- Validate some of the findings experimentally.

1.4 Contributions to Knowledge

The main contributions of this work are:

- Development of a frequency and time domain model to investigate wave generation and interaction with corrosion like damage on a beam;
- The understanding the filtering effects of damage in order to avoid false diagnostics;
- Formulation of equations to find Optimum Frequencies to be used in a SHM system;
- Discussions of the difference between longitudinal and flexural wave interaction with corrosion like damage on a beam and;
- Show clearly in frequency and time domain that reflected wave packets are more sensitive than transmitted waves in order to detect and quantify the damage;
- Conclude that longitudinal wave mode is better to be used in SHM systems than flexural wave mode;
- Presents a study of physical aspects of a longitudinal wave interacting with symmetric damage in order to understand how many wave packets are important to be considering in the a modeling to represents the physical behavior of infinite packets.

1.5 Thesis Outline

This thesis outline is as follows:

Chapter 1 presents an introduction and justification of this work, literature review, objective and contributions to knowledge;

Chapter 2 presents a brief overview about the wave motion on elastic structures to support the comprehension of the formulation used in this work;

Chapter 3 explains the modelling approach for waves propagation in the frequency domain and discuss some typical behaviors observed from numerical simulations of each parts of the structure (actuator, sensor, discontinuities and beam);

Chapter 4 presents and discusses the behavior in time domain for every study case defined in this work considering burst signals as input to excite the structure and three damage depth for discontinuities;

Chapter 5 presents the experimental tests carried out and comparisons between experimental data and results obtained by numerical simulations;

Chapter 6 presents the conclusions obtained and indicates some future studies that can be

done to complement this work;

Appendix A.1 presents and discusses the wave models of single discontinuities;

Appendix A.2 presents and discusses physical aspects of a longitudinal wave interacting with symmetric damage.

2 BRIEF OVERVIEW OF WAVE MOTION ON ELASTIC STRUCTURES

Elastic waves (or stress waves) on structures can be described as harmonic disturbances in a solid media that propagate in the elastic regime.

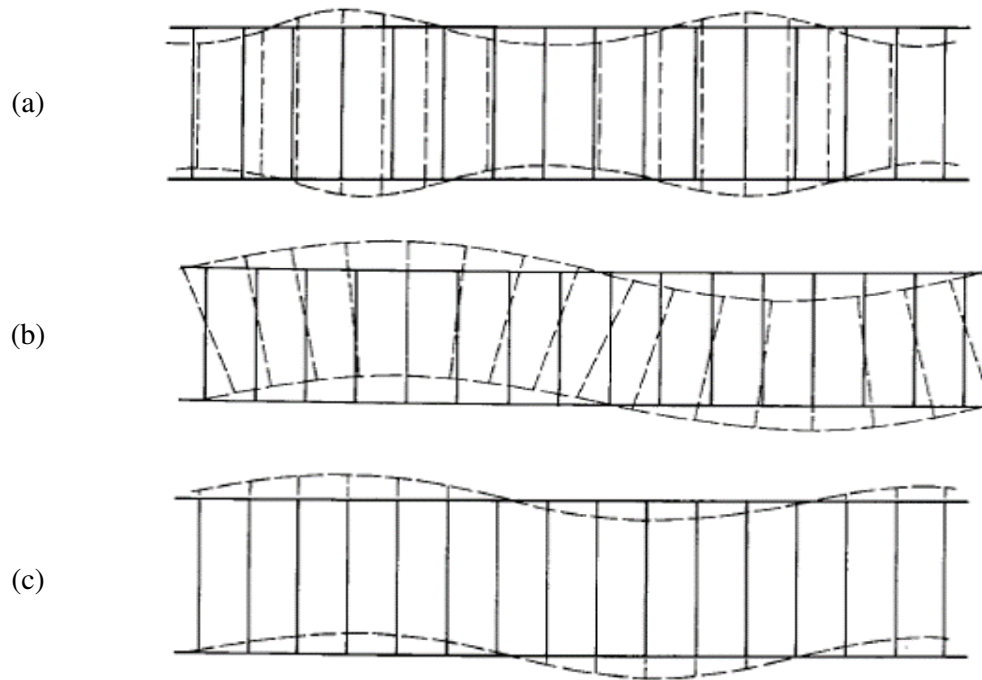
As mentioned by Fahy (2001), the modeling and analysis of wave propagation in structures is more complicated than in fluids. This is because in structures there are different wave types (longitudinal, transversal and torsional, for examples).

This chapter presents a brief overview of some important aspects of wave motion on elastic structures. More contents can be found in textbooks on the subject, such as Graff (1975), Achenbach (1984), Cremer and Heckl (1988), Auld (1990), Nayfeh (1995), Doyle (1997), Rose (1999) and Hagedorn and DasGupta (2007). Also, an explanation and interpretation of the physical behavior of structural wave motion can be found in Brennan *et al.* (2016).

2.1 Basic Waves types on Elastic Structures

There are several types of waves that can propagate in an elastic structure. The most basic ones are longitudinal, flexural and shear waves. An illustration of these kinds of waves are shown in Figure 7.

Figure 7: Illustration of the most basic waves types on elastic structures; (a) Longitudinal waves; (b) Bending waves and; (c) Shear waves.



Source: Fahy (2001)

The longitudinal waves are predominantly present on rods (due to axial forces). However, they are also present in beams, plates and tubes. Bending waves are related to transversal motion and they are also present in structures as beams, plates and tubes. The same occurs for shear waves.

2.2 Some Basic Aspects of Harmonic Wave Motion

This section introduces basic definitions of the fundamental concepts of wave propagation.

2.2.1 Phase velocity (c)

The wave speed is the speed that a wave propagates. For longitudinal waves, as showed by Brennan *et al.* (2016), the phase speed is given by

$$c_l = \sqrt{\frac{E}{\rho}} \quad (1)$$

where E is the Young's modulus and ρ is the material density. Note that c_l is dependent only on the material properties.

The wave speed for flexural waves, as showed by Brennan *et al.* (2016), is given by

$$c_f = \sqrt[4]{\frac{EI}{\rho S}} \sqrt{\omega} \quad (2)$$

where I is the second moment of area, S is cross-sectional area and ω is angular frequency.

The phase speed of a shear waves is given by:

$$c_s = \sqrt{\frac{G}{\rho}} \quad (3)$$

where G is the shear modulus.

2.2.2 Wavelength (λ)

The wavelength is the size (length) of a wave corresponding to one cycle (a period). It is related to the wavenumber by $c = \lambda f$, then

$$\lambda = \frac{c}{f} \quad (4)$$

where c is the phase speed and can be, for example, c_l , c_f or c_s .

2.2.3 Wavenumber (k)

The wavenumber is the spatial frequency of a wave (analogous to temporal frequency) and represents the number of wavelengths that occurs in a unitary distance:

$$k = \frac{\omega}{c} = \frac{2\pi}{\lambda} \quad (5)$$

2.2.4 Group Velocity (c_g)

The phase velocity for individual waves (longitudinal, flexural and shear) is defined by $c = \omega/k$. The group velocity is the phase velocity of the combined waves and is given by:

$$c_g = \frac{\Delta\omega}{\Delta k} \quad (6)$$

The group velocity is the velocity at which combined waves propagates (BRENNAN *et al.*, 2016) or is the velocity at which the energy in the combined waves is transported (CREMER *et al.*, 2005).

2.2.5 Dispersive and Non-Dispersive waves

The term dispersion is commonly confused with term dissipative. In the same way, non-dispersive is usually confused with non-dissipative. However, these nomenclatures are used to denominate different phenomenon.

Dissipation is related to the energy lost during the wave propagation. It is usually related to damping in the structures.

Dispersion is related to changes in the wave shape and occurs without energy lost. Dispersion is a non-dissipative phenomenon and involves only the speed at waves propagates.

Dispersive waves have phase speed dependent of frequency. It means that the waves in different frequencies propagate at different phase speeds. It generates a modification in the

shape of wave packet during propagation. Flexural waves in an example of dispersive waves. The phase speed of flexural waves is given by Eq. (2) and the combination of flexural waves at different frequencies propagate at group speed, given by $c_{gf} = 2c_f$ (BRENNAN *et al.*, 2016).

In the other hand, non-dispersive waves have phase speed without frequency dependency. Longitudinal waves is non-dispersive. It means that a packet of this wave mode (contains waves at different frequencies) propagate without change in the shape of waves packet. Additionally, as commented by Brennan *et al.* (2016), if a pulse of longitudinal waves is generated in a point of the structure it propagates without distortion. At this case, the group and phase speed is equal to $c_{gl} = c_l$.

2.3 Guided Waves

Guided Waves are types of waves that require a boundary for propagation. Some examples of guided waves are (ROSE, 2000, 2007):

- Waves along a free surface of a solid (Rayleigh);
- Waves at an interface between two materials (Stonely);
- Waves in a rod (Longitudinal mode);
- Waves at the surface of a plate (Shear Horizontal –SH modes);
- Waves in a beam and in a plate (Longitudinal and Flexural modes or Lamb Waves);
- Waves in a tube or pipe (Longitudinal, Flexural and Torsional modes);
- Multilayer materials;

Guided Waves are widely used for SHM especially because they can travel at large distances in structures (GIURGIUTIU, 2007) and is possible giving complete volumetric coverage of the item inspected or monitored (ROSE, 2007).

2.3.1 Waves on Beams

As presented before, in a beam longitudinal and flexural waves (bending and shear) can occur. It depends of the beam depth and the frequency of propagating wave.

To model wave propagation in a beam it is important to note the difference between Euler-Bernoulli and Timoshenko beam theories. Two fundamental assumptions in Euler-Bernoulli

theory are (BRENNAN *et al.*, 2016):

- Rotary inertia of the beam is neglected and;
- Shear stiffness is infinite.

These assumptions are generally valid for a rectangular (cross-sectional) beam when $\lambda_f \geq 10t_B$ where t_B is the thickness of the beam. When this condition does not hold, it is necessary to use the Timoshenko theory to describe the vibration of beams (BRENNAN *et al.*, 2016; GRAFF, 1975; HAGEDORN; DASGUPTA, 2007).

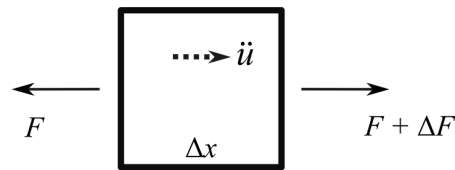
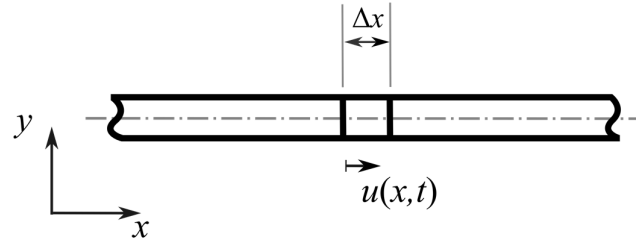
Considering the assumptions above, for a uniform Euler-Bernoulli beam two types of waves can occur: longitudinal and flexural waves. They can be considered separately or simultaneously. For a Timoshenko beam the shear effect is considered and thus shear waves can exist.

The formulation in this work involves the Euler-Bernoulli theory, and because of this a short review of this one is presented in the following section to the longitudinal and flexural bending waves.

2.3.1.1 Longitudinal Waves

The content presented in this section is based on the theory presented by Doyle (1997) for rods. Figure 8 shows a segment of beam with axial force related to a longitudinal vibration of this structure, where Δx is a short length of the structure, $u(x, t)$ is the axial (or longitudinal) displacement, x defines the horizontal direction and t is the time.

Figure 8: Segment of a beam (or rod) with loads.



Source: Adapted from Doyle (1997)

In this case only one displacement $u(x, t)$ is considered (the axial degree of freedom). For a linear elastic material the related axial stress by Hooke's Law is given by

$$\sigma_{xx} = E\varepsilon_{xx} \quad (7)$$

where ε_{xx} is the axial strain, i.e.,

$$\varepsilon_{xx} = \frac{\partial u(x, t)}{\partial x} \quad (8)$$

The resultant axial force F is related to the axial strain by

$$F = \int \sigma_{xx} dS = ES \frac{\partial u}{\partial x} \quad (9)$$

The balance of forces in that x-axis direction gives

$$-F + [F + \Delta F] = \rho S \Delta x \ddot{u} \quad (10)$$

where the product ρS is the mass density per unit length of the beam (or rod) and the two super dots indicates the second derivative. If quantities are small enough, after dividing the last equation by Δx the equation of motion becomes

$$\frac{\partial F(x,t)}{\partial x} = \rho S \frac{\partial^2 u(x,t)}{\partial t^2} \quad (11)$$

For this equation x and t are the independent variables and substituting F defined by Equation (9), the last equation can be rewritten by

$$\frac{\partial \left[ES \frac{\partial u}{\partial x} \right]}{\partial x} = \rho S \frac{\partial^2 u}{\partial t^2} \quad (12)$$

It is possible to use Equation (2) and obtain the normalized equation of motion

$$c_l^2 \frac{\partial^2 u}{\partial x^2} - \frac{\partial^2 u}{\partial t^2} = 0 \quad (13)$$

To solve the Equation (13) a propagating wave that is harmonic in time and space can be represented by

$$u(x,t) = A_r e^{j(\omega t - kx)} + A_l e^{j(\omega t + kx)} \quad (14)$$

where A_r is the amplitude of the wave propagating to the right side of beam (or rod) and A_l is the amplitude of one propagating the opposite side (the left) from that coordinate x and j is the imaginary number. It is important to make clear that notation implicitly considers a separation variables approach once the term $e^{j(\omega t \pm kx)}$ can be rewritten using a function f_t of t and another one f_x of x , i.e., $e^{j(\omega t \pm kx)} = f_t(t) f_x(x)$.

Rewriting Equation (9) considering the axial displacement given by Equation (14) results in:

$$F(x, t) = ES(-jkA_r e^{-jkx} + jkA_l e^{+jkx})e^{j\omega t} \quad (15)$$

Equations (14) and (15) can be rearranged in a matrix form to give

$$\begin{Bmatrix} u_x(x) \\ F_x(x) \end{Bmatrix} e^{j\omega t} = \begin{bmatrix} e^{-jkx} & e^{+jkx} \\ -ESjke^{-jkx} & ESjke^{+jkx} \end{bmatrix} \begin{Bmatrix} A_r \\ A_l \end{Bmatrix} e^{j\omega t} \quad (16)$$

Equation (16) can be rewritten as:

$$\mathbf{h}(x, \omega) = \mathbf{H}(\omega) \mathbf{T}(x, \omega) \mathbf{a}(\omega) \quad (17)$$

where

$$\mathbf{h}(\omega) = \{u_x \quad F_x\}^T \quad (18)$$

$$\mathbf{a}(\omega) = \{A_r \quad A_l\}^T \quad (19)$$

$$\mathbf{H}(\omega) = \begin{bmatrix} 1 & 1 \\ -ESjk & ESjk \end{bmatrix} \quad (20)$$

$$\mathbf{T}(x) = \begin{bmatrix} e^{-jkx} & 0 \\ 0 & e^{+jkx} \end{bmatrix} \quad (21)$$

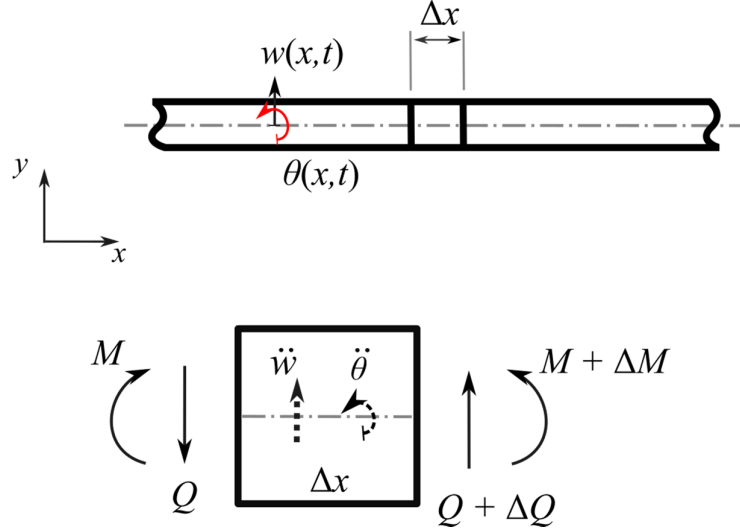
note that the dependence in k and/or x can be omitted for simplicity; $\mathbf{h}(\omega)$ is defined as the state vector, $\mathbf{a}(\omega)$ is the vector of longitudinal wave amplitudes, $\mathbf{H}(\omega)$ is the transformation matrix and $\mathbf{T}(x)$ is the spatial transformation matrix.

2.3.1.2 Flexural Waves

For the flexural waves a similar procedure can be used. This following contents are presented by Lee (2009), Doyle (1997) and Brennan *et al.* (2016). For flexural (or bending) waves, the model follows the Euler Bernoulli assumptions for beams (small deflections,

neglects shear deformation, the cross section of beam are orthogonal to the neutral axis after the flexural deformation). Figure 9 presents a segment of beam related to a flexural vibration.

Figure 9: Segment of an Euler-Bernoulli beam with flexural loads.



Source: Elaborated by the author.

The dynamic model for flexural waves in beams can be obtained from a transversal section, as shown in Figure 9, in which $w(x, t)$ is the transversal displacement, $\theta(x, t)$ is the angular displacement, Q is the shear force and M is the moment. Applying the balance of forces in the vertical direction is possible to obtain the following relation

$$-Q + [Q + \Delta Q] = \rho S \Delta x \ddot{w} \quad (22)$$

and, similarly to the moments,

$$-M + [M + \Delta M] + \Delta x Q = \rho I \ddot{\theta} \quad (23)$$

The term $\rho I \ddot{\theta} = 0$ for the Euler-Bernoulli formulation because the rotary inertia of the beam is neglected. Dividing these equations by Δx and considering it small enough, is possible to write the following equations

$$\rho S \frac{\partial^2 w}{\partial t^2} = \frac{\partial Q}{\partial x} \quad (24)$$

$$\frac{\partial M}{\partial x} + Q = 0 \quad (25)$$

Rearranging these two equation and assuming $\theta = \frac{\partial w}{\partial x}$ and $M = EI \frac{\partial \theta}{\partial x}$, the equations of flexural motion is given by

$$EI \frac{\partial^4 w}{\partial x^4}(x,t) + \rho S \frac{\partial^2 w}{\partial t^2}(x,t) = 0 \quad (26)$$

The above equation can be rewritten considering $w(x,t) = w_x(x)e^{-j\omega t}$ such that the temporal dependence can be eliminated after including the second derivative of $w(x,t)$. In this case, the resulting equation is given by

$$EI \frac{\partial^4 w_x}{\partial x^4}(x) - \omega^2 \rho S w_x(x) = 0 \quad (27)$$

and to solve this equation is assumed a particular solution $w_x(x) = A_w e^{jkx}$ such that

$$EI k^4 - \omega^2 \rho S = 0 \quad (28)$$

and the flexural wave number $k_f = k$ is given by

$$k_f = \sqrt{\omega} \left(\frac{\rho S}{EI} \right)^{1/4} \quad (29)$$

If a general solution of the partial differential equation (Eq.(27)) is desired, four roots of Equation (28) can be found, i.e., k_f , $-k_f$, jk_f and $-jk_f$, and the following expression can be written by

$$w_x(x) = A_1 e^{k_f x} + A_2 e^{-k_f x} + A_3 e^{jk_f x} + A_4 e^{-jk_f x} \quad (30)$$

The above equation allows to write a state vector $\mathbf{h}_f(\omega, x) = \{w \ \theta \ M \ Q\}^T$ in terms of the spatial derivatives such that

$$\begin{Bmatrix} w \\ \theta \\ M \\ Q \end{Bmatrix} = \mathbf{H}_f(\omega) \mathbf{T}_f(\omega, x) \begin{Bmatrix} A_1 \\ A_2 \\ A_3 \\ A_4 \end{Bmatrix} \quad (31)$$

in which the matrices $\mathbf{T}_f(\omega, x)$ and $\mathbf{H}_f(\omega)$ for the flexural waves are respectively given by

$$\mathbf{T}_f = \text{diag}(e^{k_f x}, e^{-k_f x}, e^{jk_f x}, e^{-jk_f x}) \quad (32)$$

$$\mathbf{H}_f = \begin{bmatrix} 1 & 1 & 1 & 1 \\ k_f & -k_f & jk_f & -jk_f \\ E_b I_b k_f^2 & E_b I_b k_f^2 & -E_b I_b k_f^2 & -E_b I_b k_f^2 \\ E_b I_b k_f^3 & -E_b I_b k_f^3 & -jE_b I_b k_f^3 & jE_b I_b k_f^3 \end{bmatrix} \quad (33)$$

2.4 Conclusions

This chapter presented a brief introduction of wave motion for elastic structures and some basic aspects of harmonic wave motion to provide the background to understand some physicals behind of wave propagation.

This chapter also presented the general solutions for the partial differential equations (EDP) for both longitudinal and flexural motion. It is considered the Euler-Bernoulli theory and it was shown the relation between the wavelength and the structure thickness which defines the maximum frequency for each this theory can be applied.

The presented formulation introduced the state vector which is the base of this work. In addition, it is also introduced the transformation matrix and the spatial transformation matrix after applying a matrix rearrangement of the associated EDPs.

3 WAVE MODELS IN THE FREQUENCY DOMAIN

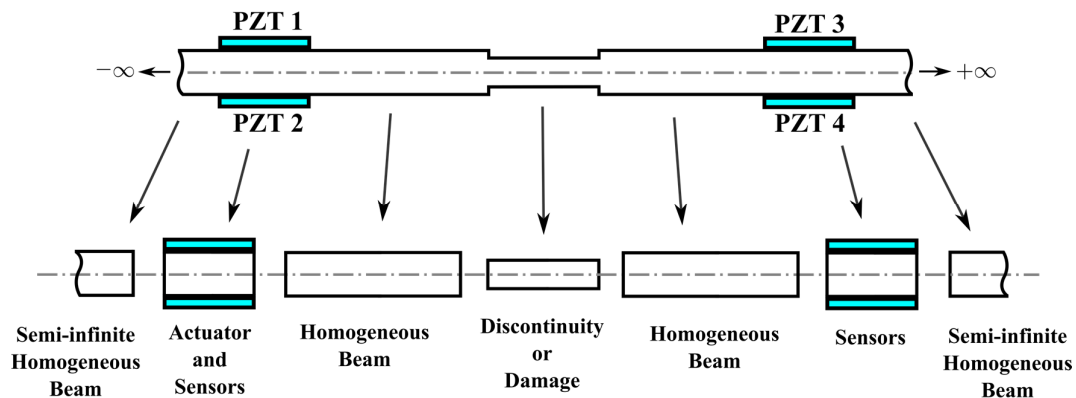
3.1 Introduction

The approach adopted in this work was previously presented and discussed by Brennan (1994), Brennan *et al.* (1997) and Ayala (2015). Some highlights about this methodology to modeling the wave propagation are:

- the approach is analytical and in the frequency domain, and it can be converted to the time domain using the Inverse Fast Fourier Transform (IFFT);
- the structure is hypothetically divided into segments that can be modelled in a simple manner;
- the basic principle of the approach is to transform the waves at each end of a segment to a state vector.

Figure 10 shows the assembled structure for the first study case and an illustration of how the structure is hypothetically divided.

Figure 10: First study case divided in segments.



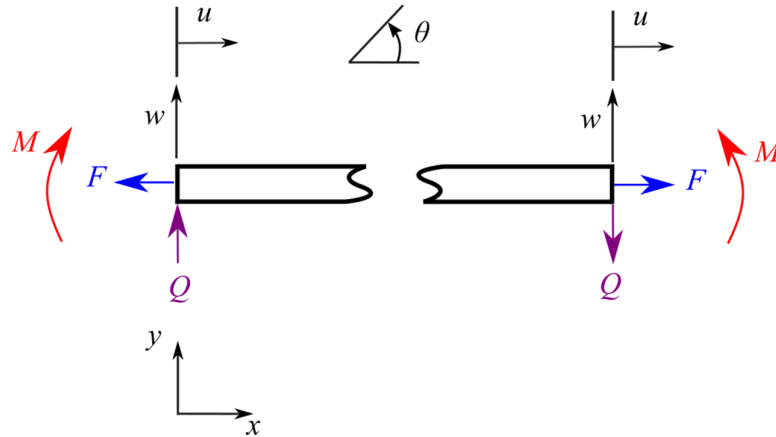
Source: Elaborated by author

The aim of this Chapter is to present the approach used to model the wave propagation in the Euler Bernoulli beam using piezoelectric elements like actuator/sensor and considering symmetric and asymmetric discontinuities. Each segment is modelled and discussed separately in different sections. However, the next section presents the overall model of waves.

3.2 Wave Model

Considering a beam segment, it is possible to see in Figure 11 the sign convention used with state vector (efforts, displacements and slopes) for each end of the segment.

Figure 11: Sign convention used with state vector.



Source: Adapted from Brennan *et al.* (1997)

In Figure 11 u is the horizontal displacement (axial), w is transversal displacement, θ is the slope, M is the moment, Q is vertical force (shear) and F is horizontal force (axial). A state vector, \mathbf{h} , can be written as:

$$\mathbf{h} = \{u \quad w \quad \theta \quad M \quad Q \quad F\}^T \quad (34)$$

Using an equivalent form considering w and u spatial derivatives in terms of x such that:

$$\mathbf{h} = \{u \quad w \quad w' \quad E_b I_b w'' \quad E_b I_b w''' \quad E_b S_b u'\}^T \quad (35)$$

where E_b is the Young's modulus of the beam, I_b is the second moment of area of beam, S_b

is the cross-sectional area of the beam, $u' = \frac{du}{dx}$ and, similarly, $w^{(i)} = \frac{d^{(i)}w}{dx^{(i)}}$.

Considering any segment of the beam, the state vector at each end of the segment is formed combining the waves amplitude, so that

$$\mathbf{h} = \mathbf{H}\mathbf{a} \quad (36)$$

where \mathbf{H} is the transformation matrix and \mathbf{a} is the vector of waves amplitudes.

The transformation matrices defined in Chapter 2 (Section 2.3.1) by Eqs. (25) and (37) can be rearranged to obtain the following 6x6 matrix for both longitudinal and flexural waves:

$$\mathbf{H} = \begin{bmatrix} 0 & 0 & 1 & 0 & 0 & 1 \\ 1 & 1 & 0 & 1 & 1 & 0 \\ k_f & jk_f & 0 & -k_f & -jk_f & 0 \\ E_b I_b k_f^2 & -E_b I_b k_f^2 & 0 & E_b I_b k_f^2 & -E_b I_b k_f^2 & 0 \\ E_b I_b k_f^3 & -jE_b I_b k_f^3 & 0 & -E_b I_b k_f^3 & jE_b I_b k_f^3 & 0 \\ 0 & 0 & jE_b S_b k_l & 0 & 0 & -jE_b S_b k_l \end{bmatrix} \quad (37)$$

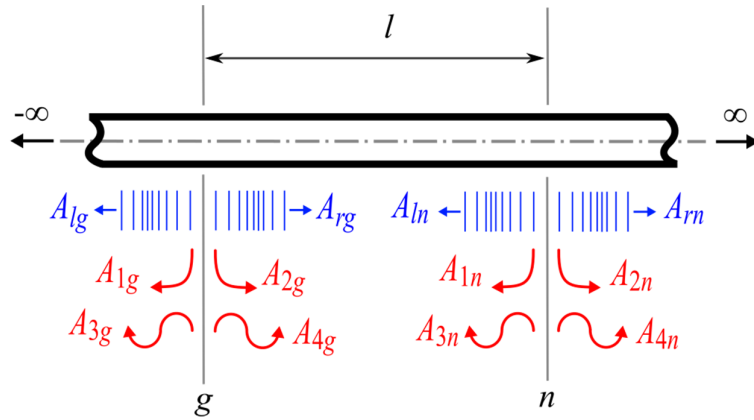
where $j = \sqrt{-1}$, k_l is the longitudinal wavenumber, k_f is the flexural wavenumber, defined by Eq.(2.6). The vector of wave amplitudes is given by:

$$\mathbf{a} = \{A_1 \ A_3 \ A_l \ A_2 \ A_4 \ A_r\}^T \quad (38)$$

where A_1 is the amplitude of near-field wave going to the left side, A_3 is the amplitude of a propagating wave travelling to the left side, A_l is the amplitude of longitudinal wave travelling to the left side, A_2 is the amplitude of near-field wave going to the right side, A_4 is the amplitude of propagating wave travelling to the right side, and A_r is the amplitude of longitudinal wave travelling to the right side. These waves can exist in each cross section of the beam or each point of beam.

Figure 12 illustrates the six waves that can exist in each cross sectional area of beam (here is showed for points g and n). Then, to denominate the waves at each point is used a subscript on nomenclature of waves corresponding to the designation of each point.

Figure 12: Waves that can exist at each cross section of an Euler-Bernoulli beam.



Source: Elaborated by author

The wave amplitudes at point n (\mathbf{a}_n) can be given by multiplying the vector of wave amplitudes at point g (\mathbf{a}_g) by the corresponding spatial transformation matrix (\mathbf{T}):

$$\mathbf{a}_n = \mathbf{T} \mathbf{a}_g \quad (39)$$

where

$$\mathbf{a}_n = \{A_{1n} \ A_{3n} \ A_{1n} \ A_{2n} \ A_{4n} \ A_{rn}\}^T \quad (40)$$

$$\mathbf{a}_g = \{A_{1g} \ A_{3g} \ A_{1g} \ A_{2g} \ A_{4g} \ A_{rg}\}^T \quad (41)$$

$$\mathbf{T} = \text{diag} \left(e^{k_r l}, e^{jk_r l}, e^{jk_l}, e^{-k_r l}, e^{-jk_r l}, e^{-jk_l} \right) \quad (42)$$

where diag indicates a diagonal matrix, $e^{(\cdot)}$ is the exponential function, l is the length of the

segment.

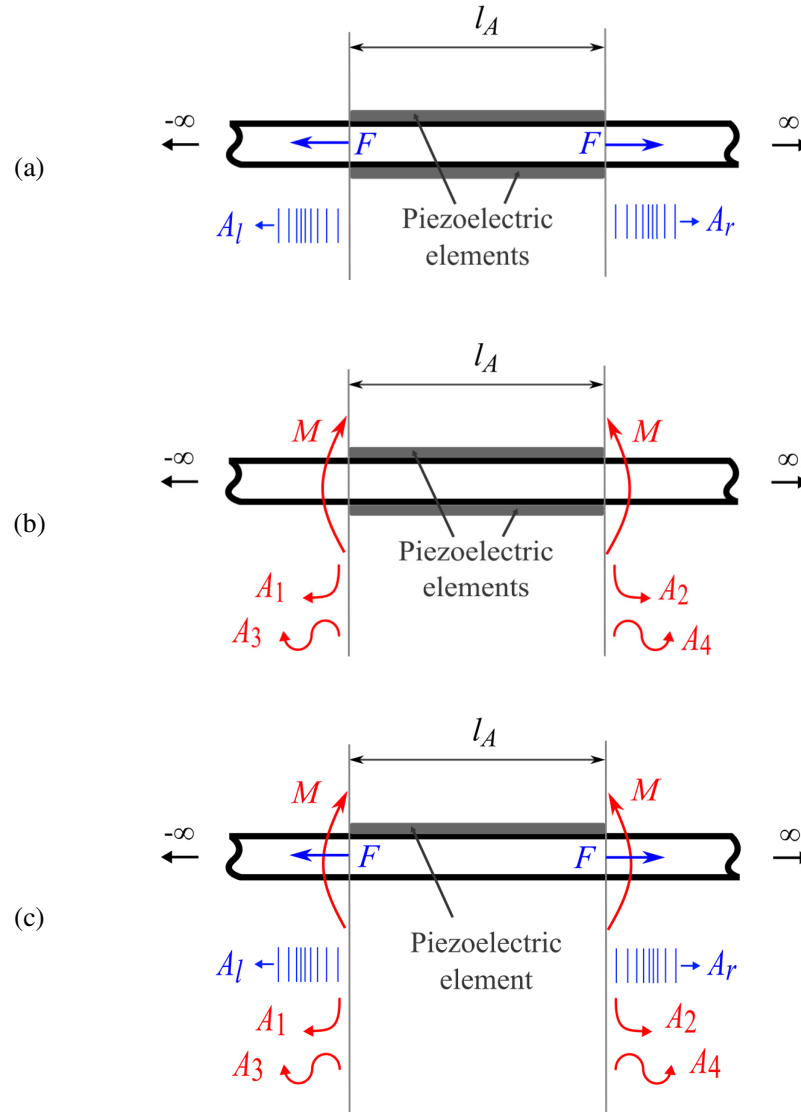
The concepts presented are employed in the next sections for each segment of beam and to model them.

3.3 Piezoelectric Actuator

Piezoelectric elements coupled in a beam can generate longitudinal and flexural waves separately or both at the same time. It depends how the electrical potentials are applied on piezoelectric patches and the poling direction of PZTs.

Longitudinal waves are generated by axial forces, Figure 13(a), and flexural waves are generated by moments, Figure 13(b). Asymmetric actuation generates a pair of forces and a pair of moments at the same time. In this case a piezoelectric element excites the structure generating both waves types, Figure 13(c).

Figure 13: Piezoelectric actuator; (a) longitudinal waves generated by a pair of forces on symmetric configuration; (b) flexural waves generated by a pair of moments on symmetric configuration and (c) longitudinal and flexural waves generated by an asymmetric actuation.



Source: Adapted from Brennan *et al.*. (1997)

3.3.1 Symmetric Actuator

As observed in Figure 13(a) and (b), a symmetric actuator consists of two piezoelectric element (piezoelectric patches fitted to opposite sides of the beam).

Longitudinal waves results from axial forces derived by in-phase potentials applied on piezoelectric elements (V_i). The waves developed are longitudinal waves travelling on the left

side (A_l) and longitudinal wave travelling on the right side (A_r) of structure.

Flexural waves result from bending moments derived after applying out-of-phase potentials on piezoelectric elements (V_o). In this case, the waves developed are the near-field wave on the left side (A_1), a near-field wave on the right side (A_2), propagating wave travelling on the left side (A_3) and propagating wave travelling on the right side (A_4).

As mentioned previously, longitudinal forces, F , and moments, M , are related to V_i and V_o , respectively, and they are given by:

$$F = \beta V_i \quad (43)$$

$$M = \alpha V_o \quad (44)$$

where β and α are constants. These coefficients are presented by Brennan *et al.* (1997) as follows:

$$\beta = \left[\frac{2E_b S_a}{6 + T(E_b / E_p)} \right] \frac{d_{31}}{t_p} \quad (45)$$

$$\alpha = \left(\frac{2E_b I_a}{t_p} \right) \left[\frac{6(1+T)}{6 + T(E_b / E_p) + 12T + 8T^2} \right] \frac{d_{31}}{t_p} \quad (46)$$

where S_a is the effective cross-sectional area of the active section (the effective area accounts for the different Young's moduli of the piezoceramic elements and the beam), E_p is the Young's modulus of the PZTs, d_{31} is the piezoelectric constant, $T = t_p / t_b$ is the thickness ratio, t_p is the PZTs thickness, t_b is the beam thickness and I_a is the effective second moment of area of the active section (the effective second moment of area accounts for the different Young's moduli of the piezoceramic elements and the beam).

Since F and M are known a simple way to obtain the amplitudes of waves generated by

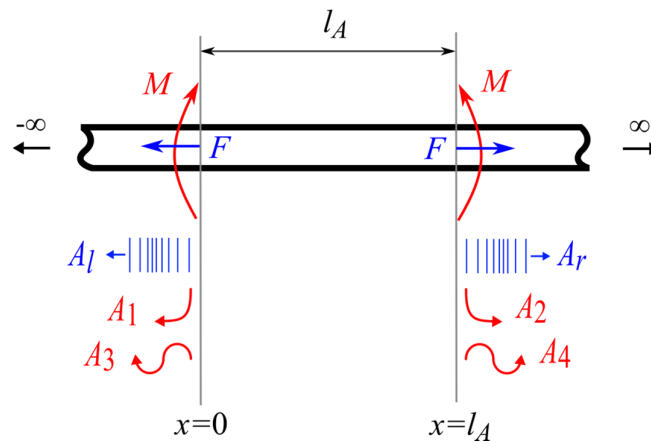
a pair of forces and a pair of moments was given by Brennan (1994) are:

$$\begin{Bmatrix} A_l \\ A_r \end{Bmatrix} = \frac{-j}{2k_f E_b S_b} \begin{bmatrix} 1 & e^{-jk_f l_A} \\ 1 & e^{jk_f l_A} \end{bmatrix} \begin{Bmatrix} -F \\ F \end{Bmatrix} \quad (47)$$

$$\begin{Bmatrix} A_1 \\ A_2 \\ A_3 \\ A_4 \end{Bmatrix} = \frac{1}{4k_f^2 E_b I_b} \begin{bmatrix} 1 & e^{-k_f l_A} \\ -1 & -e^{k_f l_A} \\ -1 & -e^{-k_f l_A} \\ 1 & e^{jk_f l_A} \end{bmatrix} \begin{Bmatrix} -M \\ M \end{Bmatrix} \quad (48)$$

where l_A is the length of actuator (of piezoelectric elements). Figure 14 presents an illustration of this model.

Figure 14: Simplified model of a piezoelectric actuator.



Source: Adapted from Brennan *et al.* (1997)

This modelling is designed simplified model of a piezoelectric actuator because it does not consider the passive effect of the actuator segments. It means that the thickness of the piezoelectric elements are neglected in the actuator model because these elements are very thin compared to the beam. It is important to highlight that the complete actuator model consider the active and passive effect of actuator and this approach is adapted here to model the discontinuities (damage).

The Eqs. (47) and (48) give the waves generated by the piezoelectric elements assuming that the thickness of piezoelectric elements are neglected. However, the complete model of actuator proposed by Brennan *et al.* (1997) is more useful when the piezo elements are thicker and the thickness and if its mechanical properties must be considered.

Working with Eqs. (43), (45) and (47) is possible to obtain the transfer function of the piezoelectric actuator for the longitudinal waves:

$$\frac{A_r}{V_i} = \frac{jS_a d_{31}(1 - e^{jk_l l_a})}{k_l S_b t_p (6 + T(E_b / E_p))} \quad (49)$$

In addition, working with Eqs. (44), (46) and (48) is possible to obtain the transfer function of the piezoelectric actuator for the flexural waves:

$$\frac{A_4}{V_o} = \frac{3d_{31}I_a(e^{jk_f l_a} - 1)(1 + T)}{k_f^2 I_p^2 I_b (6 + T(E_b / E_p) + 12T + 8T^2)} \quad (50)$$

Only the two waves (A_r and A_4) that propagate to the right side are more explored here because they interact with the damage while the near field waves (A_1 and A_2) dissipates quickly and the waves generated for the left side of the beam (A_l and A_3) propagate to infinity.

In addition, the powers transmitted by the longitudinal and flexural propagating right going waves are (BRENNAN *et al.*, 1997):

$$P_l = (1/2) E_b S_b k_l \omega |A_r|^2 \quad (51)$$

$$P_f = E_b I_b k_f^3 \omega |A_4|^2 \quad (52)$$

Figure 15 and Figure 16 present the amplitude of outgoing waves propagating to the right

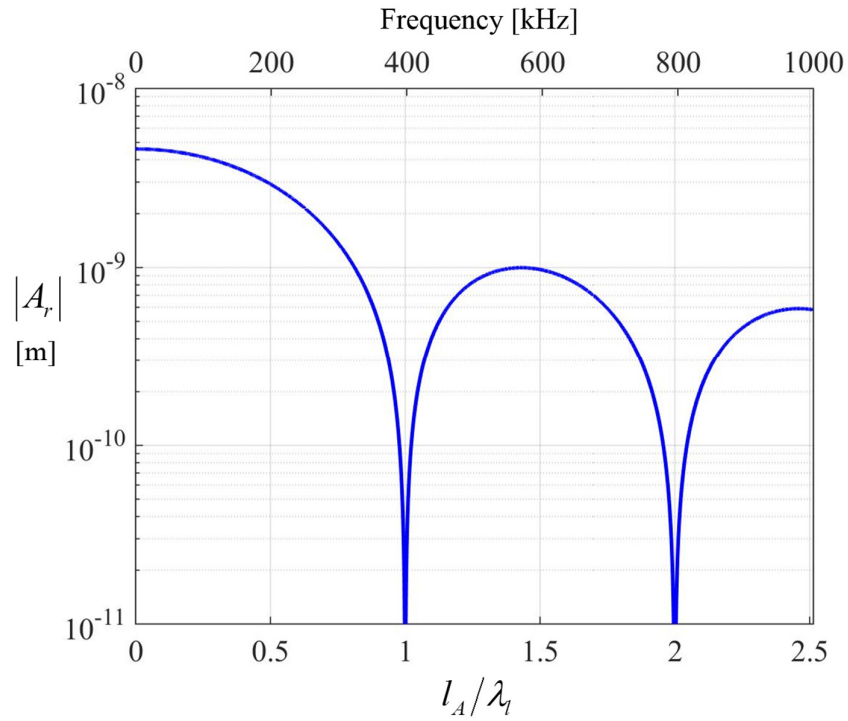
side of the infinite beam, respectively to the longitudinal and flexural types. The waves propagating to the left side are symmetric to the right side. The properties of the beam and the piezo elements are described on Table 1.

Table 1: Geometrical and material properties of infinite beam and piezoelectric elements.

Properties	PZTs	Beam
<i>Material</i>	PSI-5H4E	Al (6063-T5)
<i>Young's Modulus [N/m²]</i>	$62 \times 10^9 (Y_1^E)$	68.9×10^9
<i>Density [kg/m³]</i>	7800	2700
<i>Relative Dielectric Constant</i>	3800 (k_3^T)	--
<i>Piezoelectric Coefficient [m/V] or [C/N]</i>	$-320 \times 10^{-12} (d_{31})$	--
<i>Breadth [m]</i>	12.7×10^{-3}	12.7×10^{-3}
<i>Depth [m]</i>	2.67×10^{-4}	1.58×10^{-3}

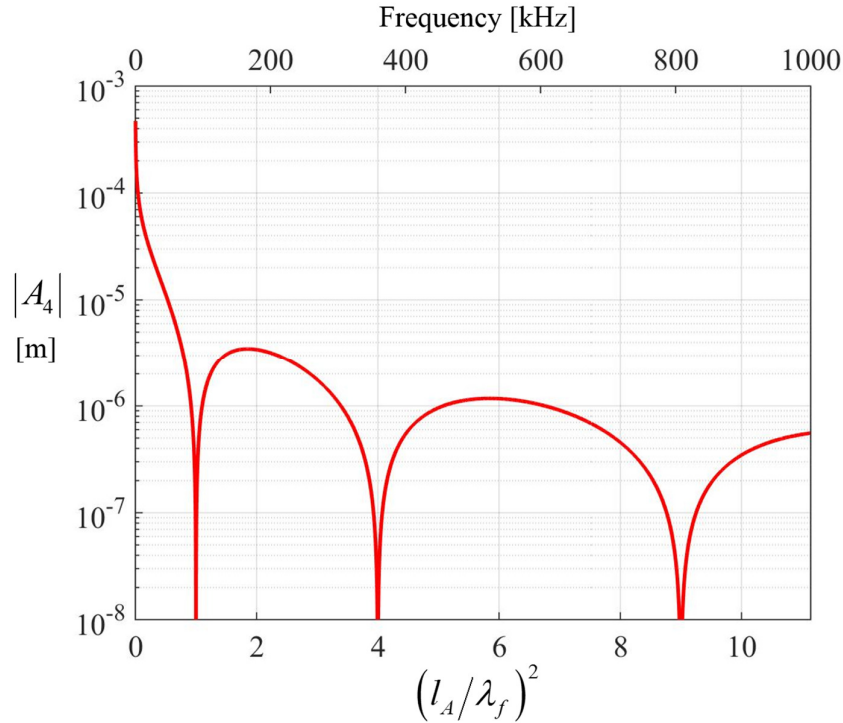
Source: Elaborated by author

Figure 15: Amplitude of longitudinal right going wave from symmetric actuator of length
 $l_A = 0.0127m$.



Source: Elaborated by author

Figure 16: Amplitude of flexural right going wave from symmetric actuator of length $l_A = 0.0127m$.



Source: Elaborated by author

Observing the behavior of waves in Figure 15 and Figure 16 is possible to note the filtering effect created by the actuator when the amplitude of waves tends to zero. This means that specifically in these frequencies the actuator is not able to excite waves on beam. These filtering effects can also be seen in time domain, as discussed in the next chapter.

Considering the longitudinal waves, to understand the filtering effects is important remember that four waves are excited by a pair of forces. It because each force causes one longitudinal wave propagating to the left and another longitudinal wave propagating to the right. The filtering effects occur due an interaction of these four waves generated by the pair of forces. A similar behavior of filtering effects occurs for flexural waves generated by the pair of moments.

These filtering effects takes place when the wavelength of each respective wave is multiple of the actuator size. They are given by this following equations:

$$\frac{l_A}{\lambda_l} = 1, 2, \dots, n \in \mathbb{N} \quad (53)$$

and

$$\frac{l_A}{\lambda_f} = 1, 2, \dots, n \in \mathbb{N} \quad (54)$$

Based on these results, for designing of SHM system is important to be careful with these frequencies. It is recommended to avoid these frequency bands because the structure is not excited appropriately.

3.3.2 Asymmetric Actuator

As presented above, an asymmetric actuator (or one-element piezoelectric actuator) generates longitudinal and flexural waves simultaneously, as illustrated by Figure 13(c).

The simplified model of the asymmetric actuator is the same presented by the symmetric actuator (see Figure 14) and the transfer functions are the same, Eqs. (49) and (50), divided by two. Similarly, Eqs. (47) and (48) can be used to obtain the first packet of waves generated by an asymmetric actuator, however the efforts (F and M) must be divided by two.

The filtering effect observed on Figure 15 and Figure 16 also occurs for asymmetric actuators and it keeps related to the actuator length, i.e., when the wavelength is multiple of actuator size, as given by Eqs. (41) and (42).

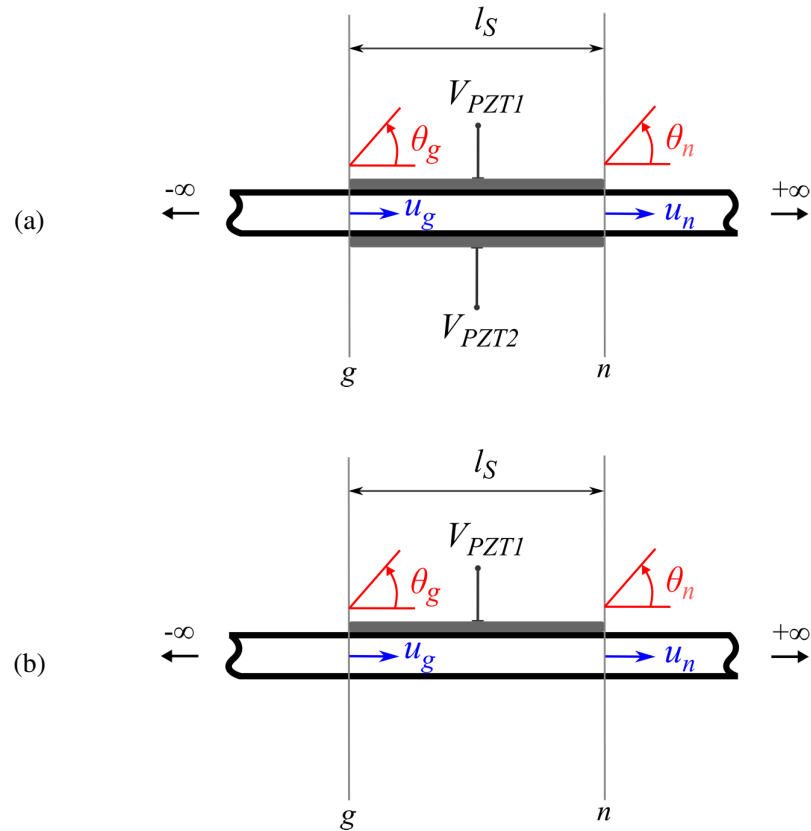
As explained for symmetric actuator these filtering effects must be considered on a design of SHM systems.

3.4 Piezoelectric Sensor

As presented by Brennan (1994) piezoelectric patches can be coupled to a beam and configured to measure strain spatially integrated over the area occupied by themselves. As introduced to the actuators, the piezoelectric sensors can be used in a symmetric or asymmetric

configuration, as shown in Figure 17.

Figure 17: Piezoelectric sensor; (a) symmetric configuration and; (b) asymmetric configuration.



Source: Adapted from Brennan *et al.* (1997)

3.4.1 Symmetric Sensor

Considering the symmetric configuration for the sensor (piezoelectric patches fitted to opposite sides of the beam) it can obtain longitudinal motion, flexural motion or both simultaneously.

The simplified model of sensor adopted here assumes that the piezoelectric elements on sensor have negligible mass and stiffness and also the strain be constant across the width of the beam and the piezoelectric elements. A longitudinal symmetric sensor has the electrical voltage given by (BRENNAN, 1994):

$$V_l = \frac{d_{31}E_p b}{C_p} (u_n - u_g) \quad (55)$$

where b is the width of piezo, C_p is the capacitance of piezo and u is the axial displacement, that for each structural point is:

$$u = A_l + A_r \quad (56)$$

and for each sensor extremity: $u_g = A_{lg} + A_{rg}$ and $u_n = A_{ln} + A_{rn}$.

The longitudinal sensor sensitivity, S_l , is the term of Eq. (55) that is multiplied by the displacement difference. It is:

$$S_l = \frac{d_{31}E_p b}{C_p} \quad (57)$$

To obtain the longitudinal sensitivity of a single element is necessary divide S_l by two.

Considering only a right going wave incite ($A_{lg} = A_{ln} = 0$) on the sensor and working with Eqs. (55), (56) and (57) is possible to find the transfer function of the symmetric sensor considering $u_n = A_{rn} = A_{rg} e^{-jk_l l_s}$:

$$\frac{V_l}{A_{rg}} = S_l (e^{-jk_l l_s} - 1) \quad (58)$$

Similarly, a flexural symmetric sensor has the electrical voltage given by (Brennan, 1994):

$$V_f = \frac{d_{31}w_p E_p b}{C_p} (\theta_n - \theta_g) \quad (59)$$

where $w_p = t_b/2 + t_p$ and θ is the slope given by:

$$\theta = k_f A_1 + jk_f A_2 - k_f A_3 - jk_f A_4 \quad (60)$$

and for each sensor extremity $\theta_g = k_f A_{1g} + jk_f A_{2g} - k_f A_{3g} - jk_f A_{4g}$ and $\theta_n = k_f A_{1n} + jk_f A_{2n} - k_f A_{3n} - jk_f A_{4n}$.

The flexural sensor sensitivity, S_f , is the term of Eq. (59) that is multiplied by the slope difference. It is:

$$S_f = \frac{d_{31} w_p E_p b}{C_p} \quad (61)$$

To obtain the flexural sensitivity of a single element is necessary divide S_f by two.

Considering only a flexural right going propagating wave incite ($A_{1g} = A_{2g} = A_{3g} = A_{1n} = A_{2n} = A_{3n} = 0$) on sensor and working with the Eqs. (59), (60) and (61) is possible to find the transfer function of the symmetric considering $A_{4n} = A_{4g} e^{-jk_f l_s}$:

$$\frac{V_f}{A_4} = -jk_f S_f (e^{-jk_f l_s} - 1) \quad (62)$$

In order to measure simultaneous the two wave types is necessary to use independent electrical connections for the piezoelectric elements that results in a sensor sensitivity of a single element (Brennan, 1994). To obtain the voltage response related to the longitudinal waves is necessary to sum the responses obtained for each single sensor:

$$V_l = V_{PZT1} + V_{PZT2} \quad (63)$$

where V_{PZT1} and V_{PZT2} are the measured electrical voltages on PZT1 and PZT2, respectively, see Figure 17(a). In other hand, to obtain the voltage response associated with the flexural motion this following equation shall be used:

$$V_f = V_{PZT1} - V_{PZT2} \quad (64)$$

As presented for the piezoelectric actuators, the filtering effects also occur for sensors and this effect still related with the length of piezoelectric elements (Eqs. (53) and (54)).

These effects must be considered on a design of a SHM system to avoid the frequencies bands where these filtering effects of sensors occurs because these frequencies bands are blind spot of sensors.

Is easy to understand these phenomena considering a harmonic wave propagating by the sensor. For wavelength multiple of the sensor length the displacement and slope in the extremities of sensor are the same. That means, the difference between then, on Eqs (43) and (47) will always be zero.

3.4.1 *Asymmetric Sensor*

Considering the asymmetric configuration for the sensor (piezoelectric patch fitted one side of the beam) it can detect longitudinal and flexural motion, simultaneously.

For longitudinal waves an asymmetric sensor has the electrical voltage given by Eqs. (55) divided by two. In analogue way for flexural waves an asymmetric sensor has the electric voltage given by Eq. (59) divided by two.

The same way, the transfer functions of symmetric sensor given by Eqs. (58) and (62) can be adapted by the asymmetric sensor just divided these equations by two.

A disadvantage to use an asymmetric sensor is due the two wave types be measured simultaneously and is not possible to separate them. However, this configuration can be useful if the group velocity allows the packet of longitudinal waves be measured separated than the packet of flexural waves.

Once again the filtering effect also occurs for asymmetric sensors as for symmetric sensors and must be considered on a design of a SHM system to avoid blind spot of sensors.

3.5 Discontinuities (damage)

In order to model the discontinuities the approach used here are based on the approach proposed by Brennan (1994) and Brennan *et al.* (1997) for actuator (complete model). However, the important part to be considered in this work is the passive effect, as used by Ayala (2015) for the symmetric damage.

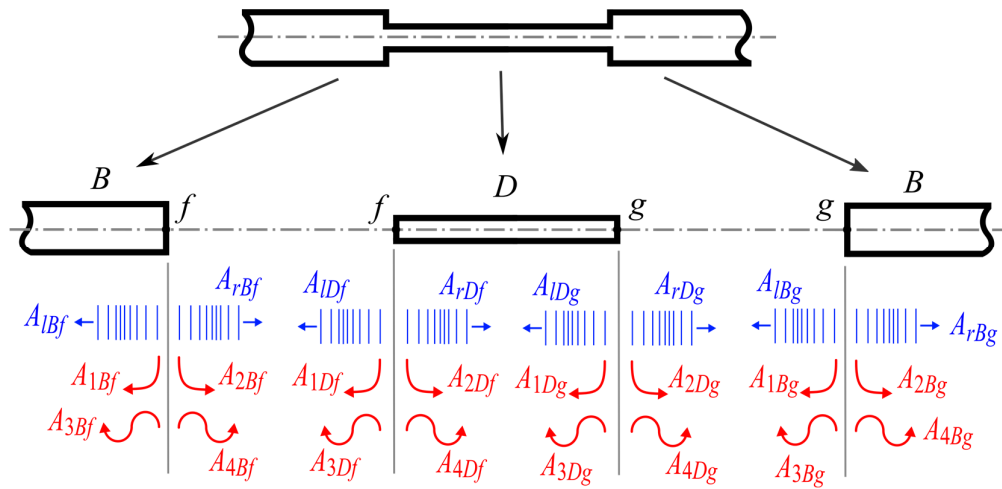
A symmetric damage occurs when the change of cross-sectional area is symmetrical to the neutral axis. To better understand the wave interaction with a symmetric damage section it is separated the damaged section in two changes of cross-sectional area. A study of waves interaction into changes of cross-sectional area (reducing and amplifying) for symmetric and asymmetric discontinuities is presented in the Appendix A.1.

3.5.1 *Symmetric Damage*

For a symmetric damage there is no scattering between longitudinal and flexural waves. In fact, the symmetric damage is as two symmetric changes of cross sectional area, reducing and amplifying in the sequence.

To model the waves behaviors in a symmetric damage is important to understand all waves presented on both area changes, see Figure 18. “B” (for beam) and “D” (for damage) call the segments and as seen before, there are six wave components at each extremity of segments.

Figure 18: Waves presented in the segments extremities of a symmetric damage.



Source: Elaborated by author

For each extremity of segments there is a state vector. By continuity, they must be the same at the same point, then:

$$\mathbf{h}_{Bf} = \mathbf{h}_{Df} \quad (65)$$

and

$$\mathbf{h}_{Bg} = \mathbf{h}_{Dg} \quad (66)$$

or

$$\mathbf{H}_B \mathbf{a}_{Bf} - \mathbf{H}_D \mathbf{a}_{Df} = \mathbf{0} \quad (67)$$

and

$$\mathbf{H}_B \mathbf{a}_{Bg} - \mathbf{H}_D \mathbf{a}_{Dg} = \mathbf{0} \quad (68)$$

where \mathbf{h}_{Bf} and \mathbf{h}_{Df} are the state vectors at extremity of beam and damage on point “ f ”, respectively. \mathbf{h}_{Bg} and \mathbf{h}_{Dg} are the state vectors at extremity of beam and damage on point “ g ”, respectively. \mathbf{H}_{Bf} and \mathbf{H}_{Df} are the transformation matrixes of beam segment and damage segment, respectively. \mathbf{a}_{Bf} and \mathbf{a}_{Df} are the vector of waves amplitudes in the extremity of beam and damage on point “ f ”. \mathbf{a}_{Bg} and \mathbf{a}_{Dg} are the vector of waves amplitudes in the extremity of beam and damage on point “ g ”, respectively. The vectors of waves amplitude are:

$$\mathbf{a}_{Bf} = \{A_{1Bf} \quad A_{3Bf} \quad A_{1Bf} \quad A_{2Bf} \quad A_{4Bf} \quad A_{rBf}\}^T \quad (69)$$

$$\mathbf{a}_{Df} = \{A_{1Df} \quad A_{3Df} \quad A_{1Df} \quad A_{2Df} \quad A_{4Df} \quad A_{rDf}\}^T \quad (70)$$

$$\mathbf{a}_{Bg} = \{A_{1Bg} \quad A_{3Bg} \quad A_{1Bg} \quad A_{2Bg} \quad A_{4Bg} \quad A_{rBg}\}^T \quad (71)$$

$$\mathbf{a}_{Dg} = \{A_{1Dg} \quad A_{3Dg} \quad A_{1Dg} \quad A_{2Dg} \quad A_{4Dg} \quad A_{rDg}\}^T \quad (72)$$

For these vectors of waves amplitude can be applied the relation of Eq. (39):

$$\mathbf{a}_{Dg} = \mathbf{T}_D \mathbf{a}_{Df} \quad (73)$$

where \mathbf{T}_D is the spatial transformation matrix of damage segment.

Considering the area discontinuity as a black box is possible to define the outgoing waves from the section change using the following equation (Brennan *et al.*, 1997):

$$\boldsymbol{\gamma} \mathbf{a}_o + \boldsymbol{\mu} \mathbf{a}_i = \mathbf{0} \quad (74)$$

where \mathbf{a}_o is the vector of outgoing waves amplitudes (reflected and transmitted), the \mathbf{a}_i is the vector of ingoing wave amplitudes (incidents), given by:

$$\mathbf{a}_o = \{A_{1B} \quad A_{3B} \quad A_{tB} \quad A_{2B} \quad A_{4B} \quad A_{rB}\}^T \quad (75)$$

$$\mathbf{a}_i = \{A_{1B} \quad A_{3B} \quad A_{tB} \quad A_{2B} \quad A_{4B} \quad A_{rB}\}^T \quad (76)$$

This way, is possible to find the outgoing waves, given by:

$$\mathbf{a}_o = -\gamma^{-1} \boldsymbol{\mu} \mathbf{a}_i \quad (77)$$

Considering the outgoing waves, \mathbf{a}_o , the waves going to left side are called reflected waves and the waves going to the right side are called transmitted waves. Similarly, to the presented notation it can be used:

$$\mathbf{a}_o = \mathbf{a}_o^- + \mathbf{a}_o^+ \quad (78)$$

where the superscript ()⁻ indicates the waves travels to the left side of structure and ()⁺ represents the waves going to the right side. Alternatively, it is possible to use the following notation:

$$\mathbf{a}_o^- = \mathbf{a}_{Ref} = \{A_{1B} \quad A_{3B} \quad A_{tB} \quad 0 \quad 0 \quad 0\}^T \quad (79)$$

$$\mathbf{a}_o^+ = \mathbf{a}_{Trans} = \{0 \quad 0 \quad 0 \quad A_{2B} \quad A_{4B} \quad A_{rB}\}^T \quad (80)$$

where \mathbf{a}_{Ref} is the vector of reflected waves and \mathbf{a}_{Trans} the vector of transmitted waves by the damage section.

Working with the Eqs. (67) and (68) to isolate the vector of waves amplitudes in the damage (\mathbf{a}_{Df} and \mathbf{a}_{Dg}). Substituting these vectors in Eq. (73) and multiplying by \mathbf{H}_D , after some rearranging is possible to write:

$$\mathbf{H}_B \mathbf{a}_{Bg} - \mathbf{H}_D \mathbf{T}_D \mathbf{H}_D^{-1} \mathbf{H}_B \mathbf{a}_{Bf} = \boldsymbol{\gamma} \mathbf{a}_o + \boldsymbol{\mu} \mathbf{a}_i \quad (81)$$

So, the matrices $\boldsymbol{\gamma}$ and $\boldsymbol{\mu}$ are given by:

$$\begin{aligned} \boldsymbol{\gamma} &= [\gamma_1 \quad \gamma_2 \quad \gamma_3 \quad \gamma_4 \quad \gamma_5 \quad \gamma_6] \\ \gamma_i &= (-\mathbf{H}_D \mathbf{T}_D \mathbf{H}_D^{-1} \mathbf{H}_B)_i \quad i = 1, 2, 3 \\ \gamma_i &= (\mathbf{H}_B)_i \quad i = 4, 5, 6 \end{aligned} \quad (82)$$

$$\begin{aligned} \boldsymbol{\mu} &= [\mu_1 \quad \mu_2 \quad \mu_3 \quad \mu_4 \quad \mu_5 \quad \mu_6] \\ \mu_i &= (\mathbf{H}_B)_i \quad i = 1, 2, 3 \\ \mu_i &= (-\mathbf{H}_D \mathbf{T}_D \mathbf{H}_D^{-1} \mathbf{H}_B)_i \quad i = 4, 5, 6 \end{aligned} \quad (83)$$

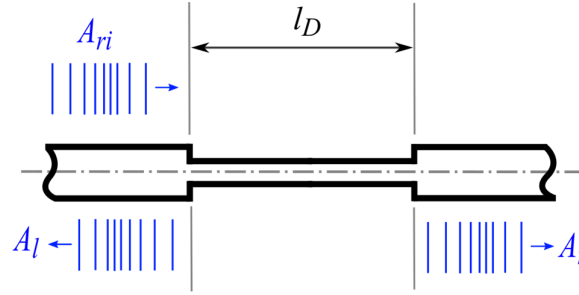
where $()_{1-6}$ denotes the columns of the respective matrices.

The formulation presented in this section could be divided in equations related to longitudinal waves (2x2 matrix order) and flexural waves (4x4 matrix order). It because they are not coupled by each other for the physical problem.

3.5.1.1 Longitudinal Incident Wave

Once a longitudinal wave affects a symmetric damage it scatter into longitudinal waves reflected and transmitted, as Figure 19, the nomenclature of waves A_{iB} and A_{rB} is simplified by A_i and A_r .

Figure 19: Scattering waves by a symmetric damage for an incident longitudinal wave.



Source: Elaborated by author

From the present approach and for the particular case of a longitudinal right going wave impinging in the cross-sectional area change is possible to write the following transfer functions:

$$\frac{A_l}{A_{ri}} = \frac{A_{lBf}}{A_{rBf}} = -\frac{(S_D^2 - S_B^2)e^{jk_l l_D} + (S_B^2 - S_D^2)e^{-jk_l l_D}}{(S_B + S_D)^2 e^{jk_l l_D} - (S_B - S_D)^2 e^{-jk_l l_D}} \quad (84)$$

$$\frac{A_r}{A_{ri}} = \frac{A_{rBg}}{A_{rBf}} = -\frac{(S_B - S_D)^2 - (S_B + S_D)^2}{(S_B + S_D)^2 e^{jk_l l_D} - (S_B - S_D)^2 e^{-jk_l l_D}} \quad (85)$$

Defining r as the cross-sectional area ratio $r = S_D/S_B$, the Eqs. (84) and (85) can be rewritten as:

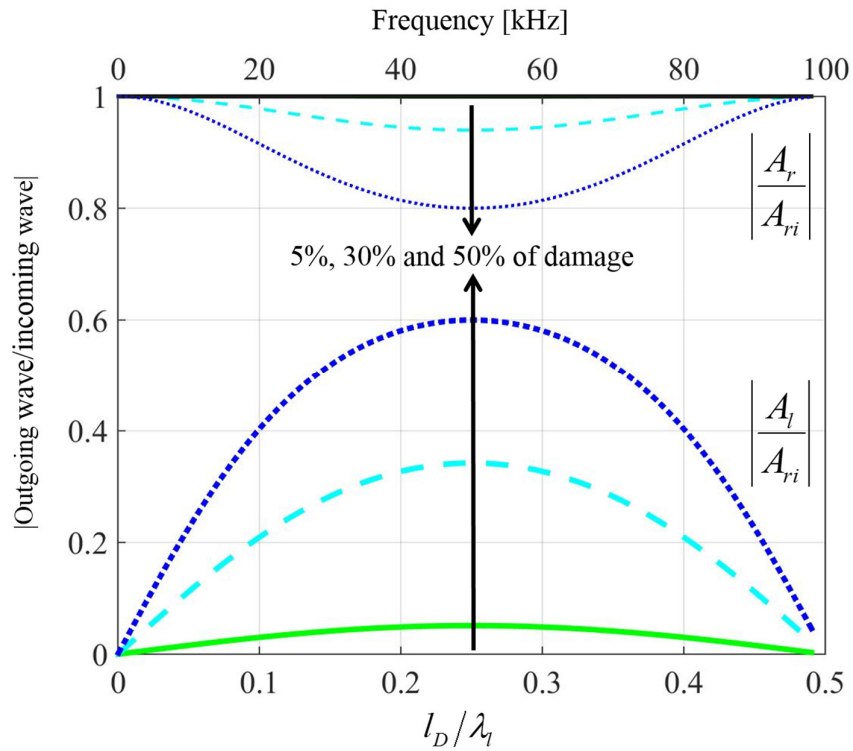
$$\frac{A_l}{A_{ri}} = \frac{A_{lBf}}{A_{rBf}} = -\frac{(r^2 - 1)e^{jk_l l_D} + (1 - r^2)e^{-jk_l l_D}}{(1 + r)^2 e^{jk_l l_D} - (1 - r)^2 e^{-jk_l l_D}} \quad (86)$$

$$\frac{A_r}{A_{ri}} = \frac{A_{rBg}}{A_{rBf}} = -\frac{(1 - r)^2 - (1 + r)^2}{(1 + r)^2 e^{jk_l l_D} - (1 - r)^2 e^{-jk_l l_D}} \quad (87)$$

Considering the parameters in Table 1 to simulate the wave interaction of an incident longitudinal wave with the symmetric damage ($l_D = 0.025m$).

Figure 20 shows the amplitude of reflected and transmitted longitudinal waves varying with the damage depth (5, 30 and 50% of thickness reduction).

Figure 20: Relation of scattering waves in a symmetric damage with $l_D = 0.025m$ and a longitudinal incident wave.



As can be noted in the figure above the reflected longitudinal waves are maximum when:

$$\left. \frac{l_D}{\lambda_l} \right|_{\max} = \frac{1+2n}{4}, n \in \mathbb{N} \quad (88)$$

and minimum when:

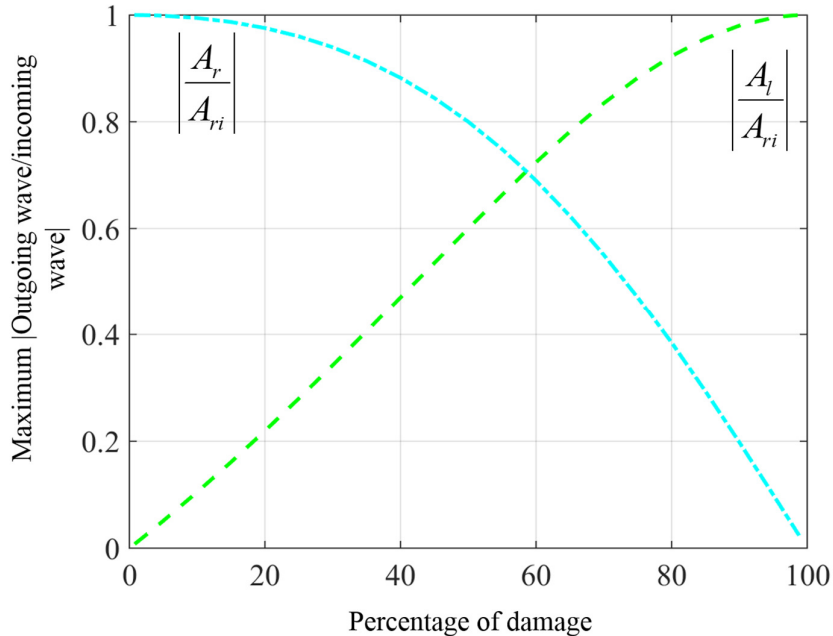
$$\left. \frac{l_D}{\lambda_l} \right|_{\min} = \frac{1+n}{2}, n \in \mathbb{N} \quad (89)$$

where l_D is the length of damage segment and λ_l the longitudinal wavelength.

Is possible to note that reflected and transmitted waves have opposite behavior, it means, when the amplitude of reflected waves are maximum the amplitudes of transmitted waves are minimum, and vice versa.

Considering the behavior presented in Figure 20, to detect and quantify a damage the best frequencies to be chosen for a longitudinal wave incident can be computed from Eq.(88). In addition, the best SHM configuration is the pulse echo (it means, using the reflected waves). It because they are more sensitivity of damage (60% of variation for a damage of 50%) than transmitted waves that present smaller variations of wave amplitudes in the presence of damage (20% of variation for a damage of 50%). It became clearer in Figure 21 where the maximum value of waves relation (outgoing by incoming) is presented in terms of the damage depth.

Figure 21: Maximum of wave amplitude ratios (reflected and transmitted) for different damage depth considering incident longitudinal wave and $l_D = 0.025m$.



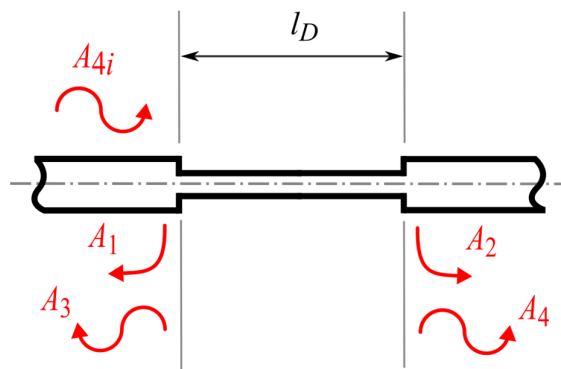
Source: Elaborated by author

It is clear to note the higher sensitivity of reflected waves than transmitted waves for damage severity below 60%.

3.5.1.2 Flexural Incident Wave

Flexural wave incident results in near-field and propagation waves (reflected and transmitted), as Figure 22, the nomenclature of waves A_{1B} , A_{2B} , A_{3B} and A_{4B} is simplified by A_1 , A_2 , A_3 and A_4 .

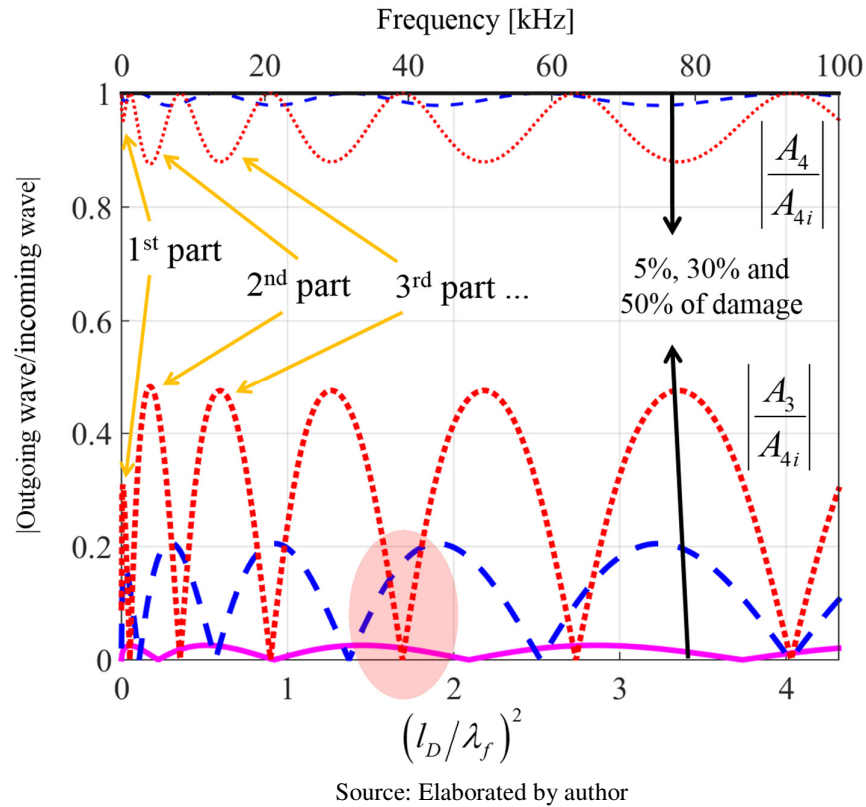
Figure 22: Scattering waves by a symmetric damage for an incident flexural propagating wave.



Source: Elaborated by author

Considering an incident flexural wave, Figure 23 shows the amplitude of reflected and transmitted flexural waves by the symmetric damage ($l_D = 0.025m$) also varying the damage depth (5, 30 and 50% of thickness reduction). The square of $(l_D/\lambda_f)^2$ is plotted to obtain a linear relationship with frequency (third axis)

Figure 23: Relation of scattering waves in a symmetric damage with $l_D = 0.025m$ and an incident flexural propagating wave.

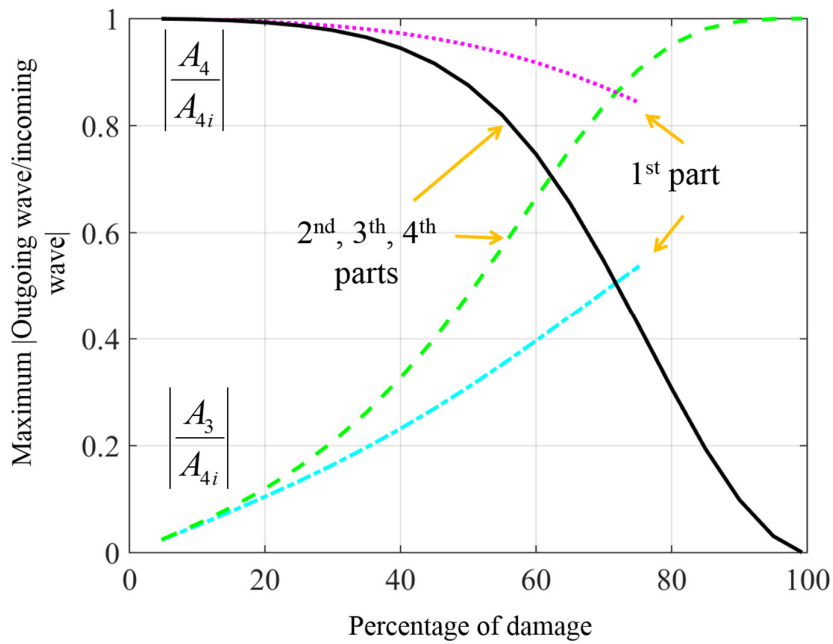


As for longitudinal waves, for flexural waves the reflected waves showed up more sensitivity to detect the damage. Nevertheless, for flexural propagation waves is more complicated to choose the best frequencies of incident wave. It because the maximum and minimum amplitude of these waves change in frequency domain depending on the damage intensity and there are many filtering effect ranges. In this case, to detect and quantify a damage in a precise way is necessary to consider these behaviors. Looking for the highlighted region by the red circle: the same frequency range that looks good to detect damage of 5% and 30% could be complicated to detect and quantify the damage of 50%. The same occurs for the flexural transmitted waves.

Comparing Figure 20 and Figure 23 is possible to see that is more complicated to use flexural waves for detect symmetric damage than longitudinal waves. To help understand the behavior of flexural waves the curve is divided in parts as showed in the Figure 23 (each part corresponds the behavior between consecutives filtering effects for any damage severity).

Figure 24 shows the maximum waves amplitude ratio by the damage severity.

Figure 24: Maximum of wave amplitude ratios (reflected and transmitted) for different damage depth considering incident flexural wave and $l_D = 0.025m$.



Source: Elaborated by author

As can be observed by Figure 24 the first part does not exist if the damage depth is high enough (higher than approximately 75%). It means that damage thickness is so thin that large wavelengths (which correspond to the first part) do not propagate. This behavior affects the wavelengths until the first filtering effect, as shown through the maximum amplitudes of transmitted and reflected flexural waves.

For flexural waves, it can be seen that the maximum reflected amplitude occurs for different values of l_D/λ_f , which varies when the damage increases. This is because, in contrast to the longitudinal wave, λ_f depends on the geometry of the cross-section in the damage. Working with the flexural wavelength of the damage is possible to find estimated functions for the maximum reflected wave amplitude:

$$\text{First part: } \frac{l_D}{\lambda_{fD}} = \frac{1}{4} - \frac{t_B - t_D}{4} \quad (90)$$

$$\text{Other parts: } \frac{l_D}{\lambda_{fD}} = \frac{1 + 2(i_p - 1)}{4} - \frac{t_B - t_D}{3}, \quad i_p = 2, 3, 4, \dots, \text{ and others} \quad (91)$$

where λ_{fD} is the flexural wavelength of the damage segment.

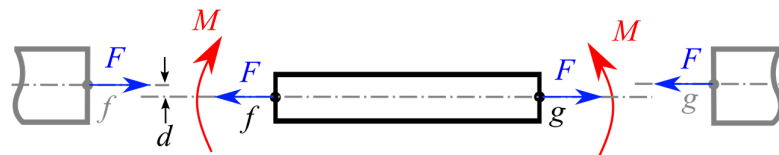
These expressions could be used to find the best frequency ranges to excite using flexural wave incident.

3.5.2 Asymmetric damage

As for the asymmetric changes, when the cross-section area of a damage is asymmetric with respect to the neutral axis of the beam there is scattering between longitudinal and flexural waves. It means that occurs mode conversion between longitudinal and flexural waves.

In order to modeling the asymmetric damage section is important to understand that the coupling between the longitudinal and flexural waves motion occurs by a moment due to the distance between the neutral axis of damaged section and adjacent beam sections, as illustrated in Figure 25.

Figure 25: Efforts on junctions of asymmetric damage section with adjacent beams.



Source: Adapted from Brennan (1997)

Considering this moment, the state vector on the junctions has to be modified to account for this:

$$\mathbf{h}_{\hat{D}f} = \mathbf{h}_{Df} + \mathbf{T}_{Asym} \mathbf{h}_{Df} \quad (92)$$

and

$$\mathbf{h}_{\hat{D}g} = \mathbf{h}_{Dg} + \mathbf{T}_{Asym} \mathbf{h}_{Dg} \quad (93)$$

where $\mathbf{h}_{\hat{D}f}$ and $\mathbf{h}_{\hat{D}g}$ are the state vectors of asymmetric damage at points “f” and “g”, respectively. \mathbf{h}_{Df} and \mathbf{h}_{Dg} are the state vectors of symmetric damage at points “f” and “g”, respectively. \mathbf{T}_{Asym} was given by (Brennan *et al.*, 1997)

$$\mathbf{T}_{Asym} = \begin{bmatrix} 0 & 0 & d & 0 & 0 & 0 \\ 0 & 0 & 0 & 0 & 0 & 0 \\ 0 & 0 & 0 & 0 & 0 & 0 \\ 0 & 0 & 0 & 0 & 0 & -d \\ 0 & 0 & 0 & 0 & 0 & 0 \\ 0 & 0 & 0 & 0 & 0 & 0 \end{bmatrix} \quad (94)$$

where $d = (t_B - t_D)/2$ is the distance between the neutral axes of each both segments.

The transformation matrix of asymmetric segment of damage is

$$\mathbf{H}_{\hat{D}} = (\mathbf{I} + \mathbf{T}_{Asym}) \mathbf{H}_D \quad (95)$$

Made these considerations the steps for the modelling of the asymmetric damage are the same presented to the symmetric damage (Section 3.3.2). And the matrices $\boldsymbol{\gamma}$ and $\boldsymbol{\mu}$ for this case are given by:

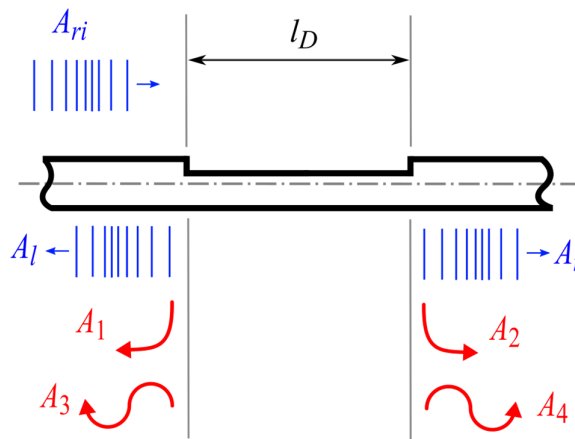
$$\begin{aligned} \boldsymbol{\gamma} &= [\gamma_1 \quad \gamma_2 \quad \gamma_3 \quad \gamma_4 \quad \gamma_5 \quad \gamma_6] \\ \gamma_i &= (-\mathbf{H}_{\hat{D}} \mathbf{T}_D \mathbf{H}_{\hat{D}}^{-1} \mathbf{H}_B)_i \quad i = 1, 2, 3 \\ \gamma_i &= (\mathbf{H}_B)_i \quad i = 4, 5, 6 \end{aligned} \quad (96)$$

$$\begin{aligned}
\boldsymbol{\mu} &= [\boldsymbol{\mu}_1 \quad \boldsymbol{\mu}_2 \quad \boldsymbol{\mu}_3 \quad \boldsymbol{\mu}_4 \quad \boldsymbol{\mu}_5 \quad \boldsymbol{\mu}_6] \\
\boldsymbol{\mu}_i &= (\mathbf{H}_B)_i \quad i = 1, 2, 3 \\
\boldsymbol{\mu}_i &= (-\mathbf{H}_D \mathbf{T}_D \mathbf{H}_D^{-1} \mathbf{H}_B)_i \quad i = 4, 5, 6
\end{aligned} \tag{97}$$

3.5.2.1 Longitudinal Incident Wave

Once a longitudinal wave affects an asymmetric damage it scatters in longitudinal waves reflected and transmitted and flexural waves reflected and transmitted, as Figure 26, the nomenclature of waves A_{lB} , A_{rB} , A_{lB} , A_{2B} , A_{3B} and A_{4B} is simplified by A_l , A_r , A_1 , A_2 , A_3 and A_4 .

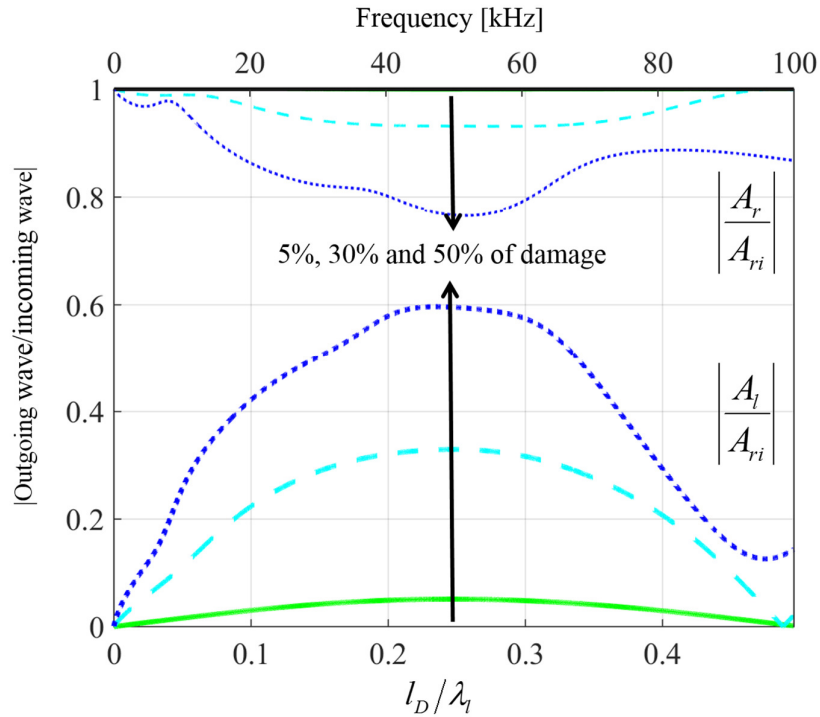
Figure 26: Scattering waves by an asymmetric damage for an incident longitudinal wave.



Source: Elaborated by author

Considering the parameters in Table 1 to simulate the wave interaction of an incident longitudinal wave with the asymmetric damage ($l_D = 0.025m$), Figure 27 shows the amplitude of reflected and transmitted longitudinal waves varying with the damage depth (5, 30 and 50% of thickness reduction).

Figure 27: Relation of longitudinal scattering waves in an asymmetric damage with $l_D = 0.025m$ and a longitudinal incident wave.

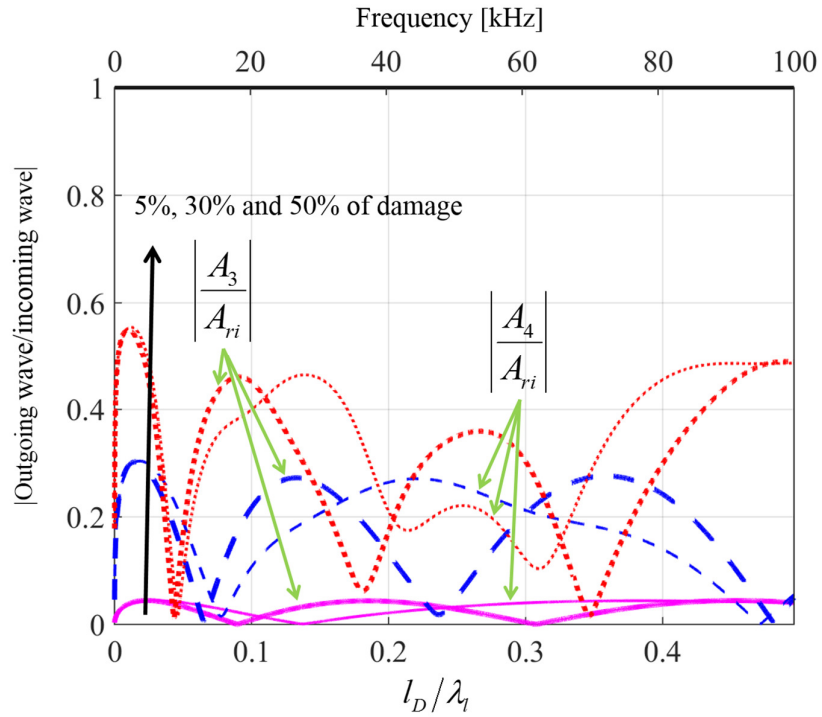


Source: Elaborated by author

The behavior observed in figure above is close to the observed in Figure 20. It means that working only with longitudinal waves (excited and sensed) to detect and/or quantify an asymmetric damage the best frequencies to be chose can be found from Eq. (88) and the pulse echo configuration (using the reflected waves) still to be the best configuration also for asymmetric damage.

Figure 28 presents the flexural waves reflected and transmitted on frequency and non-dimensional length (normalized by λ_l). As presented by this figure the flexural scattering waves by the asymmetric damage are more complicated to understand than the longitudinal scattering waves. At this case, the reflected and transmitted waves showed almost the same levels for each damage severity. However, with different optimum range

Figure 28: Relation of flexural scattering waves in an asymmetric damage with $l_D = 0.025m$ and a longitudinal incident wave.

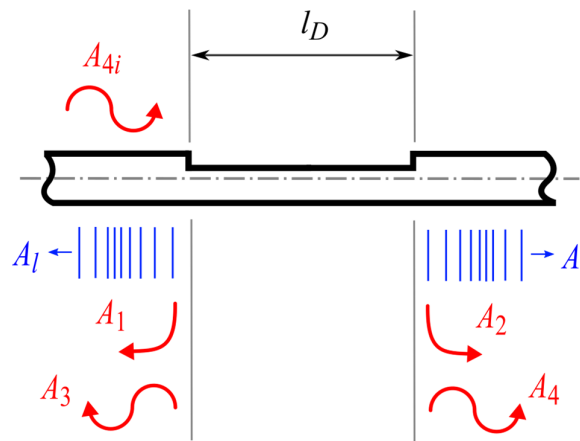


Source: Elaborated by author

3.5.2.2 Flexural Incident Wave

Considering a flexural wave (A_{4i}) reaching the asymmetric damage it scatters in longitudinal waves reflected and transmitted and flexural waves reflected and transmitted, as Figure 29, the nomenclature of waves A_{lB} , A_{rB} , A_{lB} , A_{2B} , A_{3B} and A_{4B} is simplified by A_l , A_r , A_1 , A_2 , A_3 and A_4 .

Figure 29: Scattering waves by an asymmetric damage for an incident flexural propagating wave.

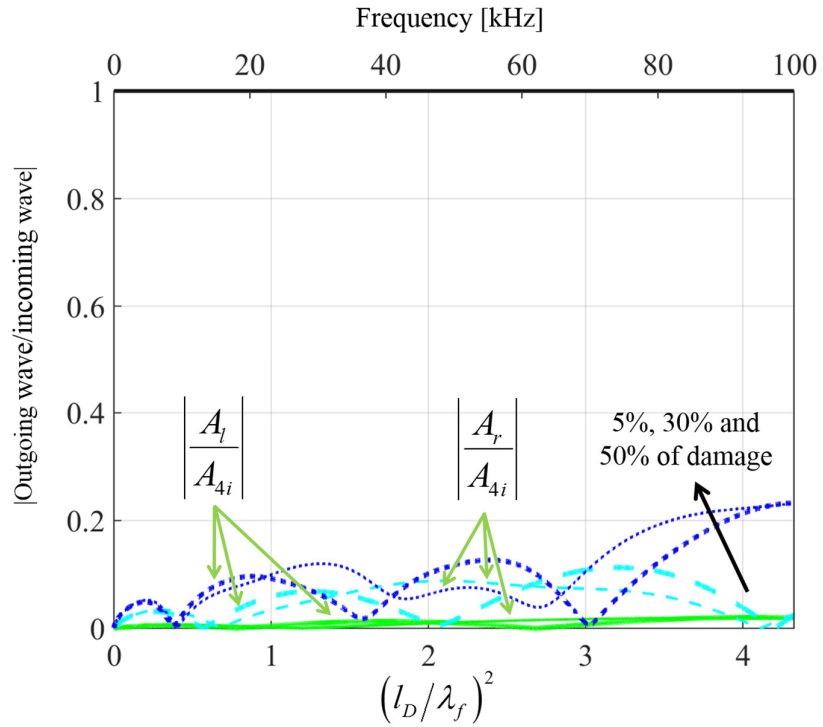


Source: Elaborated by author

Figure 30 shows the amplitude of reflected and transmitted longitudinal waves varying with the damage depth (5, 30 and 50% of thickness reduction). It is possible to note the low levels of longitudinal reflected and transmitted waves. It is possible to conclude that for a flexural incident wave in an asymmetric damage the longitudinal scattered waves are very small.

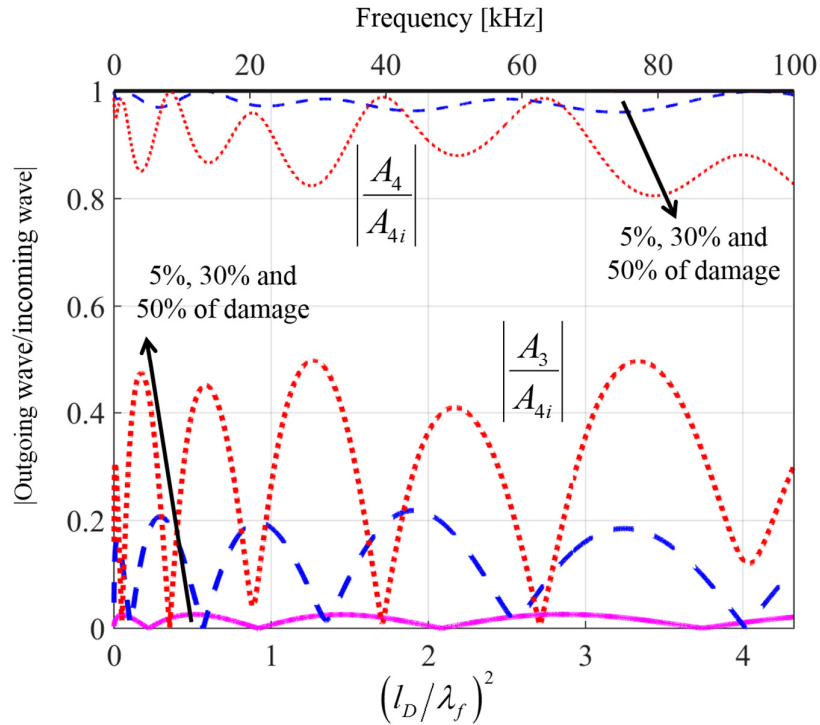
Figure 31 shows the amplitude of reflected and transmitted flexural propagating waves also varying with the damage depth. The behavior observed in this figure is close to the observed in Figure 23. It means that working only with flexural waves (excited and sensed) to detect and/or quantify an asymmetric damage the best frequencies to be chose are given by Eqs. (90) and (91). Also, the pulse echo configuration (using the reflected waves) still to be the best configuration also for asymmetric damage.

Figure 30: Relation of longitudinal scattering waves in asymmetric damage ($l_D = 0.025m$ and 50% de thickness reduction) and incident flexural wave.



Source: Elaborated by author

Figure 31: Relation of flexural scattering waves in asymmetric damage ($l_D = 0.025m$ and 50% de thickness reduction) and incident flexural wave.



Source: Elaborated by author

3.6 Conclusions

This Chapter presents the approach used in this work to obtain the wave motion in an Euler-Bernoulli beam with piezoelectric elements coupled on it and working as actuators and sensors. The models of each segment of the structures studied in this work were discussed and the wave amplitudes were presented for each condition to improve the comprehension. As shown in this text, the lengths of actuators, sensors and damage segments need to be set properly to avoid filtering effects of these elements. In practice, in the design of SHM system must to define each damage length that needs to be detect.

Symmetric damage was evaluated in this Chapter and simple transfer functions were proposed to compute the reflected and transmitted longitudinal wave amplitudes. Also, it was shown that the sensitivity of reflected longitudinal wave is higher than transmitted longitudinal one. It because the reflected wave changes more substantially if the damage depth increases, in comparison with the transmitted longitudinal wave.

The interactions of flexural waves with symmetric damage were also presented herein. It is possible to define scalar transfer functions, as done to the longitudinal wave. However, the mathematical expressions are very long and because of this only the matrix form is shown. To these waves was verified a behavior of parts for the waves amplitudes (reflected and transmitted) over frequency, similar to the case of longitudinal waves. However, for flexural ones the first part, which occurs in much lower frequency than for longitudinal waves, exhibits a maximum amplitude smaller than the other ones. In addition, while the parts keep in same frequencies for the longitudinal waves, they move to the low frequency when the damage depth increases. In practice, the maximum amplitude of flexural waves occurs in different frequencies for each damage depth.

The Chapter also discusses the longitudinal and flexural separately inciting in asymmetric damage. The main different in comparison with the symmetric damage is the coupling effect between the wave modes, whereby a longitudinal incidents waves scatter into longitudinal and flexural waves after interaction with the asymmetry, the same for flexural incident wave. However, was clear to note the resemblance between the scattered waves from symmetric and asymmetric. It means, for a longitudinal incident wave in the asymmetric damage the behavior of scattered longitudinal waves are close the behavior observed for the same wave impinge a symmetric damage. The same was observed for the interaction of flexural waves with an asymmetric damage. It was demonstrated that the general influence of the asymmetry is to introduce soft deformations on the shape of the curves for the symmetric damage. Then, the optimum frequencies (maximum amplitudes of reflected waves) defined by the symmetric damage can be used to monitor asymmetric damage.

In this sense, this Chapter introduces equations based on the damage length and wavelengths that allows to determine best frequencies ranges in the design a SHM system.

The waves behaviors discussed here in frequency domain is converted to time domain in the next chapters and supports the comprehension of them.

4 CASE STUDIES

4.1 Introduction

SHM systems usually use burst signals to generate the waves in the structure. It is a sine signal with a certain number of cycles windowed to obtain the burst in time domain. This input signal avoid abrupt excitation because the windowing and is able to excite a frequency range around the main frequency chose for the sine signal. This frequency range are bigger as the number of cycles decrease.

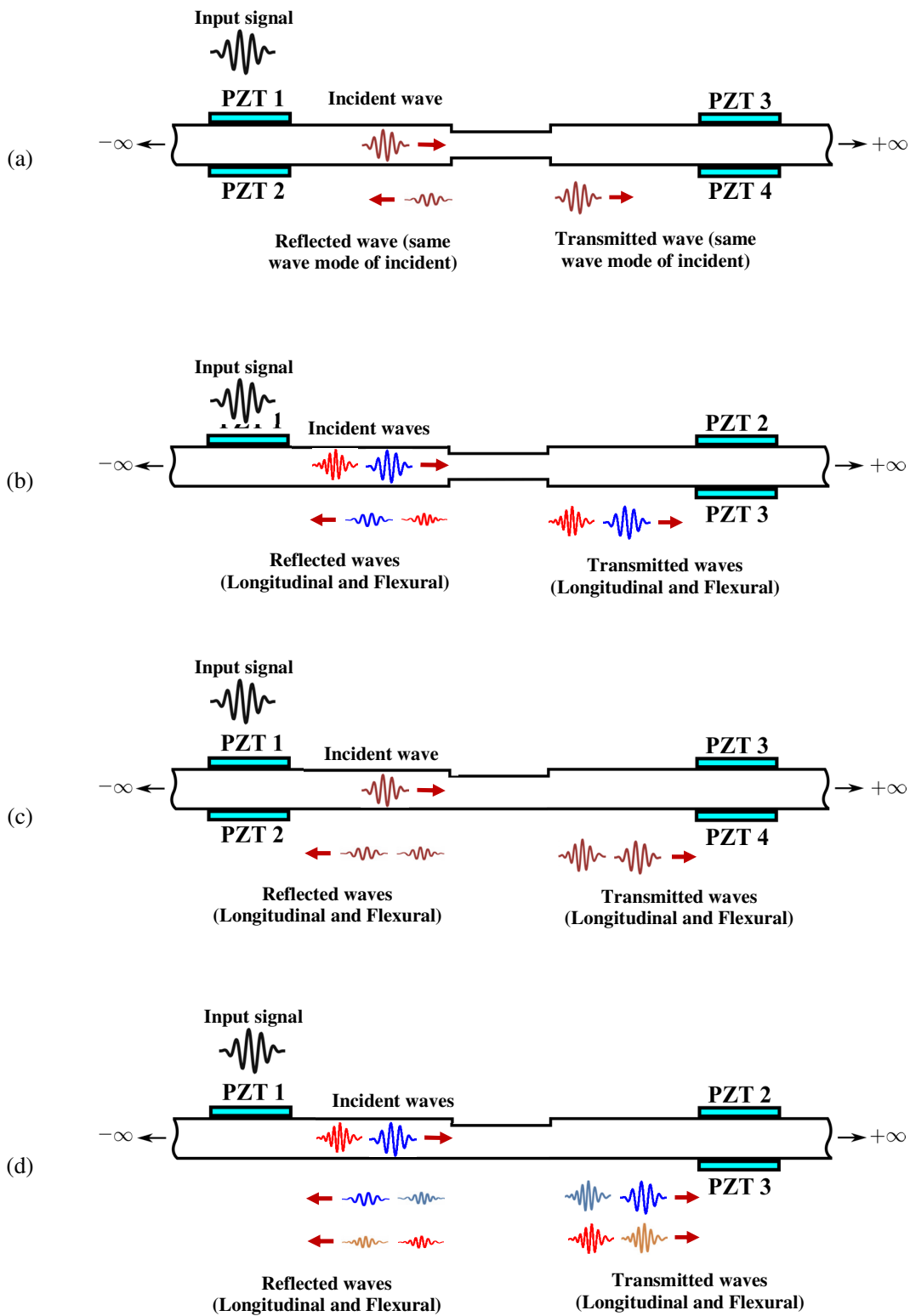
In order to understand the wave interaction with the damage in time domain generated by a burst signal and be able to sprit out the longitudinal and flexural wave packets, this Chapter presents sequential studies to discuss the main physical phenomena separated.

The aims of this chapter are present and analyze the behaviors of four study cases in order to discuss SHM strategies to detect and quantify damage. The models of segments (elements) studied in the Chapter are sequentially connected to define the complete model for the system monitored (study cases). They are:

- Case 1: symmetric actuator and symmetric damage, Figure 32 (a);
- Case 2: asymmetric actuator and symmetric damage, Figure 32 (b);
- Case 3: symmetric actuator and asymmetric damage, Figure 32 (c);
- Case 4: asymmetric actuator and asymmetric damage, see Figure 32 (d).

Figure 32 presents an illustration of the study cases considering the wave generated by the input burst signal applied in the actuator. These waves travel into the beam and impinges the damage. The scatter waves propagates and are measured by the sensors. The figure summarize the wave interaction with the damage for each case.

Figure 32: Waves behaviors for; (a) Case 1; (b) Case 2; (c) Case 3 and (d) Case 4.



Source: Elaborated by author

Figure 32 also illustrates two configurations usually used for detecting damage. In the pulse echo configuration when piezoelectric elements PZT1 and PZT2 are used as both actuator and sensor to detect the reflected waves from the damage. In the pitch-catch configuration the piezoelectric elements PZT1 and PZT2 are used as the actuator and PZT3 and PZT4 are used as sensor to detect the waves transmitted past the damage. These both SHM configuration are compared for all the cases studied in this Chapter.

4.2 Overall Aspects of Simulations

To obtain the results the models are defined in frequency domain (as presented in the Chapter 3). The electrical voltage applied in the actuator is transformed to frequency domain to be used for computing voltages measured by the sensor(s). These responses are obtained in the frequency domain and converted to time domain.

The beam and piezoelectric elements properties are presented in Table 1 (Chapter 3) and the lengths adopted to these analyses presented herein can be seen in Table 2.

Table 2: Lengths of each beam segment

Segments	Symbol	Length [mm]
<i>Actuator</i>	l_A	12.7
<i>Between actuator (or sensors) and damage</i>	l	387.5
<i>Damage</i>	l_D	25
<i>Sensors</i>	l_S	12.7

Source: Elaborated by author

For the analyses presented here a five cycles burst signal is used to generate the wave packet and different damage depths (severities of damage) are considered (5%, 30% and 50% of thickness reduction).

Figure 33 shows the five cycles burst signals applied on the piezoelectric actuator, in time (a) and frequency (b) domains. It is considered a sine-type electrical voltage with 15V of peak windowed to get the burst for a signal generated in time domain. Its representation in frequency domain is computed by using the FFT algorithm. Without loss of generality, this figure introduces then example for main frequencies of 10 and 50k Hz.

As mentioned to obtain the electrical voltage in the sensors is used an input signal in the frequency domain, (b). This signal are used as input in the complete models of the systems. The curves showed in the Chapter 3 focusing in the behavior related with the damage are present herein again for symmetric damage (Figure 34), asymmetric damage with longitudinal incident (Figure 35) and asymmetric damage with flexural incident (Figure 36). The highlighted boxes at these figure represents the frequency range excited by the burst of 10kHz (blue color) and 50kHz (red color).

Using longitudinal incident waves, the optimum frequency range to detect the damage is around 50kHz for all damage severity of symmetric, Figure 34(a), and asymmetric, Figure 35(a), configurations. However, for asymmetric configuration considering flexural incident wave, Figure 36(a), the respective frequency range is not the optimum for every scattering wave but still be a good frequency range

Working with flexural waves the main frequency of 10kHz for the burst input was chosen to avoid filtering effects of the symmetric damage, Figure 34(b), and asymmetric damage, Figure 35(b) and Figure 36(b). As can be observed at these figures, is not easy chose a frequency range for flexural waves because there are many optimum frequency ranges to detect the damage and several no good frequency range (filtering effects) in function of damage depth, as show Figure 34(b).

In order to discuss SHM strategies the next sections compare baselines with curves of damage (5, 30 and 50%) obtained by the pitch-catch and the pulse-echo SHM configurations.

Figure 33: Input burst signals for main frequency of 10kHz (blue solid line) and 50kHz (red dot-dot line): (a) time domain; (b) frequency domain.

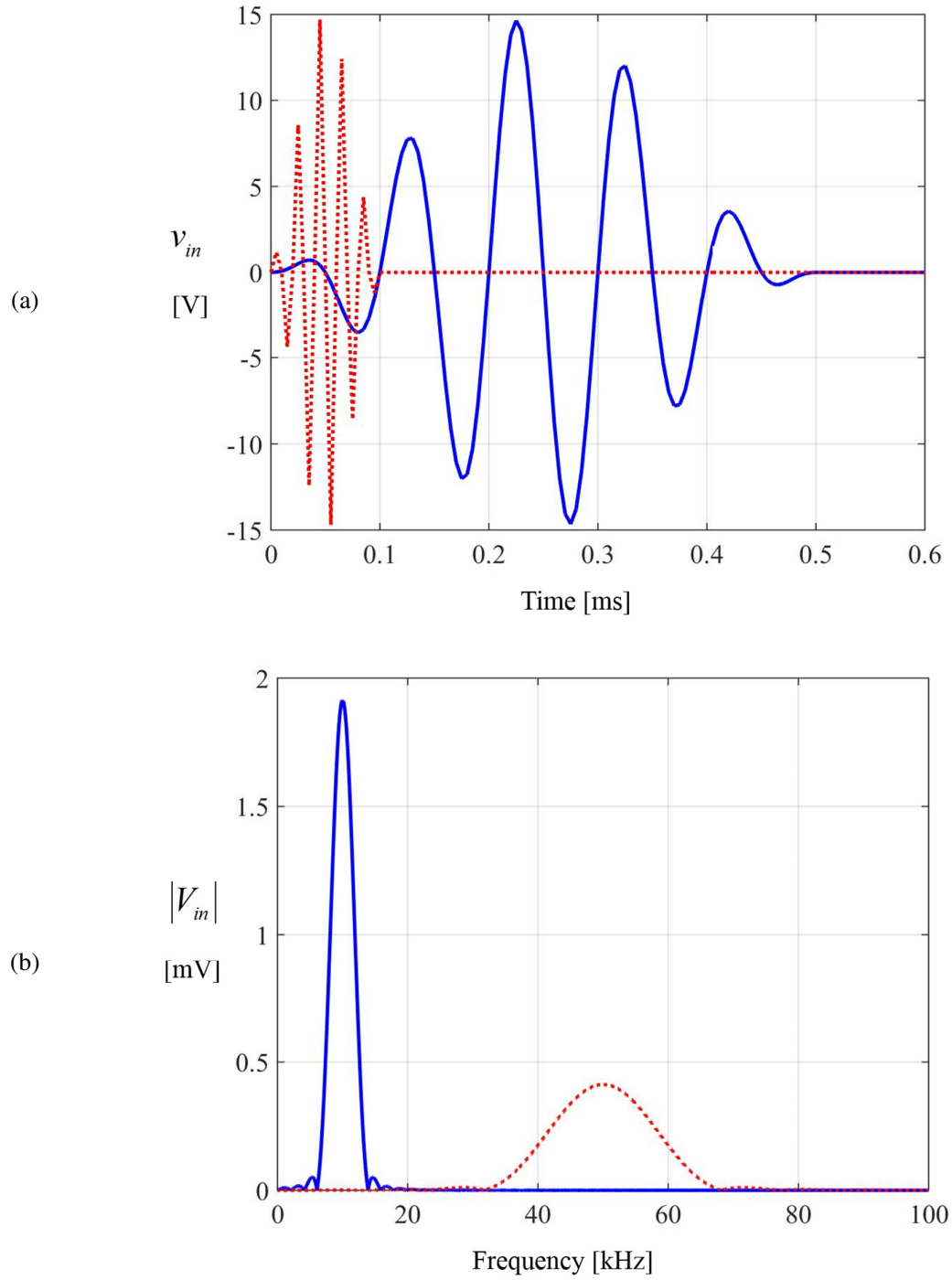
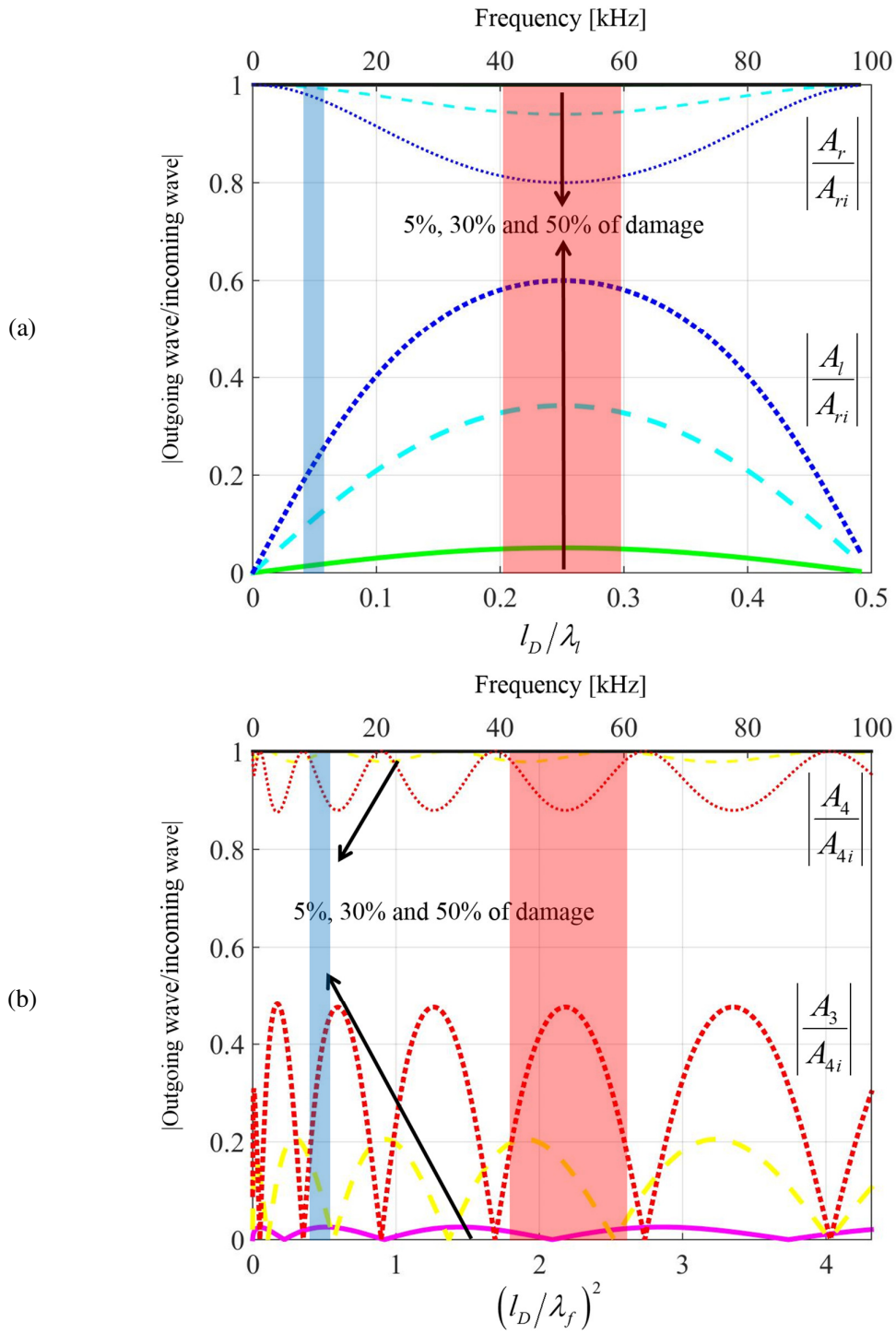
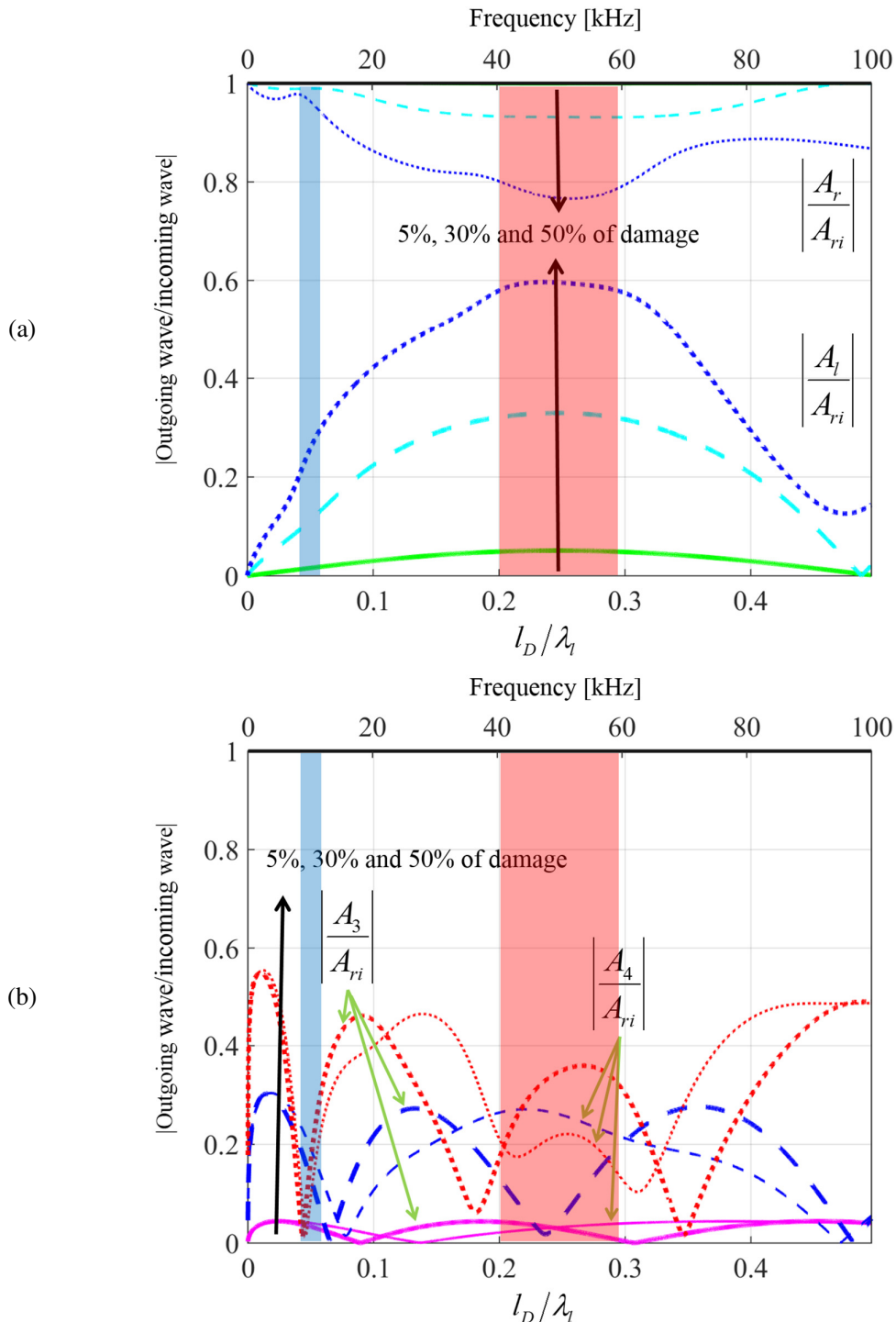


Figure 34: Reflection and Transmission coefficients (symmetric damage) in frequency domain with the highlighted excitation frequency range for input burst signals for main frequency of 10kHz (blue box) and 50kHz (red box): (a) longitudinal and; (b) flexural waves.



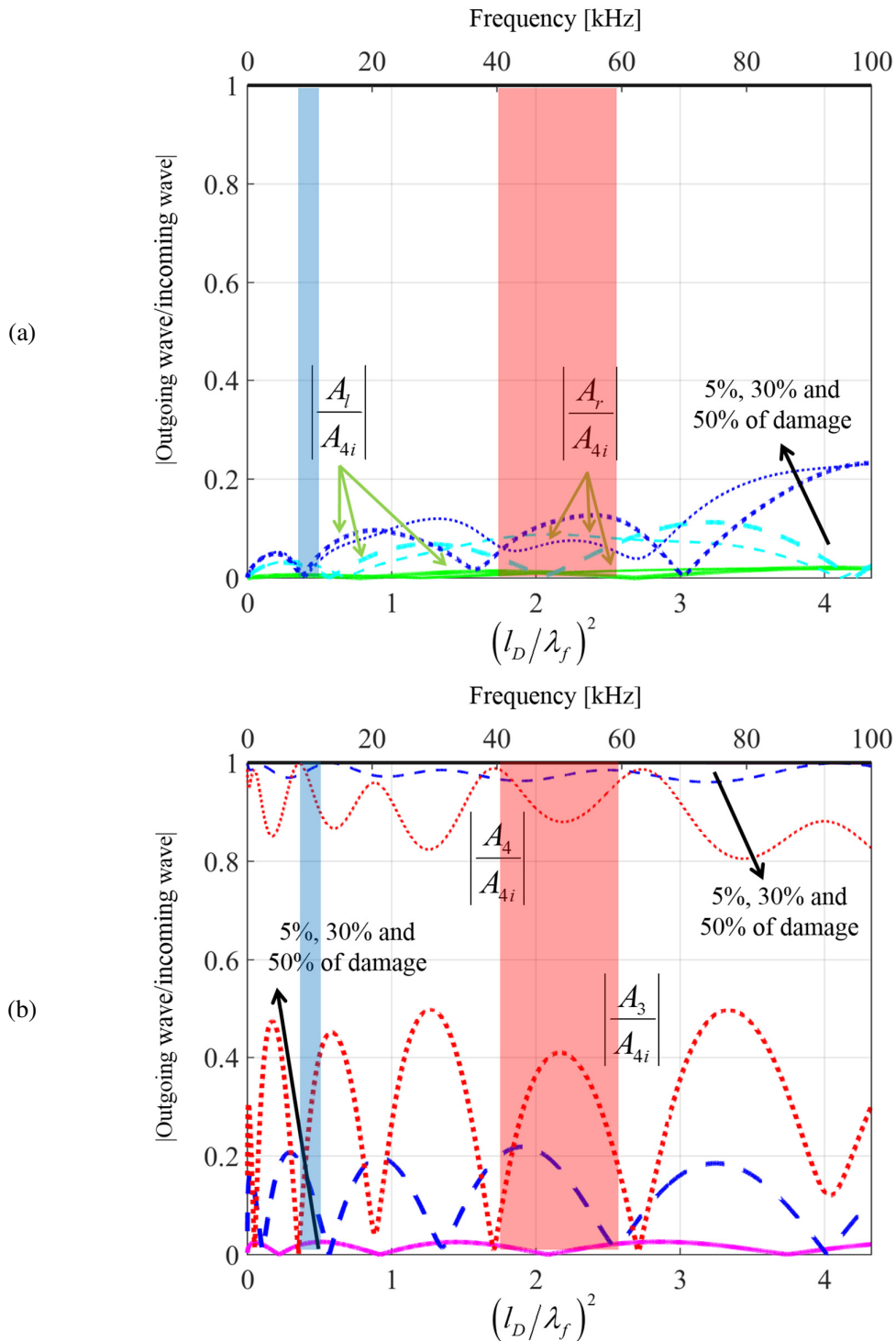
Source: Elaborated by author

Figure 35: Reflection and Transmission coefficients (asymmetric damage, longitudinal incident wave) in frequency domain with the highlighted excitation frequency range for input burst signals for main frequencies of 10kHz (blue box) and 50kHz (red box): (a) longitudinal and; (b) flexural waves.



Source: Elaborated by author

Figure 36: Reflection and Transmission coefficients (asymmetric damage, flexural incident wave) in frequency domain with the highlighted excitation frequency range for input burst signals for main frequencies of 10kHz (blue box) and 50kHz (red box): (a) longitudinal and; (b) flexural waves.

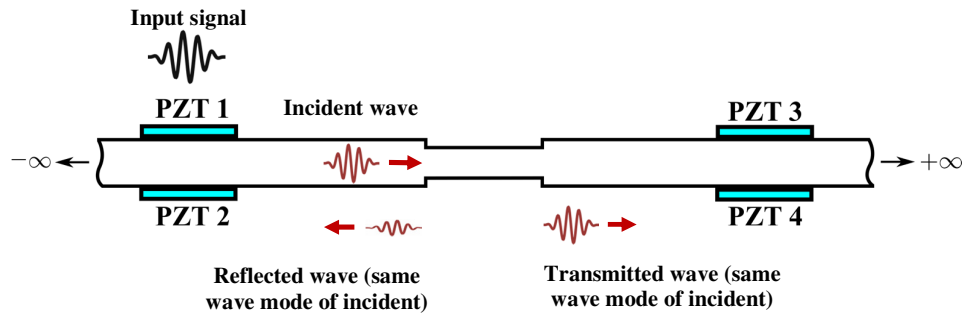


Source: Elaborated by author

4.3 Case 1: Symmetric Actuation and Symmetric Damage

Case 1 refers to an infinite Euler-Bernoulli beam with symmetric transducers and symmetric damage. Figure below shows an illustration of this structural configuration.

Figure 37: Case 1 - Waves interaction in symmetric damage (longitudinal or flexural incident).



Source: Elaborated by author

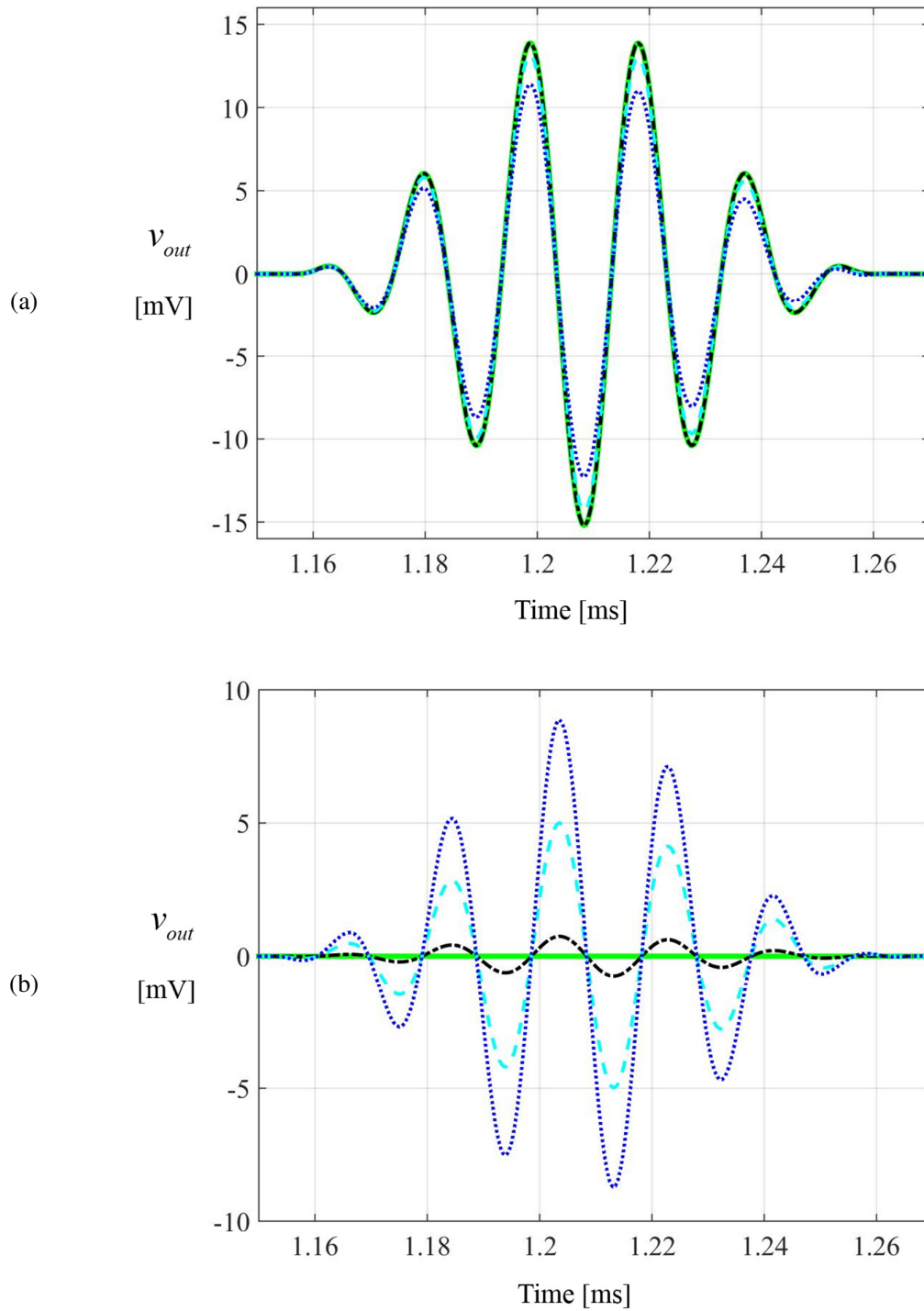
This study case are the simplest case because the wave modes can be generated separately and there are not conversion between the wave modes.

Remembering in this case due the symmetries (actuator and damage) once the incident wave is longitudinal or flexural the scattered waves are in the same wave mode of incident one.

4.3.1 Longitudinal Incident Wave

Considering a longitudinal wave generated by a pair of piezoelectric elements (symmetric actuator) for a burst signal with main frequency of 50kHz, Figure 38(a) show the electrical voltage for a pitch-catch configuration and Figure 38(b) shows the electrical voltage obtained by the piezoelectric sensor due to the reflected longitudinal wave. (pulse-echo configuration).

Figure 38: Electrical voltage signal generated by longitudinal scattered waves (at 50kHz) by symmetric damage of 5% (black dash-dot line), 30% (cyan dashed line), 50% (blue dot-dot line) compared to baseline (green solid line): (a) transmitted and; (b) reflected.



Source: Elaborated by author

While the voltage level of the pulse-echo configuration (reflected waves, Figure 38(b)) has increases about 9mV when damage severity changes 50%, the transmitted waves (Figure 38(a)) reduces only around 2.5mV for the same damage conditions.

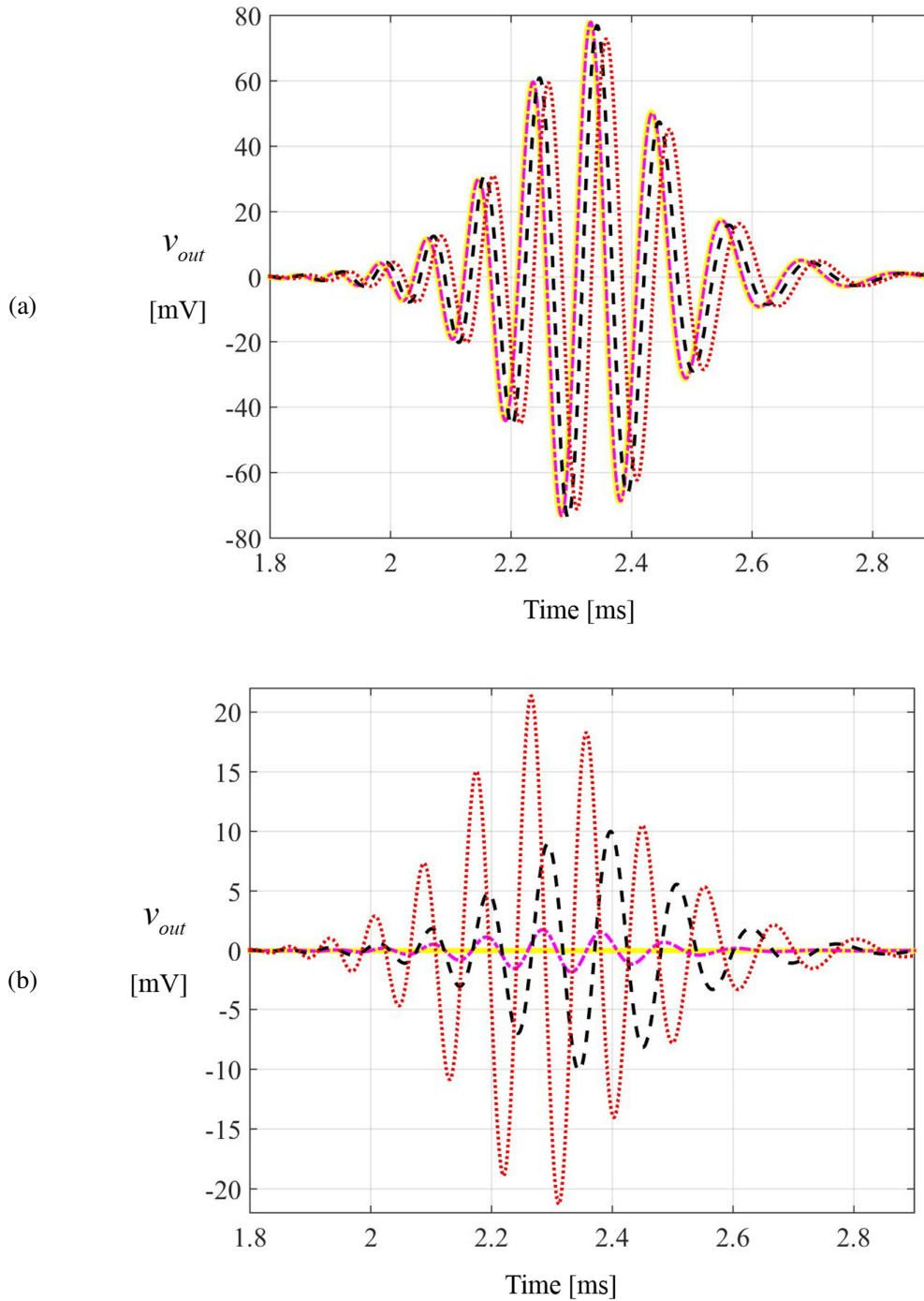
The reflected longitudinal wave, Figure 38(b), generates lower level of electrical voltage on the piezoelectric sensor compared to transmitted longitudinal waves. In another hand, the reflected longitudinal waves exhibits a great sensitivity to detect and quantify the damage once it presents significate difference of amplitudes between the signals as damage increase.

4.3.2 Flexural Incident Wave

Similarly, to the longitudinal waves, the transmitted flexural waves passing through different depths of damage do not generate significant change in the electrical voltage amplitude, as shown in Figure 39(a). Flexural reflected waves behaviors are presented in Figure 39(b). It shows the electrical voltages generated by the reflected waves for the severities of damage. Is easily to note the changes in the wave forms (dispersive effects) of the reflected and transmitted flexural waves.

As verified before, the pitch-catch configuration presents lower sensitivity to detect damage compared to the pulse-echo configuration. However, the flexural transmitted waves showed a small delay related to the damage severity. The time domain voltage generated by reflected waves can be easier used to detect a damage once it is zero for a baseline structure and changes significantly due to the damage.

Figure 39: Electrical voltage signal generated by flexural scattered waves (at 10kHz) by symmetric damage of 5% (magenta dash-dot line), 30% (black dashed line), 50% (red dot-dot line) compared to baseline (yellow solid line): (a) transmitted and; (b) reflected.



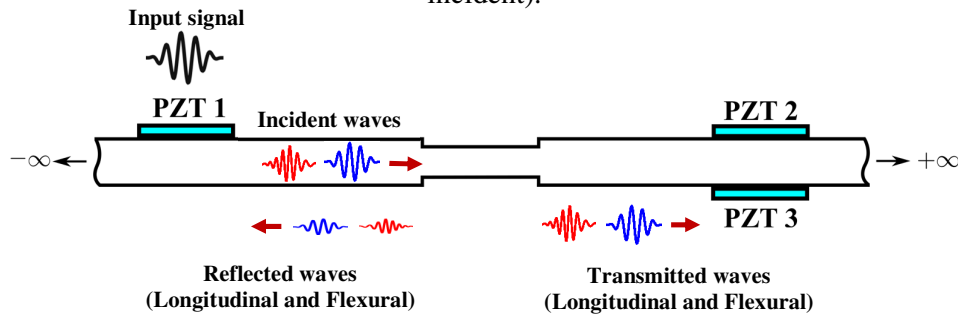
Source: Elaborated by author

4.4 Case 2: Asymmetric Actuation and Symmetric Damage

Case 2 refers to an infinite Euler-Bernoulli beam with asymmetric actuator and pulso-echo sensor, symmetric pitch-catch sensor and symmetric damage.

Figure 40 presents an illustration of the second study case considering the both wave packets generated by the actuator (longitudinal and flexural) and the interaction of these packets with the damage. The scatter waves are in the same wave mode of incident waves (there is no wave mode conversion because the symmetry of damage).

Figure 40: Case 2 - Waves interaction in symmetric damage (longitudinal and flexural incident).



Source: Elaborated by author

In other words, when the waves impinge the symmetric damage longitudinal waves (blue color in the Figure 40) scatter into longitudinal reflected and transmitted waves. And flexural waves (red color in the Figure 40) scatter into flexural reflected and transmitted waves. The final effect in time is equivalent to sum of single longitudinal and single flexural incident waves of case 1.

As both wave modes are generated the system is excited with the two burst inputs (10kHz and 50kHz).

Figure 41 shows the electrical voltage in the sensors respectively due to the transmitted and reflected waves for the burst excitation with 10kHz. It is observed two packets of wave, in which the first one (approximately in 1.2 ms) corresponds to the longitudinal wave packet and the second ($t = 1.9$ ms) corresponds to the flexural waves. It happens because the speeds of wave packets are different and longitudinal waves are faster than flexural.

From these figures, if 10kHz is used, the flexural reflected wave present higher sensitivity to detect and quantify damage than longitudinal waves. These low levels of electrical voltage generated by longitudinal waves can complicate the use of this mode (at the frequency range

of 10kHz) in a SHM system because noises.

Figure 42 presents the electrical voltage in the sensors respectively due to the transmitted and reflected waves for the burst excitation with 50kHz of main frequency. For this frequency range the longitudinal waves also exhibits important level of wave amplitude compared to flexural waves. In order to detect the damage, again the reflected waves, Figure 42(b), show better sensitivity to detection and quantification.

From Figure 42(a) is clear to note that for all transmitted waves the longitudinal packet has a little decrease of amplitude proportional to the damage severity and the flexural packet showed again a little increase in delay proportional to the damage severity.

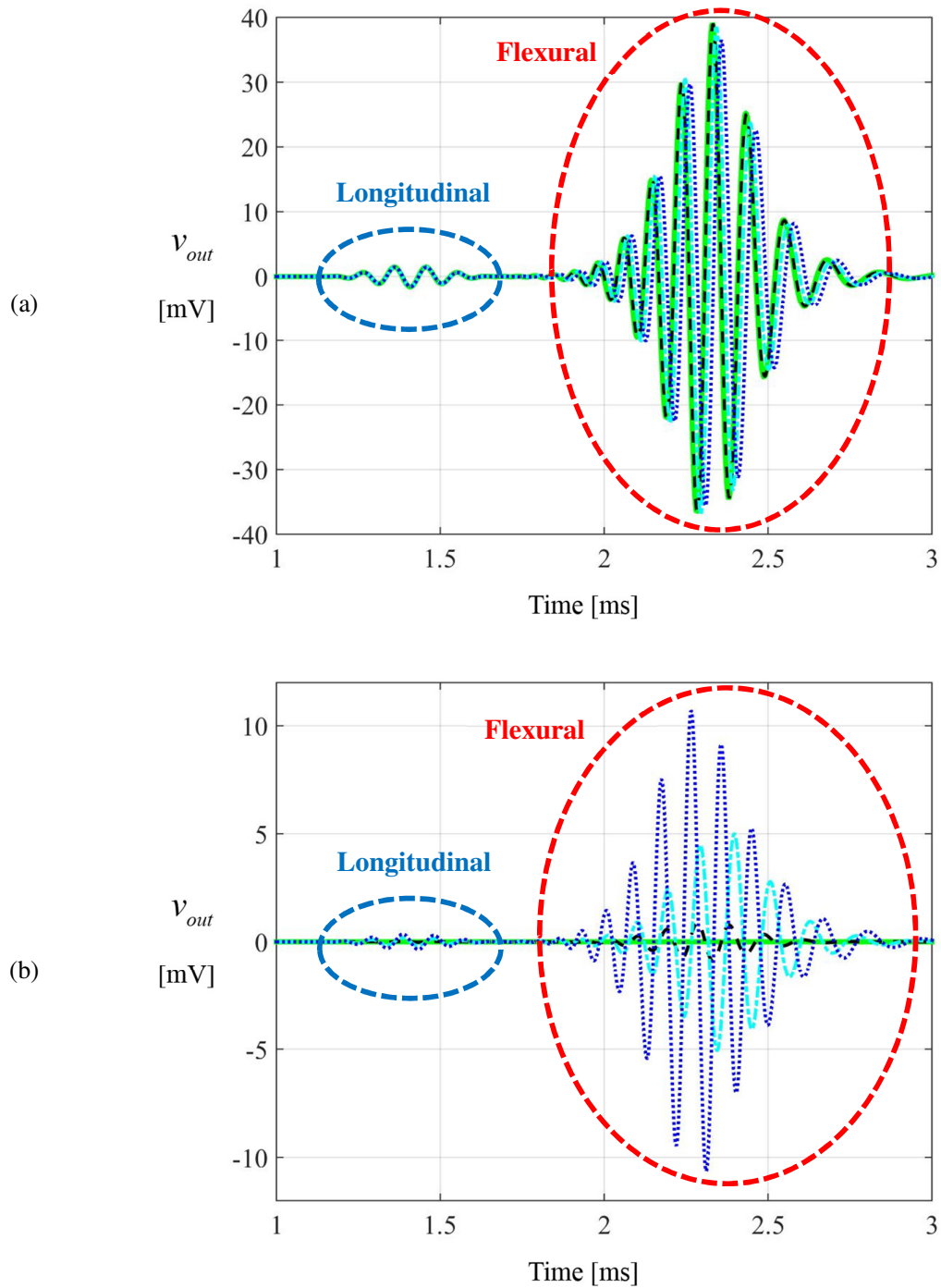
By Figure 42 (b) can be observed a bigger sensitivity of longitudinal reflected waves than flexural reflected waves for detect small damage (5%). It is possible to understand this phenomenon analyzing the behavior of flexural waves in the Figure 34(b), at this frequency range there is a filtering effect for the curve of 5% damage severity.

As observed by the behaviors presented in the Figure 42 the 50kHz frequency range is better to work with longitudinal reflected wave to detect and quantify the damage. However, flexural reflected waves is also good to detection.

This section showed that longitudinal and flexural waves have advantages and disadvantages depending of the system aims and the frequency range excited by a SHM system.

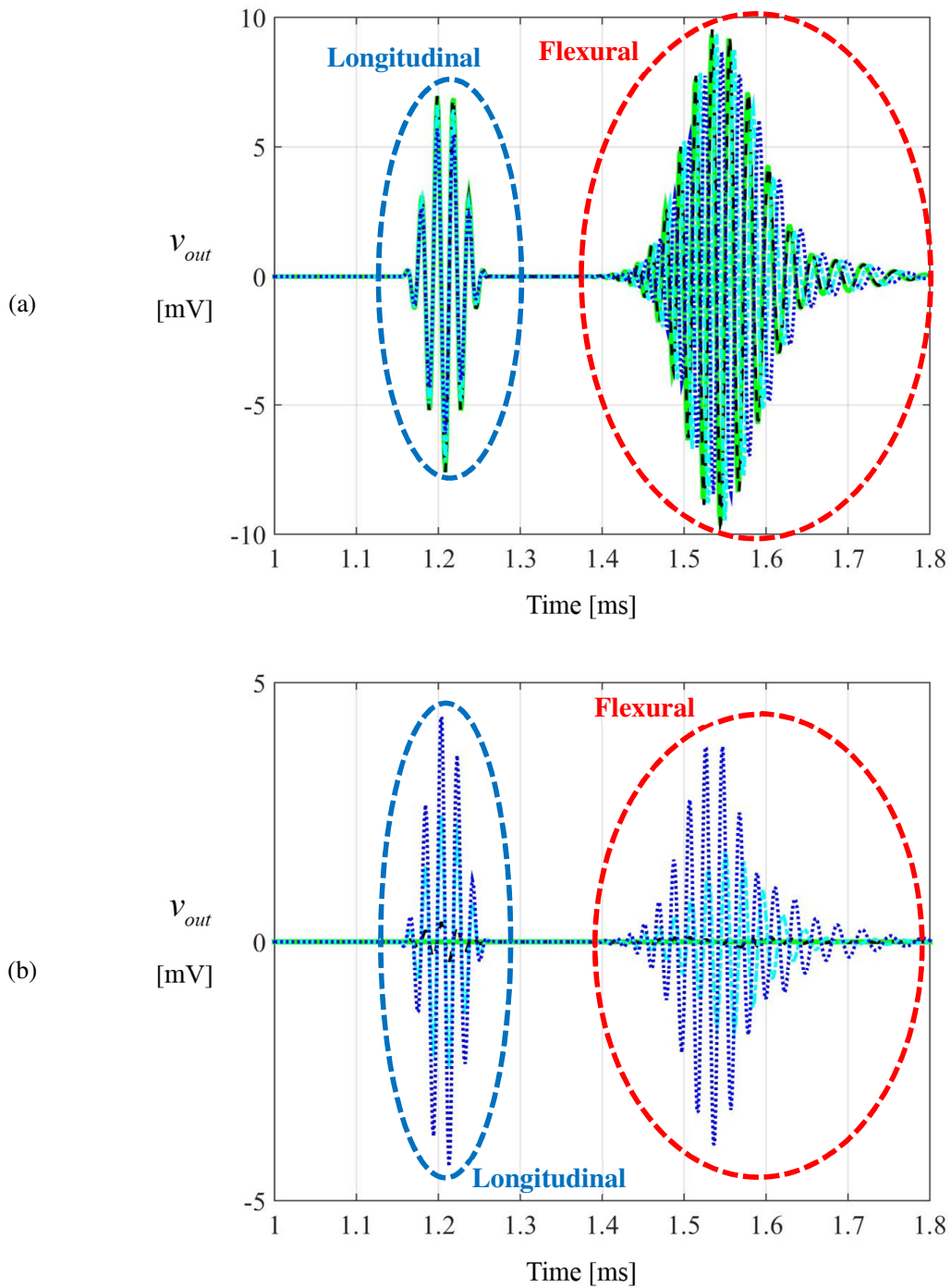
Nevertheless, this section showed how is important to understand the modification generated by the damage in the time domain curves.

Figure 41: Electrical voltage generated by scattered waves (at 10kHz) considering an asymmetric actuator and symmetric damage of 5% (black dash-dot line), 30% (cyan dashed line), 50% (blue dot-dot line) compared to baseline (green solid line): (a) transmitted and; (b) reflected.



Source: Elaborated by author

Figure 42: Electrical voltage signals generated by scattered waves (at 50kHz) considering an asymmetric actuator and symmetric damage of 5% (black dash-dot line), 30% (cyan dashed line), 50% (blue dot-dot line) compared to baseline (green solid line): (a) transmitted and; (b) reflected.

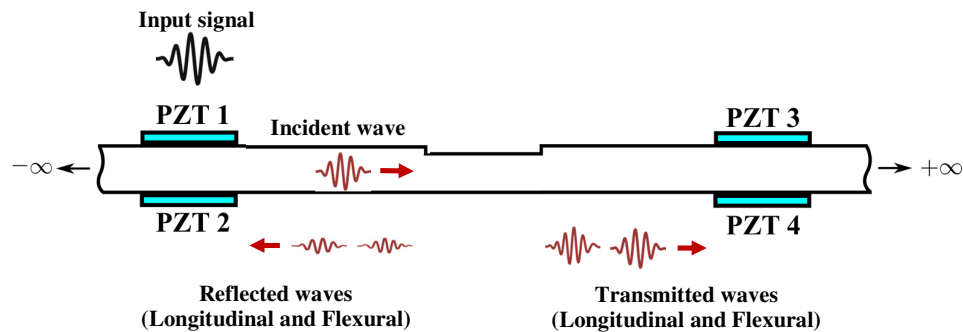


Source: Elaborated by author

4.5 Case 3: Symmetric Actuation and Asymmetric Damage

Case 3 refers to an infinite Euler-Bernoulli beam with symmetric transducers and asymmetric damage. Figure 43 presents an illustration of the third study case considering a wave packet generated by the actuator (longitudinal or flexural). This packet travels into the beam and impinges the asymmetric damage. The scatter waves are in both wave modes independently of the incident wave mode, as can be observed in the illustration.

Figure 43: Case 3 - Waves interaction in asymmetric damage (longitudinal or flexural incident).



Source: Elaborated by author

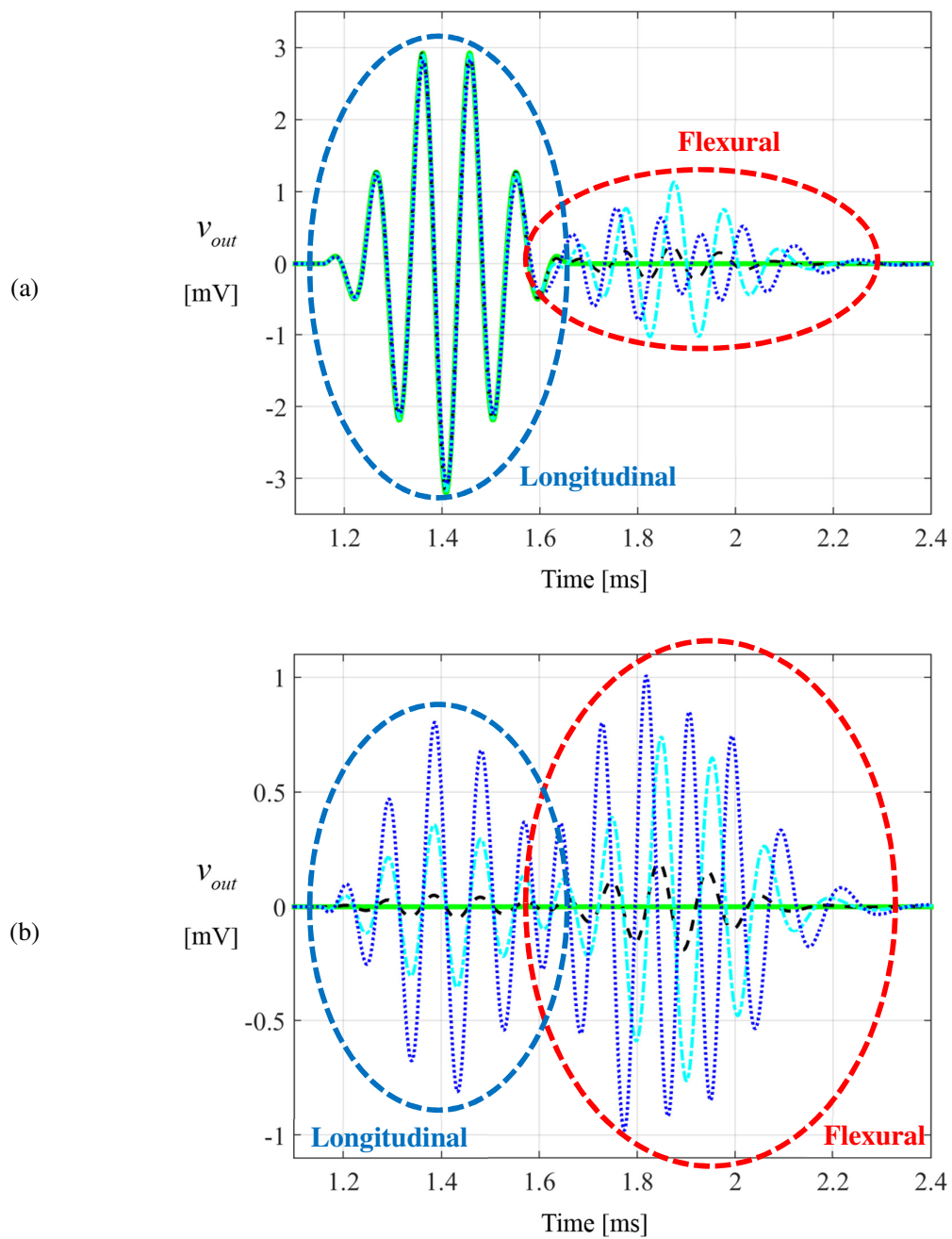
In other words, the asymmetric damage transforms longitudinal wave modes in flexural and vice versa. It means that a longitudinal wave incident into asymmetric damage scatter in longitudinal and flexural wave modes reflected and transmitted (four packets of waves). The same occurs for a flexural incident wave.

4.5.1 Longitudinal Incident Wave

Figure 44 presents the amplitudes respectively for transmitted and reflected waves generated by longitudinal waves with 10kHz of main frequency for the burst signal. Figure 45 presents the same for 50kHz.

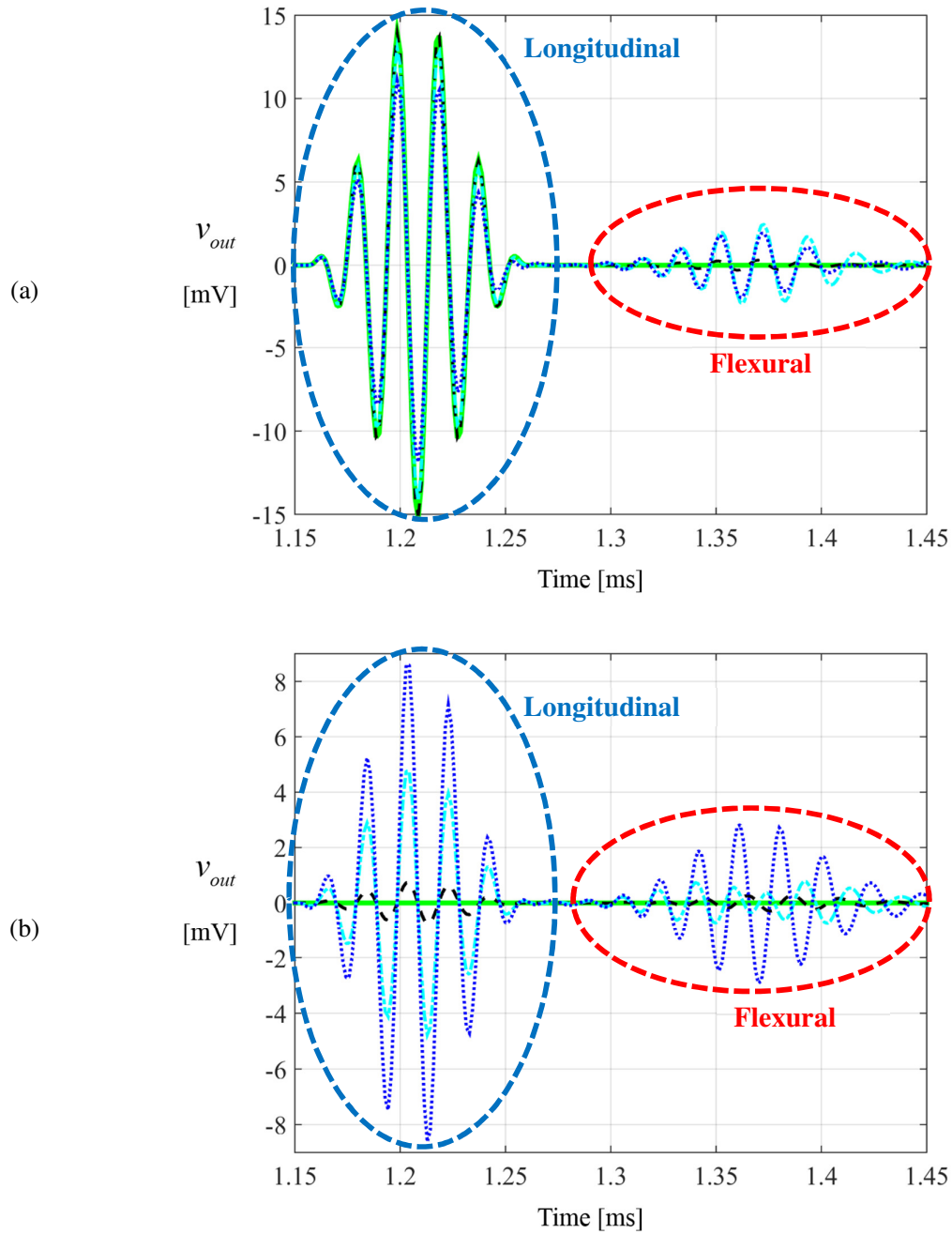
Two wave packets can be seen in all time domain graphic of this section. The first packet corresponds to the longitudinal waves packet and the second packet corresponds to the flexural part generated when the longitudinal wave impinges the asymmetric damage.

Figure 44: Electrical voltage signals generated by scattered waves (at 10kHz) considering a symmetric actuator and asymmetric damage of 5% (black dash-dot line), 30% (cyan dashed line), 50% (blue dot-dot line) compared to baseline (green solid line): (a) transmitted and; (b) reflected.



Source: Elaborated by author

Figure 45: Electrical voltage signals generated by scattered waves (at 50kHz) considering a symmetric actuator and asymmetric damage of 5% (black dash-dot line), 30% (cyan dashed line), 50% (blue dot-dot line) compared to baseline (green solid line): (a) transmitted and; (b) reflected.



Source: Elaborated by author

For the two main frequencies of inputs the new packet that appears in the transmitted waves is proportional to the damage intensity. However, the waves reflected carry two packets able to sense the damage. In the other hand, the wave packet of transmitted waves that is in the same wave mode of incident one shows more modifications than transmitted packets showed before. This is due to the incident waves split up to in four packets (no more in two packets).

As the 10kHz is an optimum frequency for flexural waves even using the incident longitudinal waves the scattered flexural waves presents high amplitudes and sensitivity to detect the damage.

The opposite occurs for 50kHz that is an optimum frequency for longitudinal waves. In this case using the longitudinal incident wave the scattered longitudinal waves by the asymmetric damage present high amplitudes and sensitivity to detect the damage.

For the frequency range of 10kHz the reflected waves, Figure 44(b), showed higher sensitivities to detect the damage compared to transmitted waves, Figure 44(a). In addition, it is noted that flexural packet of reflected waves generated can be used to detect and quantify changes in the structural health due to their different levels of electrical voltage proportional to each damage condition.

Is not clearly more, only by visual inspection of waves select which on is better to detect and quantify the damage. Is possible to see the influence of filtering effects special to quantify the damage. This generated some wave packets with no proportionality between the amplitudes of voltage levels for each damage severity.

Additionally, for reflected waves were possible to note in the Figure 45(b) a non-proportionality between damage severity and the amplitudes of flexural waves packet. It can be explained observing the frequency range excited in the Figure 35 (b). The frequency range excited involves a filtering effect close to 60kHz and this filtering effect moves in frequency depending to the damage severity, it generates the behavior observed in the flexural packet of reflected waves (cyan curve).

Nevertheless, this section showed that to detect asymmetric damage is better to work with different waves modes at the same time. It can increase the sensitivity of systems. However, is important to know the behavior of scatter waves for the frequency range chosen to avoid some incorrect conclusions (diagnostics).

4.5.2 *Flexural Incident Wave*

Figure 46 presents the amplitudes respectively for reflected and transmitted waves generated by flexural waves from a pair of actuator with 10kHz of main frequency for the burst signal. Figure 47 shows the same for 50kHz. Again, the first packet observed in time domain of these figures corresponds to the longitudinal wave packets and the second packets corresponds to the flexural part.

Is possible to note that the longitudinal wave packets (reflected and transmitted) are distorted compared to the shape of burst input signals. It occurs in this structural case because during the propagation of the flexural wave it is dispersed and when it impinges the asymmetric damage the scattered waves also carries the wave shape of incident wave (with change in wave shape).

For 10kHz the longitudinal waves packets scattered by the damage almost disappears. It is explained by filtering effects of transmitted and reflected longitudinal waves in the frequency range excited by the input. It can be seen in the Figure 36(a).

In other hand, also for 10kHz the flexural wave packets were presents and showed changes related to the damage severity. Based on these results, both transmitted and reflected waves developed changes related to the damage severity. However, reflected waves, Figure 46 (b), still to be more sensible to the damage.

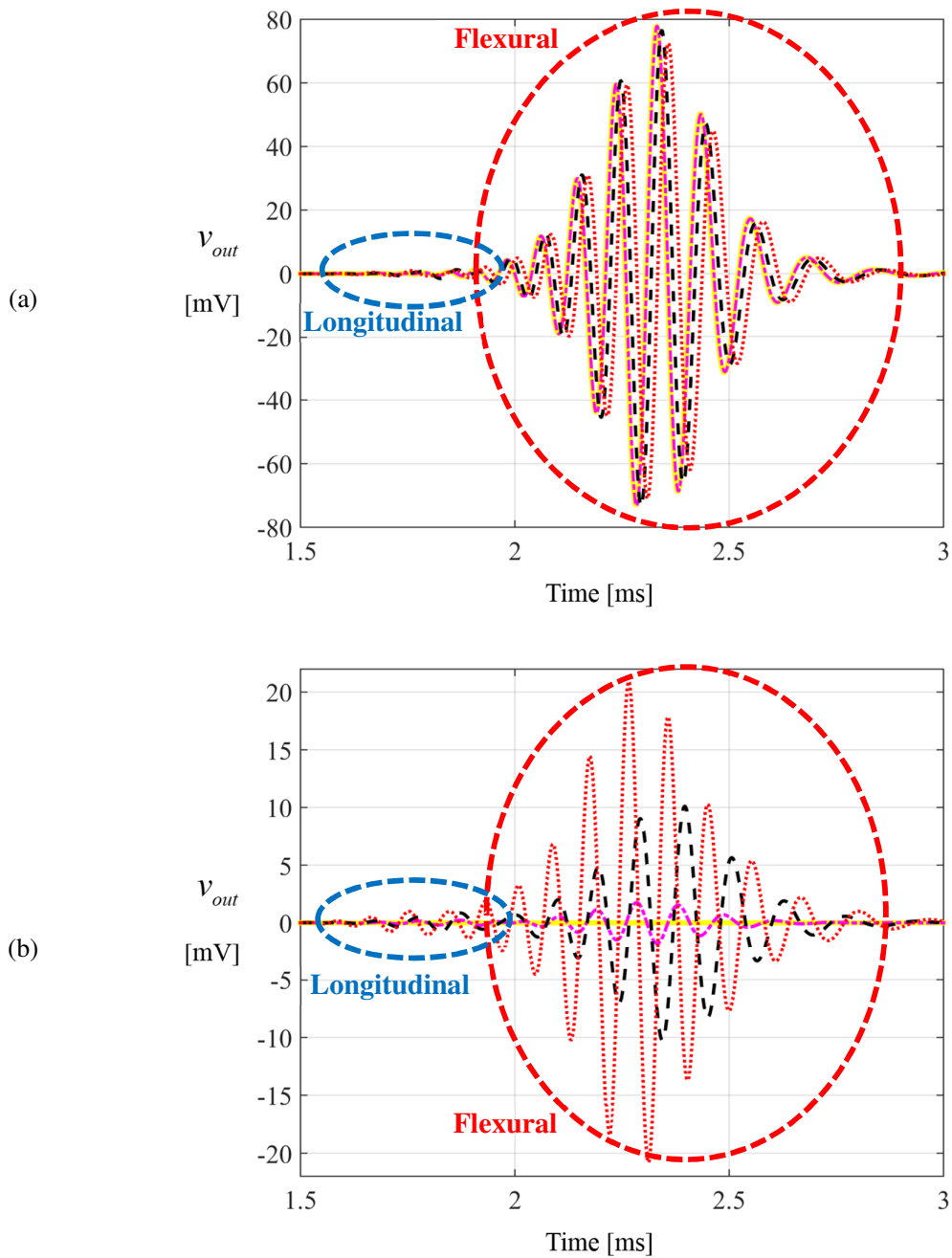
For 50kHz the longitudinal wave packets scattered were present and showed some peculiarity. One of these is that sensitivity of longitudinal transmitted is almost the same for 30 and 50% of damage. And other is that for longitudinal reflected there is some influence of a filtering effects for the damage of 30%.

For both frequency using flexural waves incident in order to detect asymmetric damage arise difficulties to use the longitudinal waves scattered by the damage because they carry many filtering effects.

However, working with flexural wave packets (reflected and transmitted) the remarks seem the same presented in Section 4.2 for the flexural components.

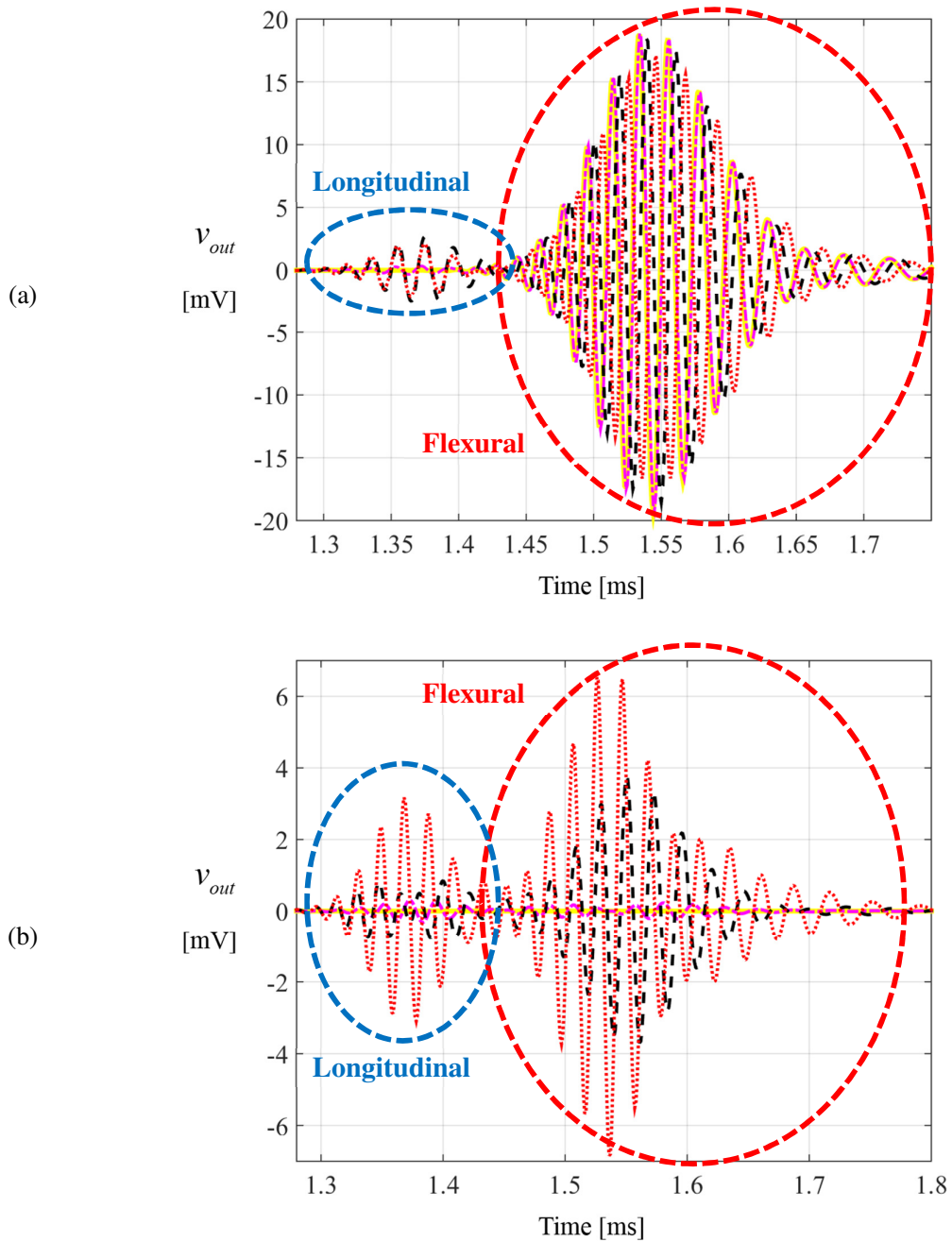
In this way, is possible to conclude that to use a flexural wave incident to detect asymmetric damage is the most complicated case presented here up to now. It because the filtering effect of starts to generate influence also in the longitudinal packets.

Figure 46: Electrical voltage signals generated by scattered waves (at 10kHz) considering an symmetric actuator and asymmetric damage of 5% (magenta dash-dot line), 30% (black dashed line), 50% (red dot-dot line) compared to baseline (yellow solid line): (a) transmitted and; (b) reflected.



Source: Elaborated by author

Figure 47: Electrical voltage signals generated by scattered waves (at 50kHz) considering an symmetric actuator and asymmetric damage of 5% (magenta dash-dot line), 30% (black dashed line), 50% (red dot-dot line) compared to baseline (yellow solid line): (a) transmitted and; (b) reflected.

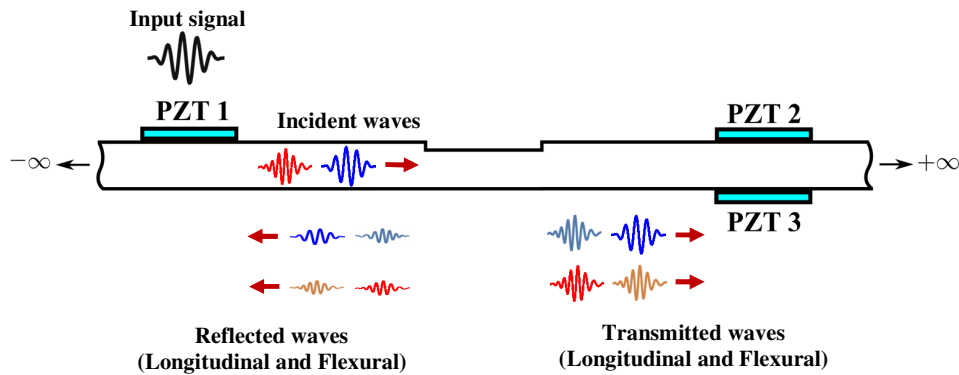


Source: Elaborated by author

4.6 Case 4: Asymmetric Actuation and Asymmetric Damage

The fourth case of interesting comprises an asymmetric actuation to excite the structure and an asymmetric damage condition. Figure 48 presents an illustration of this last study case considering waves packets generated by the actuator (longitudinal and flexural) and the interactions of these waves with the asymmetric damage. The scatter waves are in both wave mode for each incident wave packets.

Figure 48: Case 4 - Waves interaction in an asymmetric damage (longitudinal and flexural incident).



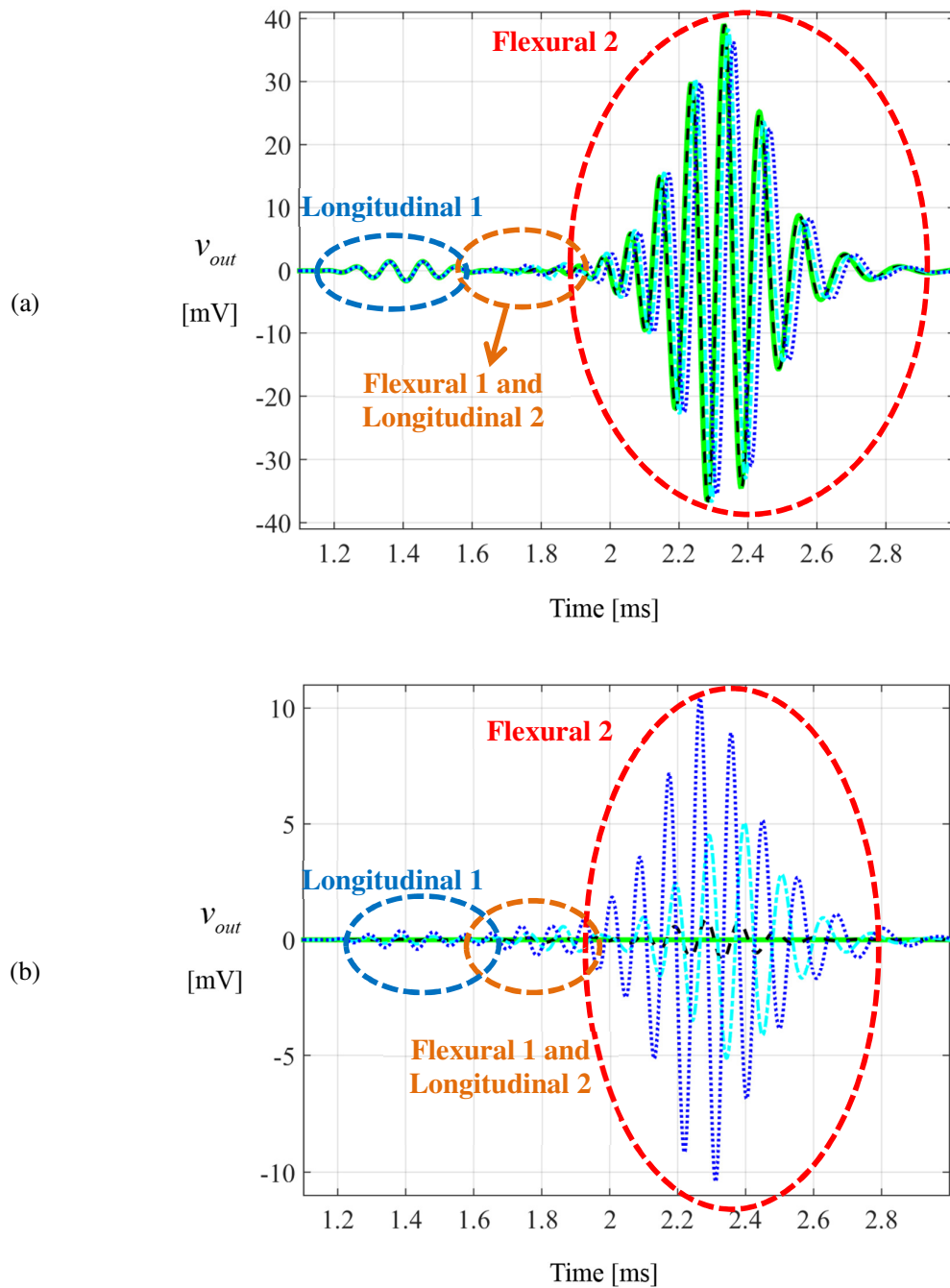
Source: Elaborated by author

It is the most complicated case presented in this work and comprises the understanding of four wave packets at each scattered wave (transmitted and reflected). These waves are the longitudinal (Longitudinal 1) and flexural (Flexural 1) waves scattered by the asymmetric damage due the packet of longitudinal wave incident and the longitudinal (Longitudinal 2) and flexural (Flexural 2) waves scattered by the damage due the packet of flexural wave incident. However, for the curves presented below is possible to note visually only three wave packets. It occurs because the superposition of two packets (Flexural 1 and Longitudinal 2).

Figure 49 presents the amplitudes of scattered waves for transmitted and reflected with 10kHz of main frequency for the burst signal.

The time domain behaviors presented in the figure here carries the same behaviors presented in the Section 4.3 for separated incident wave modes. As here the effects are summed is possible to separate the curves as present in Figure 50 for transmitted waves and in Figure 51 for reflected waves.

Figure 49: Electrical voltage signals generated by scattered waves (at 10kHz) considering a symmetric actuator and asymmetric damage of 5% (black dash-dot line), 30% (cyan dashed line), 50% (blue dot-dot line) compared to baseline (green solid line): (a) transmitted and; (b) reflected.



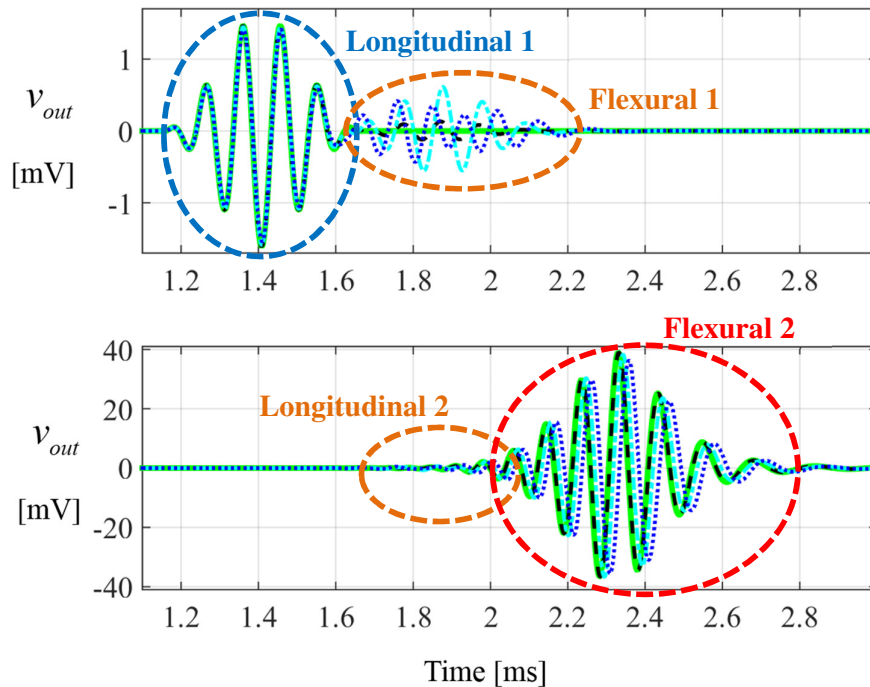
Source: Elaborated by author

As observed by Figure 49 the reflected waves showed better proportional sensitivity of damage depth. At this frequency range (10kHz) the flexural waves still developing higher amplitudes compared to longitudinal waves.

In order to separate and understand each wave packet Figure 50 presents the packets of transmitted waves obtained due longitudinal and flexural incident wave separated for input the frequency range of 10kHz.

The curves of Figure 50 are similar to the curves presented in the Figure 44(a) and Figure 46 (a). The sum of Longitudinal 1 and Flexural 1 packets are the same curve of Figure 44(a) and the sum of Longitudinal 2 and Flexural 2 are the same curve presented in Figure 46 (a).

Figure 50: Longitudinal and flexural wave packets of transmitted waves (at 10kHz) considering a asymmetric actuator and asymmetric damage of 5% (black dash-dot line), 30% (cyan dashed line), 50% (blue dot-dot line) compared to baseline (green solid line)

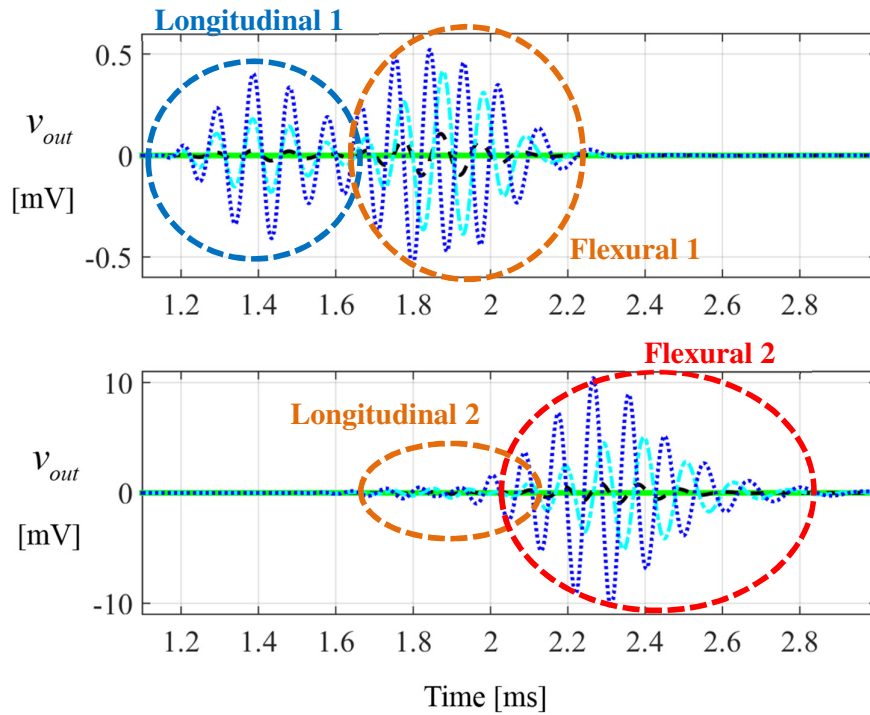


Source: Elaborated by author

For reflected waves, the sum of Longitudinal 1 and Flexural 1 packets are the same curve of Figure 44 (b) and the sum of Longitudinal 2 and Flexural 2 are the same curve presented in Figure 46 (b).

The same comments presented for each separated curves in the previous section can be employed here.

Figure 51: Longitudinal and flexural wave packets of reflected waves (at 10kHz) considering a asymmetric actuator and asymmetric damage of 5% (black dash-dot line), 30% (cyan dashed line), 50% (blue dot-dot line) compared to baseline (green solid line)



Source: Elaborated by author

Figure 52 presents the amplitudes of scattered waves for transmitted and reflected with 50kHz of main frequency for the burst signal. Figure 53 and Figure 54 present the four packets separated respectively for transmitted and reflected waves.

Figure 52: Electrical voltage signals generated by scattered waves (at 50kHz) considering a symmetric actuator and asymmetric damage of 5% (black dash-dot line), 30% (cyan dashed line), 50% (blue dot-dot line) compared to baseline (green solid line): (a) transmitted; (b) reflected.

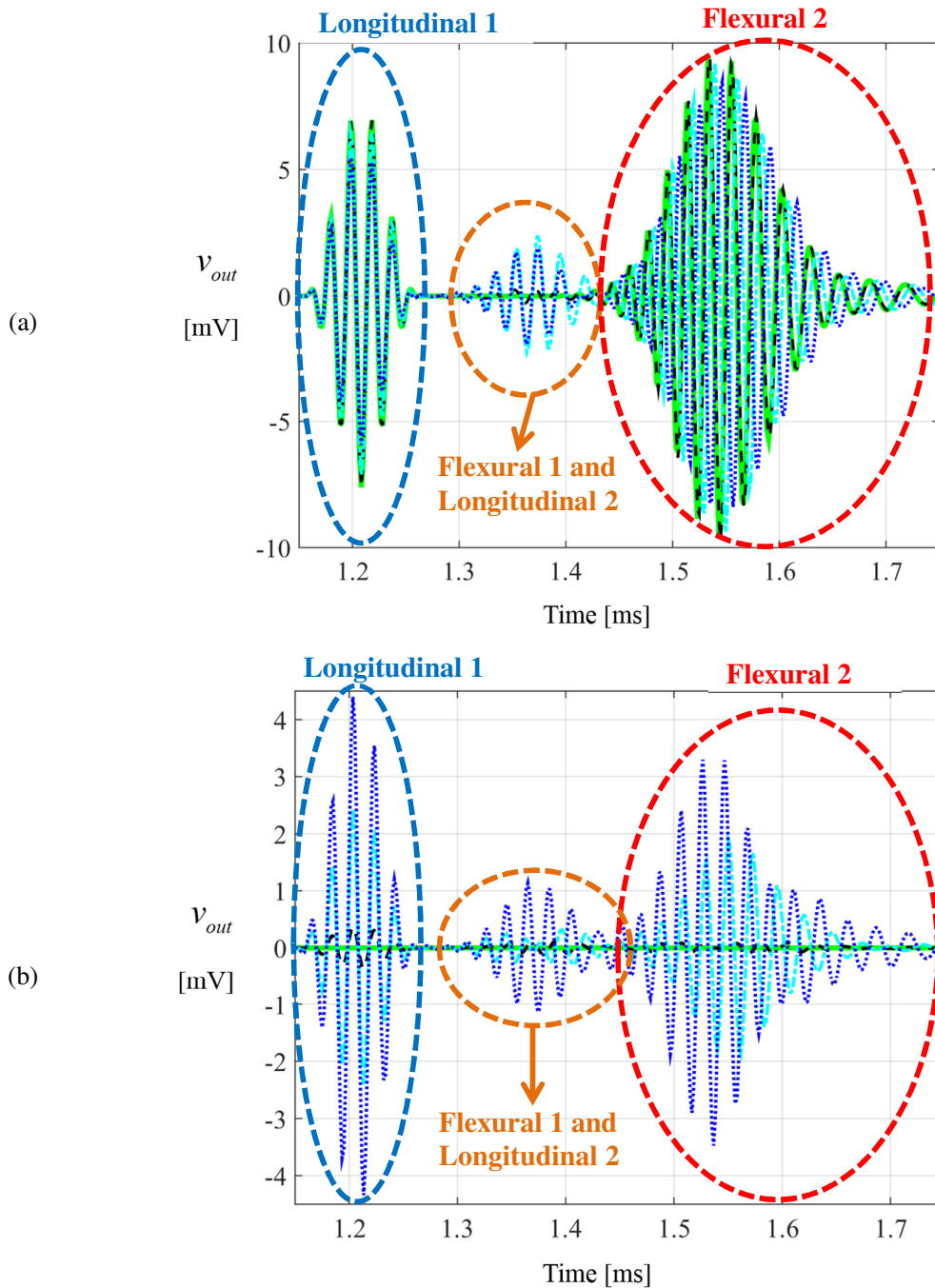
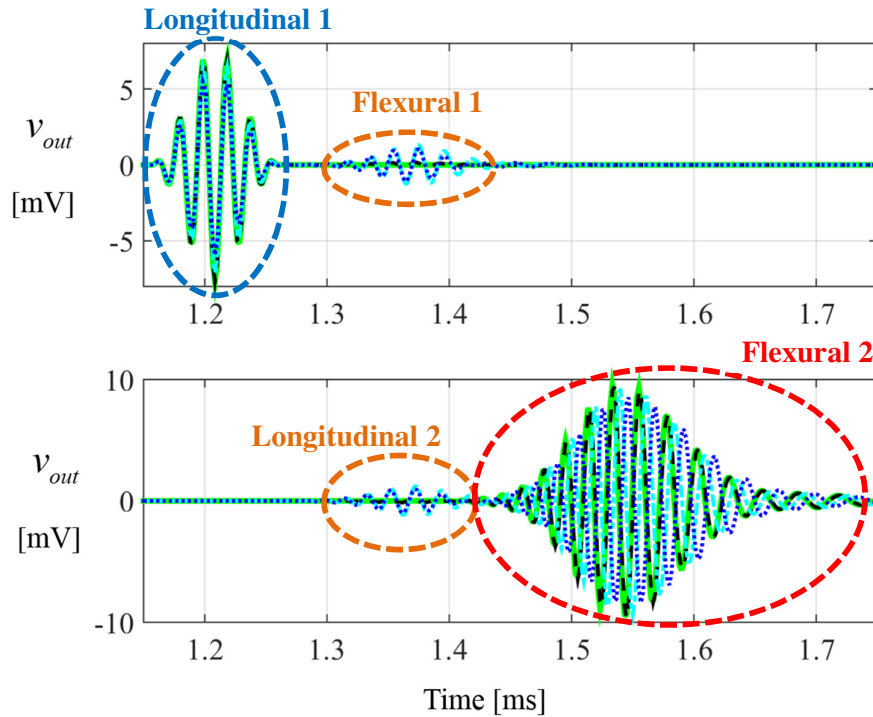


Figure 53: Longitudinal and flexural wave packets of transmitted waves (at 50kHz) considering a asymmetric actuator and asymmetric damage of 5% (black dash-dot line), 30% (cyan dashed line), 50% (blue dot-dot line) compared to baseline (green solid line).



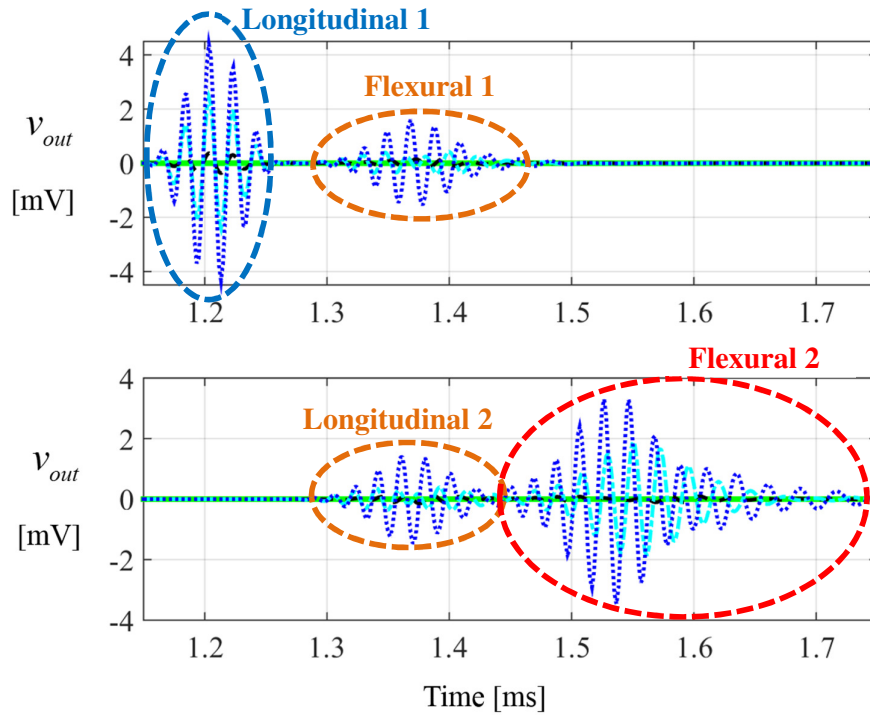
Source: Elaborated by author

For transmitted waves, the sum of Longitudinal 1 and Flexural 1 packets are the same curve of Figure 45 (a) and the sum of Longitudinal 2 and Flexural 2 are the same curve presented in Figure 47 (a).

For reflected waves, the sum of Longitudinal 1 and Flexural 1 packets are the same curve of Figure 45 (b) and the sum of Longitudinal 2 and Flexural 2 are the same curve presented in Figure 47 (b).

Again, the same comments presented for each separated curves in the Section 4.3 can be employed here.

Figure 54: Longitudinal and flexural wave packets of reflected waves (at 50kHz) considering a asymmetric actuator and asymmetric damage of 5% (black dash-dot line), 30% (cyan dashed line), 50% (blue dot-dot line) compared to baseline (green solid line)



Source: Elaborated by author

4.7 Conclusions

This chapter expands the comprehension of the physical aspects of waves propagation in time domain. Here is presented the results obtained in time domain using the complete wave model for four case studied in order to understand the main behaviors of this systems in time domain for two different frequency ranges excited by burst signals of five cycles. It was 10kHz and 50kHz. These frequencies were chosen to avoid filtering effects for flexural waves (10kHz) and for longitudinal waves (50kHz).

For the first study case as clear to note that the presence of a damage results in variations of amplitudes in the longitudinal packets (reflected and transmitted). For flexural packets the amplitude of waves changes and there are delays related with damage severity.

The second study case add the separated behaviors showed in the first case. It can be very helpful because the sensitivity of wave modes are summed. However, as observed and

discussed is important to know if the frequency range excited presents low levels of responses for some wave mode.

For the third study case, was observed a wave mode scattering in two wave modes after interaction with asymmetric damage. Using a longitudinal incident wave is recommended to work with the reflected longitudinal wave packet because the proportionality change generated as damage increase. The reflected flexural waves packet need to be carefully analyzed in order to not obtain false negatives and mistakes in the quantification of damage, as showed Figure 45(a). For a flexural wave incident is recommended to use scattered flexural waves because the scattered longitudinal waves starts to presents several filtering effects too.

The fourth case is the most complicated case because comprise all observations presented for the third case. The phenomenon occur together and is important to separate them in order to analyze the effects and choose good SHM strategies.

The most important general conclusion for all study case is that reflected waves showed more sensitivity to detect and quantify the damage than transmitted waves.

Another very important general conclusion is that longitudinal wave incidents are easier to use for SHM systems than flexural incidents. It is because they are not dispersive, there present few filtering effects ranges compared to flexural waves and there are no delays related with damage severity.

However, in order to work with longitudinal waves is necessary to choose a good frequencies range to excite the longitudinal waves, otherwise the amplitude of this waves can be very small and the changes of amplitude related with the damage are difficult to measure.

The studies and conclusions presented here are very important to guide a development of SHM systems. As observed, many physical effects can generate mistakes in the diagnostics. In this sense, predict and understand the behavior of guided waves in the structure monitored is very important. The next chapter expand the discussions presented here and compare the results simulated with experimental data.

5 PARTIAL VALIDATION

5.1 Introduction

The objective of this Chapter is to present the experimental results in order to compare with simulated results and partially validate the models for the complete system.

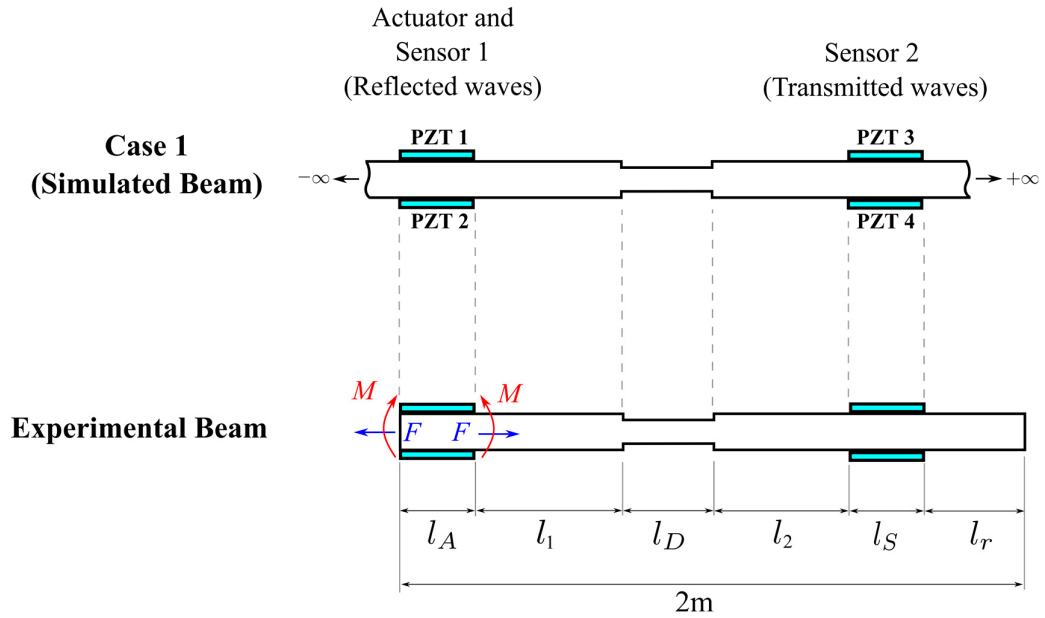
The experimental setup is presented and explained. The data measured are in time domain and can be directly compared to the time domain results from correspondent simulations, as presented in the Chapter 4.

The configuration of the first study case (Section 4.3) is chosen to be validated here considering longitudinal incident wave. There are some differences between the structural system simulated and the structural system of experiments. It is mainly concentrated in the fact of the beam simulated is an infinite beam and in the experiments the beam is finite.

5.2 Experimental Beam

The experimental beam consists of an aluminum beam (6063-T5). Figure 55 illustrates the experimental beam and compares it with the respective simulated beam. As can be observed, the piezoelectric elements were bonded in opposite side of beam and the actuator was attached in a beam extremity in order to avoid reflected waves at this border.

Figure 55: Experimental and simulated beams.



Source: Elaborated by author

The beam and piezoelectric elements properties are presented in Table 1 (Chapter 3) and the lengths adopted to these analyses presented herein can be seen in Table 2. The distance l_1 was chosen considering the phase speed of the fastest wave packet (longitudinal) to avoid superposition (in time) of the reflected wave packet with the input signal. In other hand the distances l_2 and l_r were chosen to avoid superposition of the first packet reflected in the right extremity with the packet of longitudinal waves transmitted by damage.

Table 3: Lengths of each experimental and simulated beams.

Segments	Symbol	Length [mm]
<i>Actuator</i>	l_A	12.7
<i>Between actuator (or Sensor 1) and damage</i>	l_1	1300
<i>Between Sensor 2 and damage</i>	l_2	250
<i>Damage</i>	l_D	25
<i>Sensors</i>	l_S	12.7
<i>Between Sensor 2 and the beam extremity</i>	l_r	400

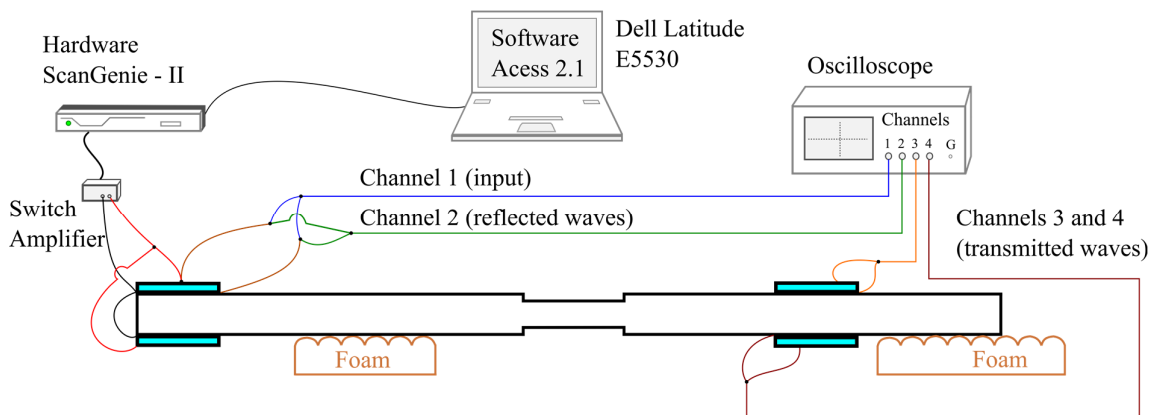
Source: Elaborated by author

5.3 Experimental Setup

Figure 56 presents an illustration of the experimental apparatus used and the Figure 57 a photographic of it that is mainly composed by

- An aluminum beam with 2 meter of length (6063-T5);
- Accelent Technologies ScanGenie –II hardware;
- Accelent Technologies Access 2.1 Software
- Oscilloscope Tektronik TBS1064 (60MHz, 1GS/s);
- Piezoelectric elements (PSI-5H4E from Piezo Systems).

Figure 56: Illustration of the experimental setup.



Source: Elaborated by author

Figure 57 Photographic of the experimental setup



Source: Elaborated by author

In order to generate input signals and apply them on the structure is used the ScanGenie – II, which operates together with the Access 2.1 Software. This system is commonly used for Lamb Waves analysis and it has capacity to work with high frequencies. However, in these tests the Accelent system was just used to excite the actuator.

The data were acquired using the oscilloscope. It has four channels and they were used to measure the input signal (Channel 1), the reflected waves (Channel 2) and transmitted waves (Channel 3 and 4), as showed in Figure 56. The data were recorded on an external drive (USB Pendrive) and post-processed in another computer.

Soft foams supported the beam in order to behave as a free beam. The temperature of the laboratory was between 25-28°C. Next section shows the comparison of simulated results and the experimental curves.

5.4 Comparison

The major difference between the structural system of the first study case (Section 4.3) and the structural system of experiments is concentrated in the fact of the beam simulated is an infinite beam and the experimental beam is finite.

The symmetric damage in the beam was about 30% of thickness reduction (15% of reduction for each side of the beam). The damage were made by a milling machining had a final precision of 0.02mm.

The central frequencies used for the burst inputs were 25kHz, 35kHz and 45kHz. Figure 58 presents these experimental inputs in time and frequency domain.

Figure 58: Input burst signals for main frequency of 25kHz (blue solid line), 35kHz (black dot-dot line) and 45kHz (red dashed-dot line): (a) time domain; (b) frequency domain.

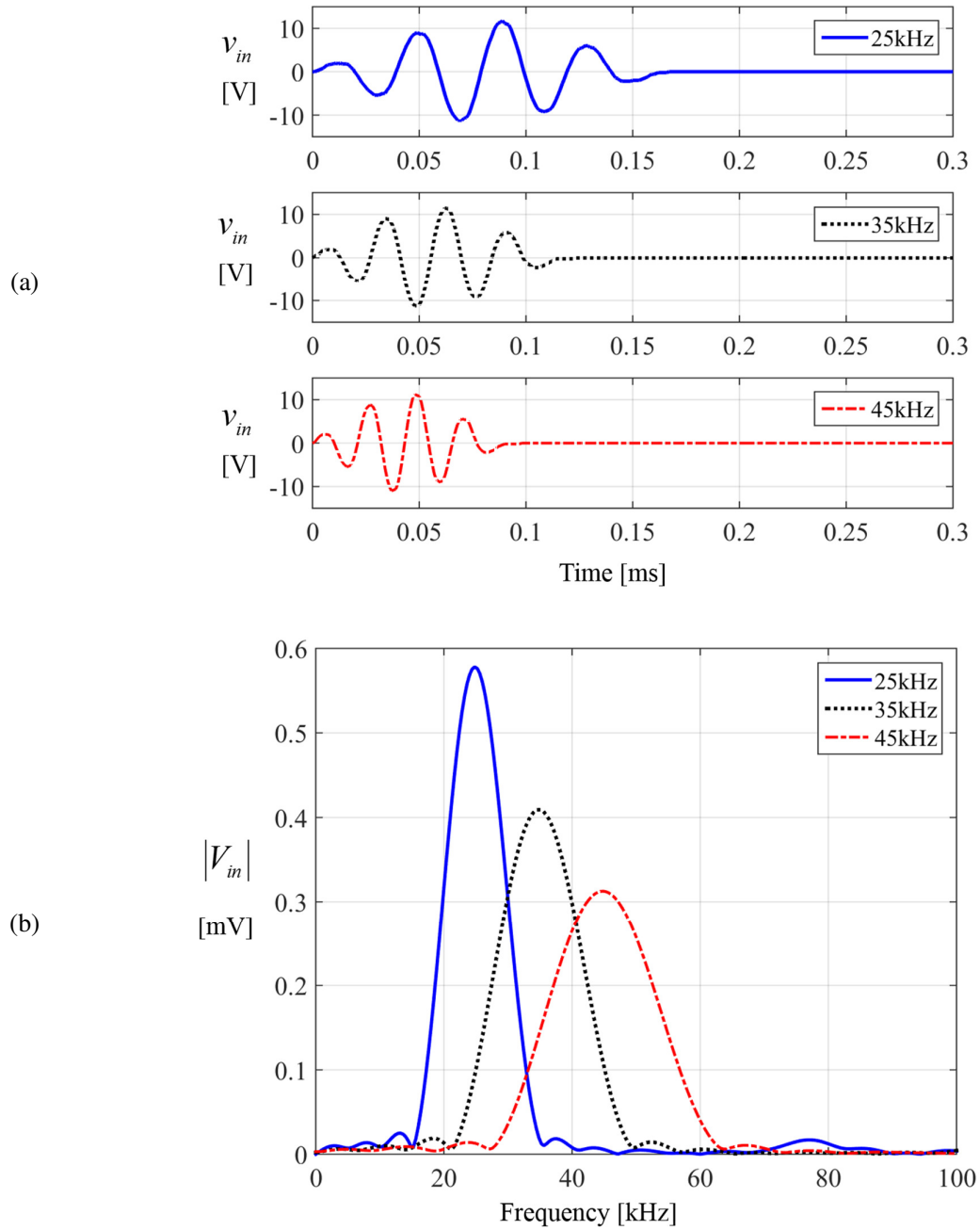
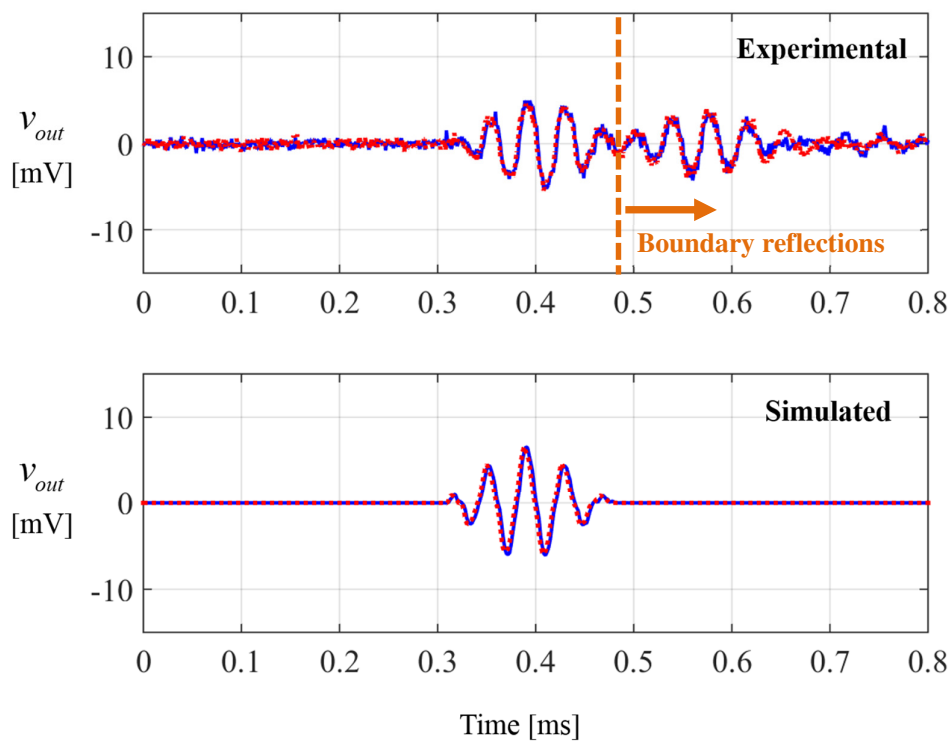


Figure 59 presents the experimental and simulated results for the pitch-catch configuration (transmitted waves) obtained by the Sensor 2 considering the input burst of 25kHz. As can be observed in the experimental curves the sensor also measured packets of waves related to boundary reflections from the right extremity (near the Sensor 2). However, the reflected waves arrives the sensor after the first packet of transmitted waves pass through it.

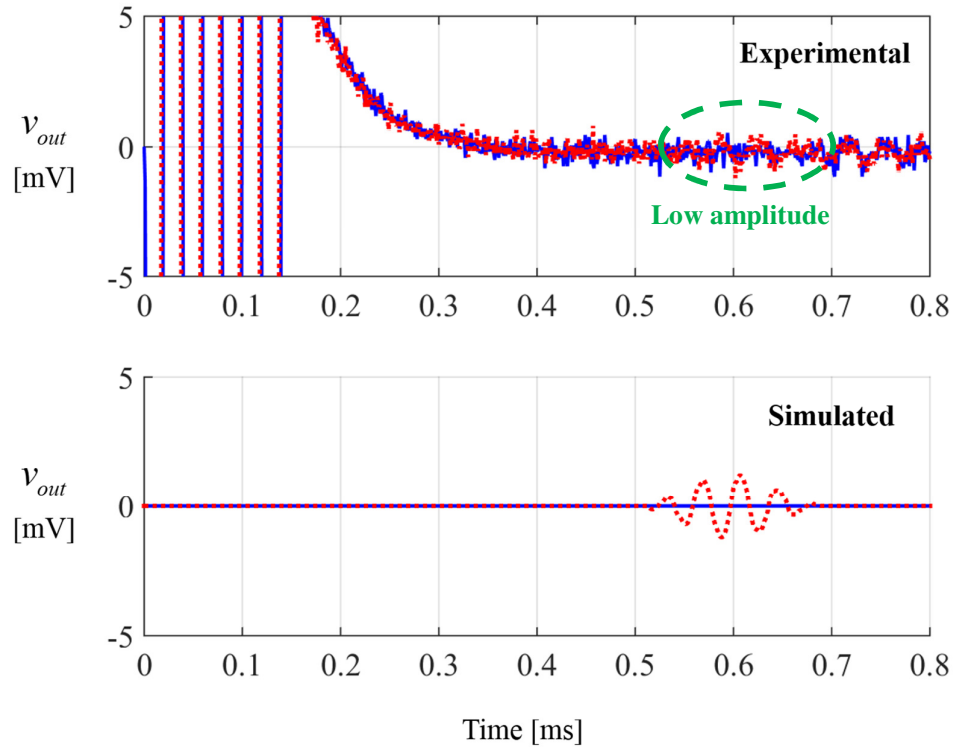
Figure 59: Comparison between simulated and experimental transmitted waves (25kHz) for baseline (blue solid line) and damage (red dot-dot line) conditions.



Source: Elaborated by author

Figure 60 presents the experimental and simulated results for the pulse-echo configuration (reflected waves) obtained by the Sensor 1 considering the input burst of 25kHz. As can be observed in the experimental curves was difficult to the experimental system to measure the longitudinal wave because the small amplitude. As discussed in the Chapter 3 the behavior of longitudinal waves at this frequency range does not exhibits the maximum amplitude because the optimum frequency range is around 50kHz for this length of damage.

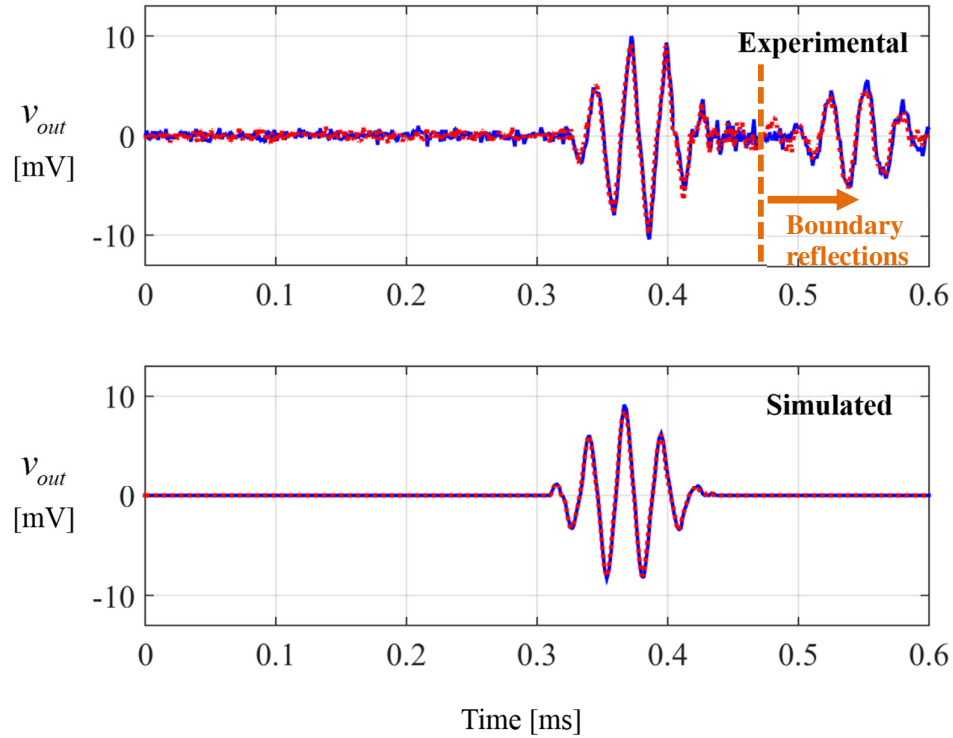
Figure 60: Comparison between simulated and experimental reflected waves (25kHz) for baseline (blue solid line) and damage (red dot-dot line) conditions.



Source: Elaborated by author

Figure 61 presents the experimental and simulated results for the pitch-catch configuration (transmitted waves) obtained by the Sensor 2 considering the input burst of 35kHz. Again the boundary influence can be observed in the experimental data. However, it still does not interact with the first packet of transmitted longitudinal wave.

Figure 61: Comparison between simulated and experimental transmitted waves (35kHz) for baseline (blue solid line) and damage (red dot-dot line) conditions.

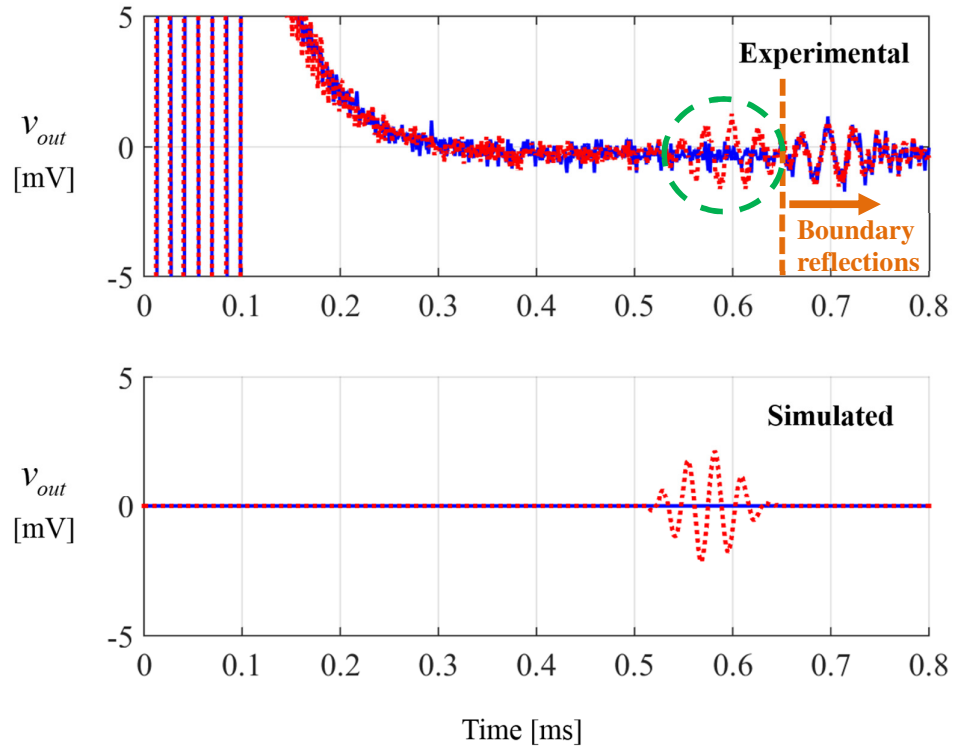


Source: Elaborated by author

Figure 62 presents the experimental and simulated results for the pulse-echo configuration (reflected waves) obtained by the Sensor 1 considering the input burst of 35kHz. As can be observed in the experimental curves, the amplitude of reflected packet is higher than obtained for the frequency range of 25kHz.

The second wave packet observed in the experimental curves of Sensor 1 is the first transmitted wave packet (by the damage) that propagates into the beam and reflects by the boundary and, then, propagates back to the Sensor 1.

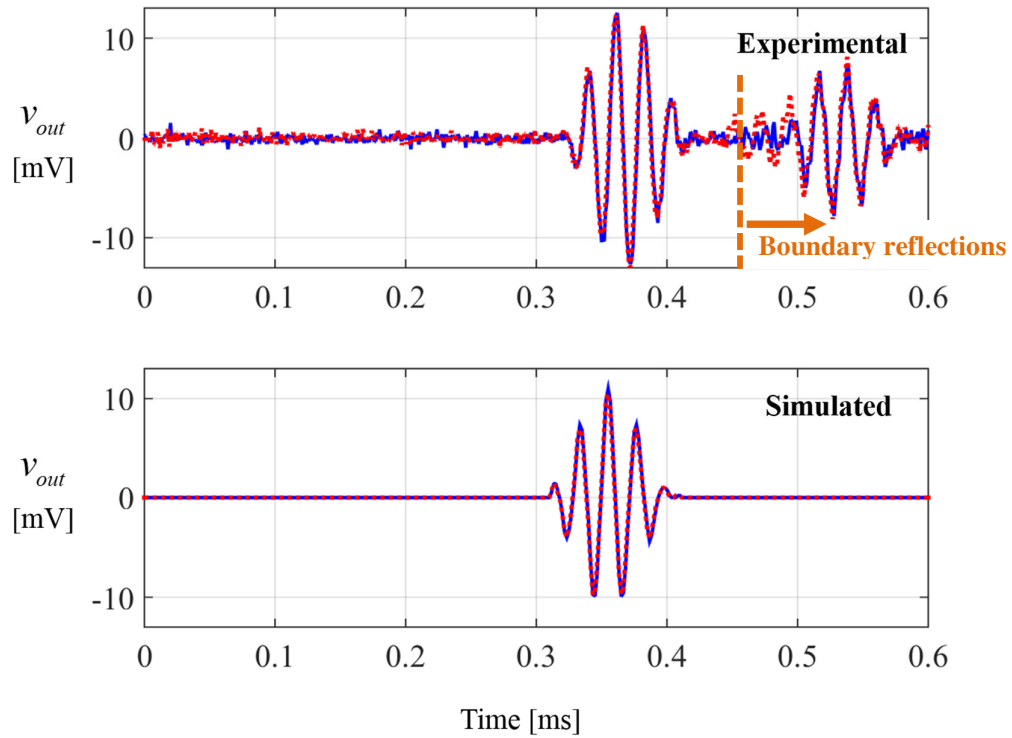
Figure 62: Comparison between simulated and experimental reflected waves (35kHz) for baseline (blue solid line) and damage (red dot-dot line) conditions.



Source: Elaborated by author

At least Figure 63 presents the experimental and simulated results for the pitch-catch configuration (transmitted waves) obtained by the Sensor 2 considering the input burst of 45kHz. The wave packet reflected at boundary can be observed in the experimental data. However, it still does not interact with the first packet of transmitted longitudinal wave.

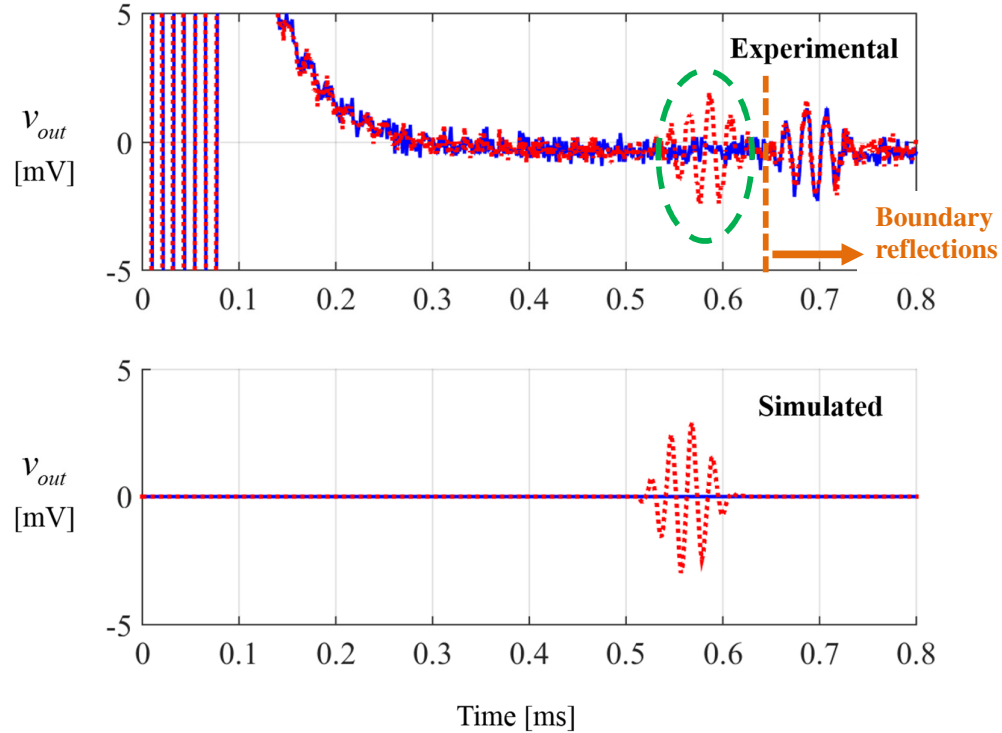
Figure 63: Comparison between simulated and experimental transmitted waves (45kHz of central frequency).



Source: Elaborated by author

Figure 64 presents the experimental and simulated results for the pulse-echo configuration (reflected waves) obtained by the Sensor 1 considering the input burst of 45kHz. At this case, the frequency range coincide with the optimum frequency range to detect the symmetric damage using a longitudinal wave incident. As can be observed the reflected wave packet is very sensible to detect the damage.

Figure 64: Comparison between simulated and experimental reflected waves (45kHz) for baseline (blue solid line) and damage (red dot-dot line) conditions.



Source: Elaborated by author

5.5 Conclusions

This chapter improves the comprehension of the physical aspects of waves propagation in time domain considering experimental curves. Here is presented the results obtained in time domain using the first study case and longitudinal incident wave into the damage.

The experimental setup was presented and explained and the behavior of the complete system was presented in time domain for three different frequency ranges excited by burst signals of five cycles (25kHz, 35kHz and 45kHz).

The results were discussed for the three frequency ranges and their results show good agreement between simulation and experimental results.

In conclusion, the correspondent model (first study case for a longitudinal incident wave) is validated and as consequence, the general observation of this work that reflected waves is better to detect the damage than transmitted waves (special in the optimum frequency range)

is also validated for the presented system. It because the amplitude change of the first packet reflected by the damage are visually higher than the amplitude change of the first packet transmitted by the damage, especially in the frequency range of 45kHz.

6 FINAL CONSIDERATIONS

In order to contribute for understanding of longitudinal and flexural waves behaviors interacting with corrosion-like damage, this thesis presented a study of these guided waves interacting with symmetric and asymmetric damage in an Euler-Bernoulli beam. The work was carried out considering an infinite aluminum beam with piezoelectric transducers used as actuators and sensors. It was also explored symmetric and asymmetric configurations of actuation.

Chapter 2 presented a brief introduction of wave motion for elastic structures and some basic aspects of harmonic wave motion to provide the background to understand some physicals behind of wave propagation. This chapter also presented the general solutions for the partial differential equations (EDP) for both longitudinal and flexural motion.

Chapter 3 presents the approach used in this work to obtain the wave motion in the studied configurations. As showed, the lengths of actuators, sensors and damage segments need to be set properly to avoid filtering effects of these elements. In practice, in the design of SHM system must to define each damage length that needs to be detect.

A general conclusion firstly presented in the Chapter 3 is that the sensitivity of reflected wave is higher than transmitted one. It because the reflected wave changes more substantially if the damage depth increases, in comparison with the transmitted longitudinal wave. Another one is that longitudinal waves are simplest to be used in a SHM system because its nature no dispersive. That means the optimum frequencies for a SHM system are not dependent of the damage severity. In other hand, for flexural waves there are many filtering effects to be avoided and the optimum frequencies ranges for SHM systems are depend of damage severity.

Chapter 4 expands the comprehension of the physical aspects of waves propagation in time domain. The results presented were obtained from simulations of the complete systems studied. The wave behavior of the study Case 2 in time domain is a superposition of the behaviors presented for the study Case 1 considering separate incident waves (longitudinal and flexural). The same for the Case 4 (asymmetric actuator and asymmetric damage) such behaviors are the superposition of presented for Case 3 for separated incident waves.

The most important general conclusion for all study case presented in the Chapter 4 is again that reflected waves showed more sensitivity to detect and quantify the damage than transmitted waves. Another general conclusion is that longitudinal wave incidents are easier to use for SHM systems than flexural incidents in order to avoid filtering effects.

However, in order to work with longitudinal waves is necessary to choose a good frequencies range to excite the longitudinal waves, otherwise the amplitude of this waves can be very small and the changes of amplitude related with the damage are difficult to measure.

A partial validation of the models is presented in the Chapter 5. It was for the Case 1 considering longitudinal incident waves. Good agreement between simulates curves and experimental data was observed. The results were discussed for the three frequency ranges and the general observation of this work that reflected waves is better to detect the damage than transmitted waves (special in the optimum frequency range) is also validated for the presented system. It because the amplitude change of the first packet reflected by the damage are visually higher than the amplitude change of the first packet transmitted by the damage, especially in the frequency range of 45kHz (optimum frequency range).

As this work considers the Euler-Bernoulli theory, which limits the frequency range for which the analysis are valid. However, attending its assumptions, it allows to predict the longitudinal and flexural waves behavior accurately to design a SHM system, as demonstrated in this thesis through experimental tests.

This work shows that the effectiveness of a SHM system depends on the frequency of the excitation selected. The criterions of this selection must consider the lengths of the actuator, sensors, and length of damage which desires to be monitored. Note that because of this, the length of damage must be an initial requirement to design a SHM system. Besides these lengths, for practical applications, once a damage can be detected if it takes place between a piezo actuator and a sensor, the length between these transducers should be well known to the analyst to separate the waves generated by the actuator from other ones reflected on the structure ends (the boundary conditions).

6.1 Further works

Future works can be derived from the studies and conclusions presented in this thesis, some of them are

- To adapt the state model presented in the Chapter 3 comprising the Timoshenko theory in order to increase the operational frequency range and understand the behavior of shear waves interacting with symmetric and asymmetric damage;
- To adapt the models considering more realistic corrosion like damage;
- Study the influence of damage length (l_D) for symmetric and asymmetric damage

configurations;

- Carry out more experiments in order to validate the flexural wave behaviors for symmetric damage;
- Validate experimentally the longitudinal and flexural waves interaction with asymmetric damage;
- Expands the approach presented in the Appendix A.2 for flexural waves in order to understand how many packets are enough to represent the physical interaction of flexural waves with symmetric damage;
- Investigates how guided waves interact with corrosion damage in more complex structures (plates, shells and thick beams);
- Adapt the models presented for asymmetric damage to model a crack ($l_D \rightarrow 0$)

REFERENCES

- ACHENBACH, J. D. *Wave propagation in elastic solids*, New York: North-Holland, 1984.
- ADAMS, D. E. *Health monitoring of structural materials and components: methods and applications*. Chichester; West Sussex: John Wiley & Sons, 2007.
- ALLEYNE, D. N.; CAWLEY, P. The interaction of Lamb waves with defects. *IEEE Transactions on Ultrasonics, Ferroelectrics, and Frequency Control*, Pistacaway, v. 39, n. 3, p. 381-397, 1992.
- AULD, B. A. *Acoustic fields and waves in solids*. 2. ed. v. 1-2. [S. l.], Kreigerishing, 1990.
- AYALA, P. C. *Detecção de danos em estruturas guiadas usando ondas de alta frequência*. 2015. 83 f. Dissertação (Mestrado em Engenharia Mecânica) – Faculdade de Engenharia, Universidade Estadual Paulista – UNESP, Ilha Solteira, 2015.
- BALAGEAS, D.; FRITZEN, C.-P.; GÜEMES, A. *Structural health monitoring*. Oxford: Hermes Science, 2006.
- BRENNAN, M. J. *Active control of waves on one-dimensional structures*. 1994. 365 f. Thesis (Doctoral) - Faculty of Engineering and Applied Science, Institute of Sound and Vibration Research - ISVR, University of Southampton, Southampton, 1994.
- BRENNAN, M. J.; ELLIOTT, S. J.; PINNINGTON, R. J. The dynamic coupling between piezoceramic actuators and a beam. *Journal of the Acoustical Society of America*, Melville, v. 102, n. 4, p. 1931–1942, 1997.
- BRENNAN, M. J.; TANG, B.; ALMEIDA, F. C. L. Waves motion in elastic structures. In: LOPES JR., V.; STEFFEN JR., V.; SAVI, M. A. (ed.). *Dynamics of smart systems and structures, concepts and applications*. London: Springer, 2016.
- BOLLER, C.; CHANG, F-K.; FUJINO, Y. *Encyclopedia of structural health monitoring*. New York: John Wiley & Sons, 2009.
- BOLLER, C.; STASZEWSKI, W. J.; TOMLINSON, G. *Health Monitoring of Aerospace Structures*, Hoboken, NJ: Wiley. 2004,
- CHAN, H.; MASSEREY, B.; FROMME, P. High frequency guided ultrasonic waves for hidden fatigue crack growth monitoring in multi-layer model aerospace structures. *Smart Materials and Structures*, Bristol, v. 24, p. 1–10, 2015.
- CHANG, P. C.; FLATAU, A.; LIU, S. C. Review paper: health monitoring of civil infrastructure. *Structural Health Monitoring*, London, v. 2, p. 257–67, 2003.
- CHEW, D.; FROMME, P. Monitoring of corrosion damage using high-frequency guided ultrasonic waves. In: SPIE 9064, HEALTH MONITORING OF STRUCTURAL AND BIOLOGICAL SYSTEMS 2014, 2014. San Diego. *Proceedings [...]* Bellingham: ASML, 2014.

CIANG, C. C.; LEE, J.-R.; BANG, H.-J. Structural health monitoring for a wind turbine system: a review of damage detection methods. *Measurement Science and Technology*, Bristol, v. 19, p. 122001, 2008.

CREMER, L.; HECKL, M.; PETERSSON, B. A. T. *Structure-borne sound: structural vibrations and sound radiation at audio frequency*. 3rd ed. Belin: Springer, 2005.

DILIGENT, O.; GRAHN, T.; BOSTRÖM, A.; CAWLEY, P.; LOWE, M. J. S. The low-frequency reflection and scattering of the S0 Lamb mode from a circular through-thickness hole in a plate: Finite Element, analytical and experimental studies. *The Journal of the Acoustical Society of America*, Melville, v. 112, p. 2589, 2002. DOI: 10.1121/1.1512292, 2002.

DEMMA, A.; CAWLEY, P.; LOWEA, M.; ROOSENBRAND, A. G.; PAVLAKOVIC, B. The reflection of guided waves from notches in pipes: a guide for interpreting corrosion measurements. *NDT&E Int.*, London, v. 37, p. 167–80, 2004.

DOEBLING, S. W.; FARRAR, C. R.; PRIME, M. B. A summary review of vibration-based damage identification methods. *Shock and Vibration Digest*, Thousand Oaks, v. 30, n. 2, p. 91–105, 1998.

DOYLE, J. *Wave propagation in structures: spectral analysis using fast discrete fourier transforms*. New York: Springer, 1997. 2nd ed. (Mechanical Engineering Series)

ERVIN, B. L.; KUCHMA, D. A.; BERNHARD, J. T.; REIS, H. Monitoring corrosion of rebar embedded in mortar using high-frequency guided ultrasonic waves. *Journal of Engineering Mechanics*, Reston, v. 135, n. 1, p. 9–19, 2009.

FAHY, F. J., *Foundations of engineerig acoustics*. San Diego; London: Academic Press, 2001.

FARHIDZADEH, A.; SALAMONE, S. Reference- free corrosion damage diagnosis in steel strands using guided ultrasonic waves. *Ultrasonics*, Amsterdam, v. 57, p. 198-208, 2015.

GAO, H.; ROSE, J. L. Goodness dispersion curves for ultrasonic guided wave based SHM: a sample problem in corrosion monitoring. *The aeronautical Journal*, Cambridge, v. 114, n. 1151, p. 49-56, 2010.

GAO, Y.; BRENNAN, M. J.; JOSEPH, P. F. On the effects of reflections on time delay estimation for leak detection in buried plastic water pipes. *Journal of Sound and Vibration*, London, v. 325, p. 649-663, 2009.

GIURGIUTIU, V. *Structural health monitoring with piezoelectric wafer active sensors*. San Diego; London: Academic Press, 2007.

GIURGIUTIU, V.; ROMAN, C.; LIN, B.; FRANKFORTER, E. Omnidirectional piezo-optical ring sensor for enhanced guided wave structural health monitoring. *Smart Materials and Structures*, Bristol, v. 24, p. 1–13, 2015.

- GONSALEZ, C. G. *Metodologias para reconhecimento de padrões em sistemas SHM utilizando a técnica da impedância eletromecânica (E/M)*. 2012. 116 f. Dissertação (Mestrado em Engenharia Mecânica) - Faculdade de Engenharia, Universidade Estadual Paulista “Júlio de Mesquita Filho”, Ilha Solteira, 2012.
- GONSALEZ, C. G.; DA SILVA, S.; BRENNAN, M. J.; LOPES JR., V. Structural damage detection in an aeronautical panel using analysis of variance. *Mechanical Systems and Signal Processing*, London, v. 52-53, p. 206-216, 2015.
- GRAFF, K. F. *Wave motion in elastic solids*, Oxford: Clarendon, 1975.
- HAGEDORN, P.; DASGUPTA, A. *Vibrations and waves in continuous mechanical systems*. New York: Wiley, 2007.
- HARRI, K.; GUILLAUME, P.; VANLANDUIT, S. On-line damage detection on a wing panel using transmission of multisine ultrasonic waves. *NDT&E Int.*, London, v. 41, p. 312–317, 2008.
- HIGUTI, R. T.; MARTÍNEZ-GRAULLERA, O.; MARTÍN, C. J.; LUIS ELVIRA, A. O.; ESPINOSA, F. M. Damage characterization using guided-wave linear arrays and image compounding techniques, *IEEE Transactions on Ultrasonics, Ferroelectrics and Frequency Control*, Piscataway, v. 159, n. 9, p. 1985–1995, 2010.
- INMAN, D. J.; FARRAR, C. R.; LOPES JR., V.; STEFFEN JR., V. *Damage prognosis for aerospace, civil and mechanical systems*. Chichester: John Wiley & Sons, 2005.
- KAMAL, A.; GIURGIUTIU, V. Shear horizontal wave excitation and reception with shear horizontal piezoelectric wafer active sensor (SH-PWAS). *Smart Materials and Structures*, Bristol, v. 23, n. 8, p. 085019, 2014
- KOLALOWSKI, P. Structural health monitoring: a review with the emphasis on low-frequency methods. *Engineering Transactions*, Warsaw, v. 55, n. 3, p. 239–275, 2007.
- MANKINS, J. C. *Technology readiness levels: a white paper*. [S. l.]: NASA, Office of Space Access and Technology, Advanced Concepts Office, 1995.
- MASSEREY, B.; FROMME, P. Surface defect detection in stiffened plate structures using Rayleigh-like waves. *NDT&E Int.*, London, v. 42, p. 564–72, 2009.
- MASSEREY, B.; FROMME, P. Fatigue crack growth monitoring using high-frequency guided waves. *Structural Health Monitoring*, London, v. 12, p. 484–493, 2013.
- MASSEREY, B. AND FROMME, P. In-situ monitoring of fatigue crack growth using high frequency guided waves. *NDT&E Int.*, London, v. 71, p. 1–7, 2015.
- MASSEREY, B.; FROMME, P. Analysis of high frequency guided wave scattering at a fastener hole with a view to fatigue crack detection. *Ultrasonics*, Amsterdam, v. 76, p. 78–86, 2017.

- MASSEREY, B.; RAEMY, C.; FROMME, P. High-frequency guided ultrasonic waves for hidden defect detection in multi-layered aircraft structures. *Ultrasonics*, Amsterdam, v. 54, p. 1720–1728, 2014.
- MITRA, M.; GOPALAKRISHNAN, S. Guided wave based structural health monitoring: A review. *Smart Materials and Structures*, Bristol, v. 25, n. 5, p. 053001, 2016.
- MOREAU, L.; CALEAP, M.; VELICHKO, A.; WILCOX, P. D. Scattering of guided waves by through-thickness cavities with irregular shapes. *Wave Motion*, Amsterdam, v. 48, p. 586-602, 2011.
- MOREAU, L.; CALEAP, M.; VELICHKO, A.; WILCOX, P. D. Scattering of guided waves by flat-bottomed cavities with irregular shapes. *Wave Motion*, Amsterdam, v. 49, p. 375-387, 2012.
- NAYFEH, A. H. *Wave Propagation in layered anisotropic media with applications to composites*. Netherlands: Elsevier Science, 1995.
- OPPENHEIM, A. V.; WILLSKY, A. S. *Sinai e sistemas*. New York: Pearson, 2010.
- OSTACHOWICZ, W.; KUDELA, P.; KRAWCZUK, M.; ZAK, A. *Guided waves in structures for SHM: the time-domain spectral element method*. New York: Wiley, 2012.
- PALACZ, M. Spectral methods for modelling of wave propagation in structures in terms of damage detection: a review. *Applied Sciences*, Bucharest, v. 8, p. 1124, 2018. DOI:10.3390/app8071124.
- PRADO, V. T.; HIGUTI, R. T.; KITANO, C.; MARTÍNEZ-GRAULLERA, O.; ADAMOWSKI, J. C. Lamb mode diversity imaging for non-destructive testing of plate-like structures. *NDT&E International*, London, v. 159, p. 86–95, 2013.
- PODDAR, B.; GIURGIUTIU, V.; PODDAR, B.; GIURGIUTIU, V. Experimental validation of analytical model for lamb wave interaction with geometric discontinuity. In: 2015 SMART STRUCTURES AND NDE, 2015, San Diego. *Proceedings [...]* [S. l.: s. n.], 2015. p. 9437-9469.
- ROSE, J. L. *Ultrasonic waves in solid media*. Cambridge: Cambridge University Press, 1999.
- ROSE, J. L. An introduction to ultrasonic guided waves. In: MIDDLE EAST NDT CONFERENCE AND EXHIBITION, 4th., 2007, Kingdom of Bahrain. *Proceeding [...]* [S. l.: s. n.], 2007.
- ROSE, J. L. Guided wave nuances for ultrasonic nondestructive evaluation. *IEEE Transactions on ultrasonics, ferroelectrics, and frequency control*, Piscataway, v. 47, n. 3, p. 575-583, May 2000.
- ROY, S.; LADPLI, P.; CHANG, F. Load monitoring and compensation strategies for guided-wave based structural health monitoring using piezoelectric transducers. *Journal of Sound and Vibration*, London, v. 351, p. 206–220, 2015.

ROY, S.; LONKAR, K.; JANAPATI, V.; CHANG, F. A novel physics-based temperature compensation model for structural health monitoring using ultrasonic guided waves, *Structural Health Monitoring*, London, v. 13, n. 3, p. 321–342, 2014.

RULLI, R. P., GONSALEZ BUENO, C. G., DOTTA, F. AND SILVA, P. A. Damage detection systems for commercial aviation. In LOPES JR., V.; STEFFEN JR., V.; SAVI, M. A. (ed). *Dynamics of smart systems and structures, concepts and applications*. New York: Springer, 2016. p. 329-342.

SANTOS, L. G. D. Embraer perspective on the challenges for the introduction of scheduled shm (s-shm) applications into commercial aviation maintenance programs. *Key engineering materials*, Pfaffikon, v. 558, p. 323-330, 2013.

RYTTER, A. *Vibrational based inspection of civil engineering structures*. 1993. 193 f. Thesis (Ph. D. Dissertation) - Department of Building Technology and Structural Engineering, Aalborg University, Denmark, 1993.

SAE INTERNATIONAL. *Guidelines for implementation of structural health monitoring on fixed wing aircraft ARP 6461*. [S. l.]: SAE International, 2013. 95 p.

SHARMA, S.; MUKHERJEE, A. Longitudinal guided waves for monitoring chloride corrosion in reinforcing bars in concrete. *Structural Health Monitoring*, London, v. 9, n. 6, p. 555-13, 2010.

SHEN, Y.; GIURGIUTIU, V. Wave form revealer: an analytical framework and predictive tool for the simulation of multi-modal guided wave propagation and interaction with damage. *Structural Health Monitoring*, London, v. 13, p. 491-511, 2014.

SHEN, Y.; GIURGIUTIU, V. Effective non-reflective boundary for Lamb waves: theory, finite element implementation, and applications. *Wave Motion*, Amsterdam, v. 58, p. 22–41, 2015.

SHEN, Y.; GIURGIUTIU, V. Combined analytical FEM approach for efficient simulation of Lamb wave damage detection. *Ultrasonics*, Amsterdam, v. 69, p. 116-128, 2016.

SOLIMAN, M.; BARONE, G.; FRANGOPOL, D. M. Fatigue reliability and service life prediction of aluminum naval ship details based on monitoring data. *Structural Health Monitoring*, London, v. 14, p. 3-19, 2015.

STEPINSKI, T.; UHL, T.; STASZEWSKI, W. J. *Advanced structural damage detection: from theory to engineering applications*. Chichester, West Sussex: Wiley, 2013.

SU, Z.; YE, L.; LU, Y. Guided lamb waves for identification of damage in composite structures: a review. *Journal of Sound and Vibration*, London, v. 295, p. 753–80, 2006.

SU, Z.; WANG, C.; PAN, N.; YE, L.; ZHOU, L.-M. Assessment of delamination in composite beams using shear horizontal (SH) wave mode. *Composites Science and Technology*, Kidlington, v. 67, p. 244–251, 2007.

TAKIY, A. E.; KITANO, C.; HIGUTI, R. T.; GRANJA, S. C. G.; PRADO, V. T. Ultrasound imaging of immersed plates using high-order Lamb modes at their low attenuation frequency bands. *Mechanical Systems and Signal Processing*, London, v. 96, p. 321-332, 2017.

TERRIEN, N.; ROYER, D.; LEPOUTRE, F.; DÉOM, A. Numerical predictions and experiments for optimizing hidden corrosion detection in aircraft structures using Lamb modes. *Ultrasonics*, Amsterdam, v. 46, p. 251-265, 2007.

VIKTOROV, I. A. *Rayleigh and lamb waves: physical theory and applications*. New York: Plenum Press, 1967.

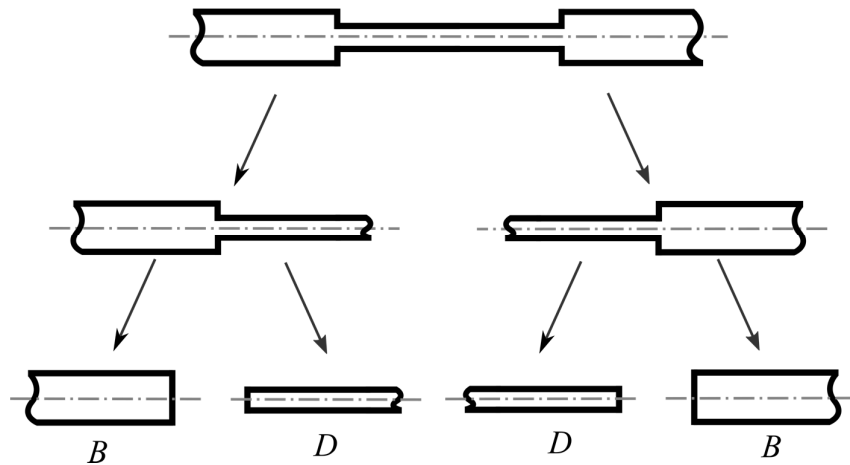
WILCOX, P. D.; VELICHKO, A.; DRINKWATER, B. W.; CROXFORD, A. J.; TODD, M. D. Scattering of plane guided waves obliquely incident on a straight feature with uniform cross-section. *The Journal of the Acoustical Society of America*, New York, v. 128, p. 2715, 2010. DOI: 10.1121/1.3488663.

A.1 WAVE MODELS OF SINGLE DISCONTINUITIES

As in Chapter 3, in order to model the discontinuities the approach used here are based is the passive effects of approach proposed by Brennan (1994) and Brennan *et al.* (1997) for actuator (complete model).

To better understand the wave interaction with a symmetric damage section is interesting to separate the damaged section in two changes of cross-sectional area, as illustrated on Figure 65. “B” (for beam) and “D” (for discontinuity) call the segments.

Figure 65: Division of a symmetric damage section.



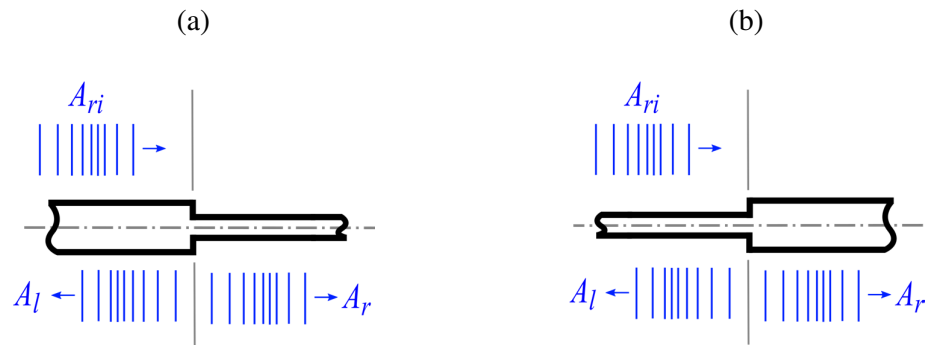
Source: Elaborated by author

The aims of this Appendix is presents the models for changes of sectional area (symmetric and asymmetric) and some analysis of the scattered wave's coefficients.

A.1.1 Symmetric Change of Cross-Sectional Area

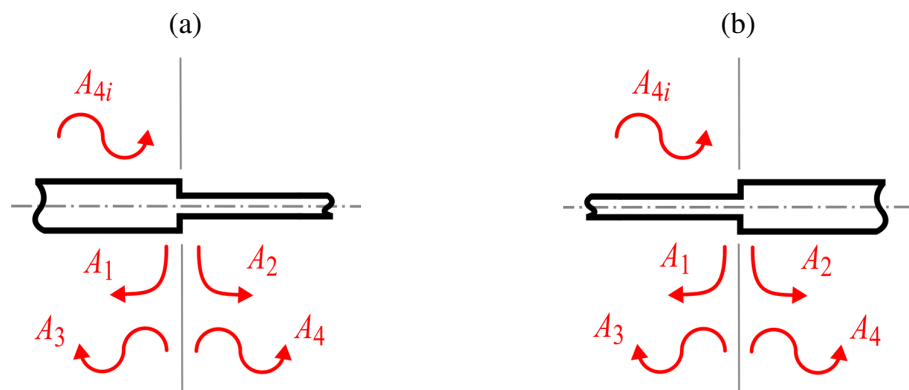
Analyzing each part of Figure 65 and considering longitudinal and flexural waves incidents, Figures 66 and 67 show the scattering of waves for symmetric reducing and amplifying cross-sectional area change. As can be noted, longitudinal wave incident scatter in longitudinal waves reflected and transmitted, as Figure 66. Likewise that a flexural wave incident results in near-field and propagation waves (reflected and transmitted), as Figure 67.

Figure 66: Scattering waves by symmetric change of cross sectional area considering a longitudinal incident wave; (a) Reducing and; (b) Amplifying.



Source: Elaborated by author

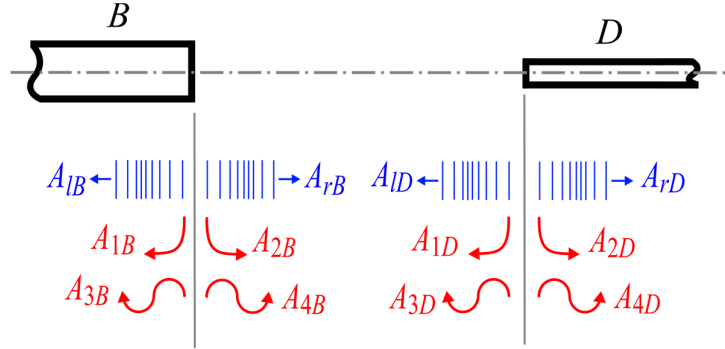
Figure 67: Scattering waves by symmetric change of cross sectional area considering an incident flexural propagating wave; (a) Reducing and; (b) Amplifying.



Source: Elaborated by author

To obtain the reflected and transmitted waves from a cross sectional area is important first see all waves presented on the area change, as Figure 68.

Figure 68: Waves presented on the area change.



Source: Elaborated by author

For each segment (B and D) at the area change there is a state vector that by continuity, they must be the same:

$$\mathbf{h}_B = \mathbf{h}_D \quad (98)$$

or

$$\mathbf{H}_B \mathbf{a}_B - \mathbf{H}_D \mathbf{a}_D = \mathbf{0} \quad (99)$$

where \mathbf{h}_B and \mathbf{h}_D are the state vectors at extremity of beam and discontinuity, respectively. \mathbf{H}_B and \mathbf{H}_D are the transformation matrixes of beam segment and discontinuity segment, respectively. \mathbf{a}_B and \mathbf{a}_D are the vector of waves amplitudes in the extremity of beam and discontinuity, respectively, the vectors of waves amplitude are:

$$\mathbf{a}_B = \{A_{1B} \quad A_{3B} \quad A_{1B} \quad A_{2B} \quad A_{4B} \quad A_{rB}\}^T \quad (100)$$

$$\mathbf{a}_D = \{A_{1D} \quad A_{3D} \quad A_{1D} \quad A_{2D} \quad A_{4D} \quad A_{rD}\}^T \quad (101)$$

Considering the area discontinuity as a black box is possible to define the outgoing waves from the section change using the following equation (Brennan *et al.*, 1997):

$$\boldsymbol{\gamma}\mathbf{a}_o + \boldsymbol{\mu}\mathbf{a}_i = \mathbf{0} \quad (102)$$

where \mathbf{a}_o is the vector of outgoing waves amplitudes (reflected and transmitted), the \mathbf{a}_i is the vector of ingoing wave amplitudes (incidents), given by:

$$\mathbf{a}_o = \{A_{1B} \ A_{3B} \ A_{tB} \ A_{2D} \ A_{4D} \ A_{rD}\}^T \quad (103)$$

$$\mathbf{a}_i = \{A_{1D} \ A_{3D} \ A_{tD} \ A_{2B} \ A_{4B} \ A_{rB}\}^T \quad (104)$$

and the matrices are given by:

$$\boldsymbol{\gamma} = [(\mathbf{H}_B)_1 \ (\mathbf{H}_B)_2 \ (\mathbf{H}_B)_3 \ (-\mathbf{H}_D)_4 \ (-\mathbf{H}_D)_5 \ (-\mathbf{H}_D)_6] \quad (105)$$

$$\boldsymbol{\mu} = [(-\mathbf{H}_D)_1 \ (-\mathbf{H}_D)_2 \ (-\mathbf{H}_D)_3 \ (\mathbf{H}_B)_4 \ (\mathbf{H}_B)_5 \ (\mathbf{H}_B)_6] \quad (106)$$

where $(\)_{1-6}$ denotes the columns of the respective matrices, the $\boldsymbol{\gamma}$ and $\boldsymbol{\mu}$ are given writing Eq. (99) equal to Eq. (74).

This way, is possible to find the outgoing waves, given by:

$$\mathbf{a}_o = -\boldsymbol{\gamma}^{-1}\boldsymbol{\mu}\mathbf{a}_i \quad (107)$$

Considering the outgoing waves, \mathbf{a}_o , the waves going to left side are called reflected waves and the waves going to the right side are called transmitted waves. Similarly, to the presented

notation it can be used:

$$\mathbf{a}_o = \mathbf{a}_o^- + \mathbf{a}_o^+ \quad (108)$$

where the superscript ()⁻ indicates the waves travels to the left side of structure and ()⁺ represents the waves going to the right side. Alternatively, it is possible to use the following notation:

$$\mathbf{a}_o^- = \mathbf{a}_{Ref} = \{A_{1B} \quad A_{3B} \quad A_{lB} \quad 0 \quad 0 \quad 0\}^T \quad (109)$$

$$\mathbf{a}_o^+ = \mathbf{a}_{Trans} = \{0 \quad 0 \quad 0 \quad A_{2D} \quad A_{4D} \quad A_{rD}\}^T \quad (110)$$

where \mathbf{a}_{Ref} is the vector of reflected waves and \mathbf{a}_{Trans} the vector of transmitted waves.

A.1.1.1 Longitudinal Incident Wave

From the approach present and for the particular case of a longitudinal right going wave incite in the cross-sectional area change is possible to write the following transfer functions:

$$\frac{A_l}{A_{ri}} = \frac{A_{lB}}{A_{rB}} = \frac{S_B - S_D}{S_B + S_D} \quad (111)$$

$$\frac{A_r}{A_{ri}} = \frac{A_{rD}}{A_{rB}} = \frac{2S_B}{S_B + S_D} \quad (112)$$

where S_B and S_D are the cross-sectional areas of the beam and discontinuity, respectively.

Defining r as the cross-sectional area ratio:

$$r = \frac{S_D}{S_B} \quad (113)$$

The Eqs. (68) and (69) can be rewritten as:

$$\frac{A_l}{A_{ri}} = \frac{A_{lB}}{A_{rB}} = \frac{1-r}{1+r} \quad (114)$$

$$\frac{A_r}{A_{ri}} = \frac{A_{rD}}{A_{rB}} = \frac{2}{1+r} \quad (115)$$

A.1.1.2 Flexural Incident Wave

From the approach present and for the particular case of a flexural right going wave incite in the cross-sectional area change is possible to write the following transfer functions:

$$\frac{A_3}{A_{4i}} = \frac{A_{3B}}{A_{4B}} = -\frac{jI^2k^4 + 2Ik^3 - 2jIk^2 - 2Ik + j}{I^2k^4 + 2Ik^3 + 2Ik^2 + 2Ik + 1} \quad (116)$$

$$\frac{A_4}{A_{4i}} = \frac{A_{4D}}{A_{4B}} = \frac{2Ik^3 + 2Ik^2 + 2k + 2}{I^2k^5 + 2Ik^4 + 2Ik^3 + 2Ik^2 + k} \quad (117)$$

where $I = I_D/I_B$ is the ratio of second moment of inertia for the discontinuity and beam, $k = k_{jD}/k_{jB}$ is the ratio of flexural wavenumbers for the discontinuity and beam.

The Eqs. (116) and (117) can be rewritten as:

$$\frac{A_3}{A_{4i}} = \frac{A_{3B}}{A_{4B}} = \frac{2h\sqrt{h}(h-1) - j(h^2-1)^2}{(h^2+1)^2 + 2h\sqrt{h}(h+1)} \quad (118)$$

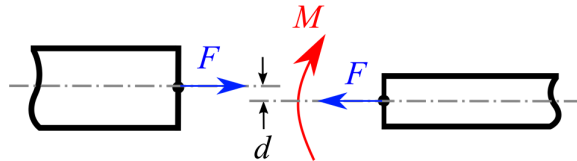
$$\frac{A_4}{A_{4i}} = \frac{A_{4D}}{A_{4B}} = \frac{2\sqrt{h}(h^2+1)(\sqrt{h}+1)}{(h^2+1)^2 + 2h\sqrt{h}(h+1)} \quad (119)$$

where $h = t_D/t_B$ is the ratio of depth for the discontinuity and beam.

A.1.2 Asymmetric Change of Cross-Sectional Area

Due the asymmetry of area change occurs a moment, proportional to the distance between the neutral axis of the beam segments, as illustrated on Figure 69.

Figure 69: Efforts on the asymmetric change of cross-sectional area.



Source: Elaborated by author

This way, the state vector on the junctions has to be modified to account for this:

$$\mathbf{h}_{\hat{D}} = \mathbf{h}_D + \mathbf{h}_{Asym} \quad (120)$$

where $\mathbf{h}_{\hat{D}}$ is the state vector of asymmetric damage, \mathbf{h}_D is the state vector of symmetric damage, and \mathbf{h}_{Asym} is the state vector containing the efforts related with the moment due the distance between the neutral axis, given by:

$$\mathbf{h}_{Asym} = \{\theta d \quad 0 \quad 0 \quad -Fd \quad 0 \quad 0\}^T \quad (121)$$

or

$$\mathbf{h}_{Asym} = \mathbf{T}_{Asym} \mathbf{h}_D \quad (122)$$

Where \mathbf{T}_{Asym} is given by:

$$\mathbf{T}_{Asym} = \begin{bmatrix} 0 & 0 & d & 0 & 0 & 0 \\ 0 & 0 & 0 & 0 & 0 & 0 \\ 0 & 0 & 0 & 0 & 0 & 0 \\ 0 & 0 & 0 & 0 & 0 & -d \\ 0 & 0 & 0 & 0 & 0 & 0 \\ 0 & 0 & 0 & 0 & 0 & 0 \end{bmatrix} \quad (123)$$

Working with Eqs. (120) and (122) is possible to write:

$$\mathbf{h}_{\hat{D}} = (\mathbf{I} + \mathbf{T}_{Asym}) \mathbf{h}_D \quad (124)$$

and

$$\mathbf{H}_{\hat{D}} = (\mathbf{I} + \mathbf{T}_{Asym}) \mathbf{H}_D \quad (125)$$

Made these considerations the way to model the interactions of waves at an asymmetric cross-sectional area change is the same as presented by the symmetric case, Section A.1. But here the vectors of waves and states for the symmetric case need to be replaced by respective vectors for the asymmetric case. The same for the transformation matrix (\mathbf{H}). This way, the matrices $\boldsymbol{\gamma}$ and $\boldsymbol{\mu}$ become:

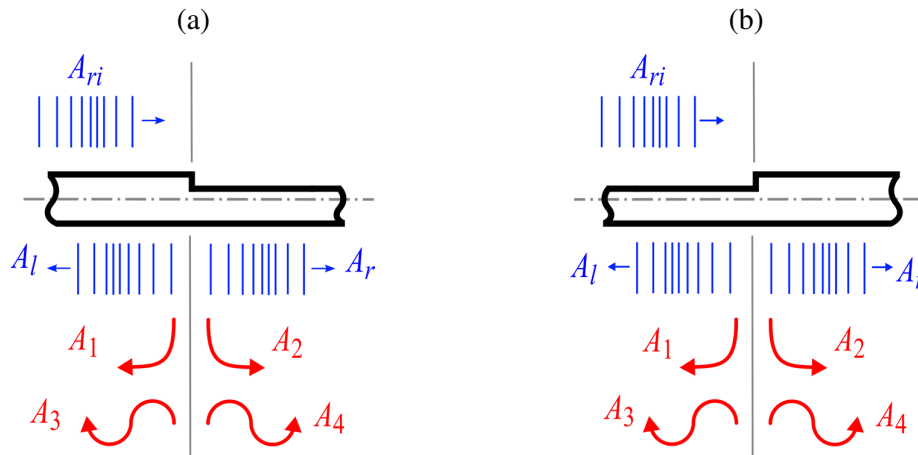
$$\gamma = [(\mathbf{H}_B)_1 \quad (\mathbf{H}_B)_2 \quad (\mathbf{H}_B)_3 \quad (-\mathbf{H}_{\hat{D}})_4 \quad (-\mathbf{H}_{\hat{D}})_5 \quad (-\mathbf{H}_{\hat{D}})_6] \quad (126)$$

$$\mu = [(-\mathbf{H}_{\hat{D}})_1 \quad (-\mathbf{H}_{\hat{D}})_2 \quad (-\mathbf{H}_{\hat{D}})_3 \quad (\mathbf{H}_B)_4 \quad (\mathbf{H}_B)_5 \quad (\mathbf{H}_B)_6] \quad (127)$$

A.1.2.1 Longitudinal Incident Wave

This way, for asymmetric change of cross-sectional area a longitudinal wave incident scatter in longitudinal and flexural waves (reflected and transmitted), as Figure 70.

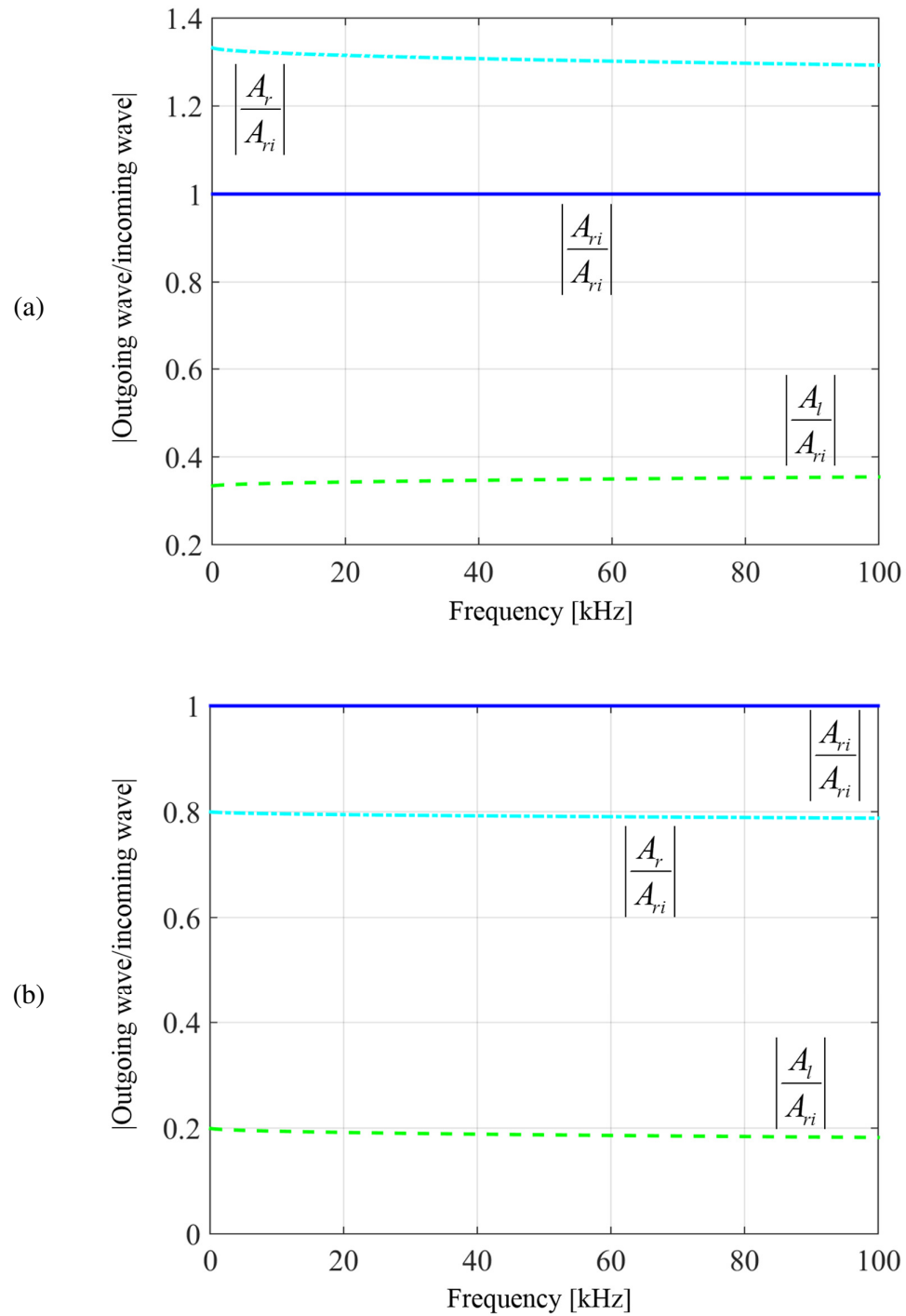
Figure 70: Scattering waves by an asymmetric change of cross sectional area considering a longitudinal incident wave; (a) Reducing and; (b) Amplifying.



Source: Elaborated by author

Then, considering a right going longitudinal waves, as figure above, focus on the asymmetric change of cross-sectional area, for the system described on Table 3.1 some analyses of reflected and transmitted waves for reducing 50% of cross-sectional area and amplifying 50% of cross-sectional area can be seen on Figure 71 and Figure 72.

Figure 71: Amplitude of longitudinal scattering waves by asymmetric change of cross sectional area considering an incident longitudinal wave; (a) Reducing 50% and; (b) Amplifying 50%.



Source: Elaborated by author

As can be noted on Figure 71(a) reducing the cross-sectional area the amplitude of transmitted wave are higher than the incident wave. It occurs because the impedance of the segment “D” is smaller than the impedance of segment “B”. This way, the segment “D” represents smaller resistance to the wave propagation than the segment “B”, as consequence, the amplitude of wave in the segment “D” become bigger.

In the other hand, the amplitude of reflected wave are smaller than the amplitude of incident wave because the impedance of wave propagation medium is the same (segment “B”) and occurred a division of incident wave power on the cross-sectional change. The power of longitudinal incident wave was divided for power of longitudinal reflected and transmitted, and power of flexural reflected and transmitted.

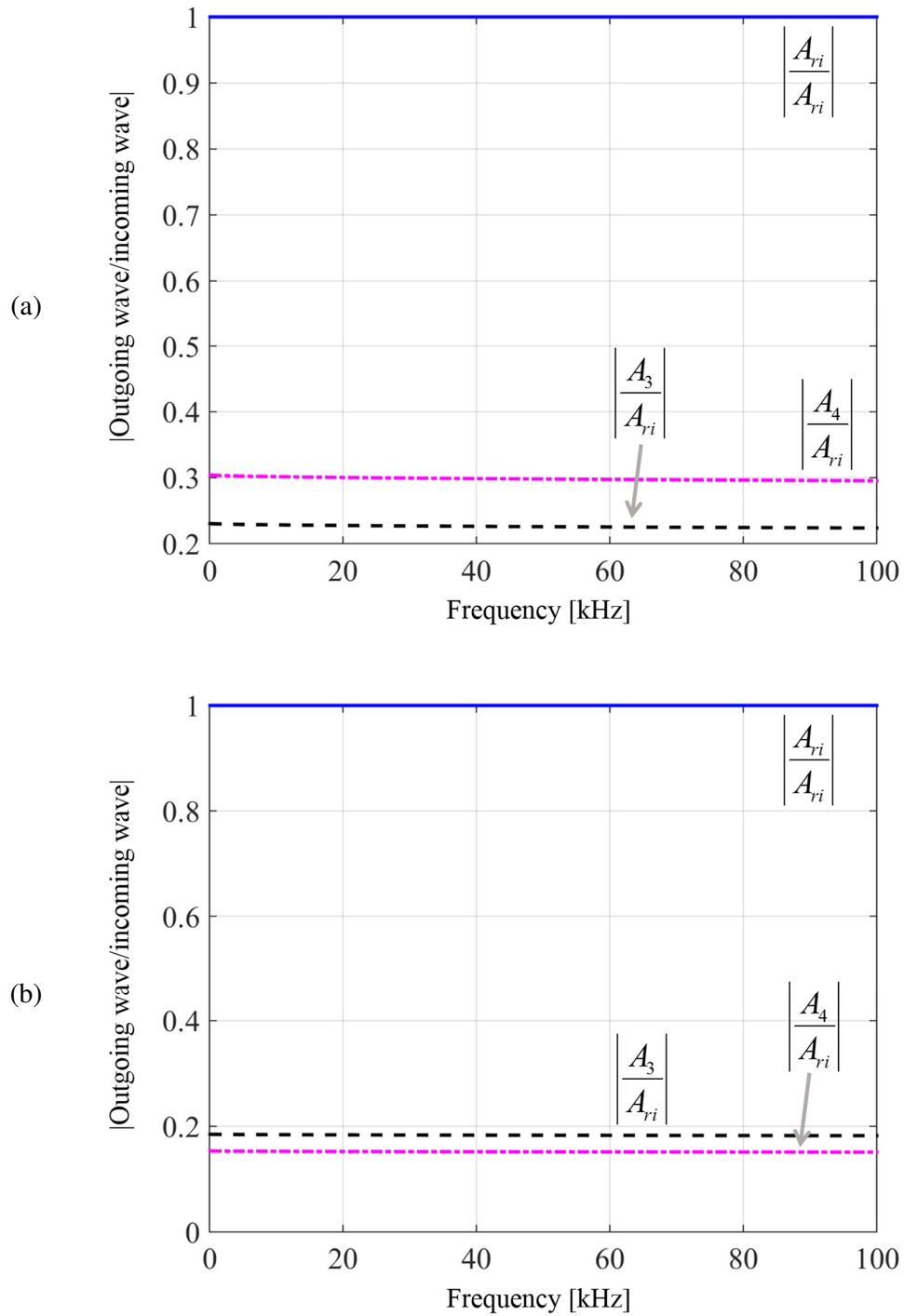
However, as there is scattering between longitudinal and flexural waves the relation of transmitted and reflected waves by the incident wave are not linear as for the symmetric cross-sectional area change.

Similar behaviors can be noted amplifying the cross-sectional are, Figure 71(b), however, the impedance of segment “D” become bigger than the impedance of segment “B” and the transmitted wave reduce it’s amplitude.

For flexural scattering waves, Figure 72, the transmitted wave reducing the cross-sectional area are bigger then the reflected wave. And when the cross-sectional area is amplified is the opposite.

However, as the incident wave are a longitudinal wave the biggest amount of wave power keep in the longitudinal waves (reflected and transmitted).

Figure 72: Amplitude of flexural scattering waves by asymmetric change of cross sectional area considering an incident longitudinal wave; (a) Reducing 50% and; (b) Amplifying 50%.

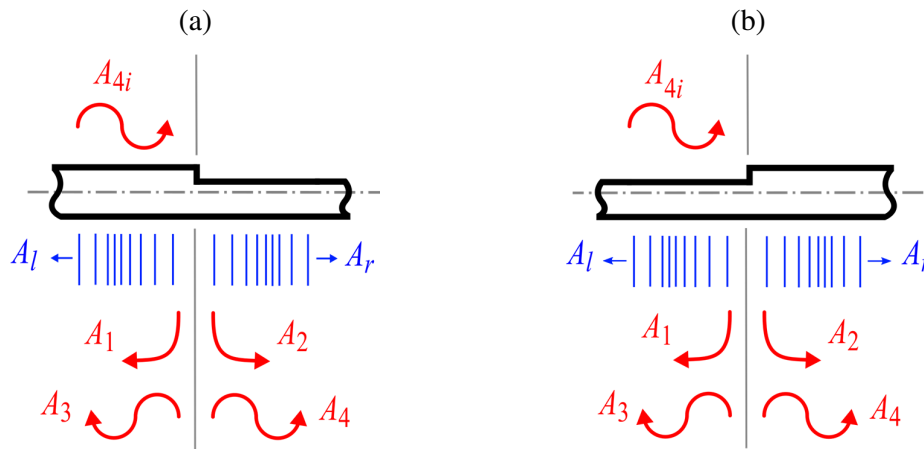


Source: Elaborated by author

A.1.2.1 Flexural Incident Wave

Likewise as presented by longitudinal waves incidents, Figure 70, a flexural wave incident results in longitudinal and flexural waves (reflected and transmitted), as Figure 73.

Figure 73: Scattering waves by an asymmetric change of cross sectional area considering an incident flexural propagating wave; (a) Reducing and; (b) Amplifying.



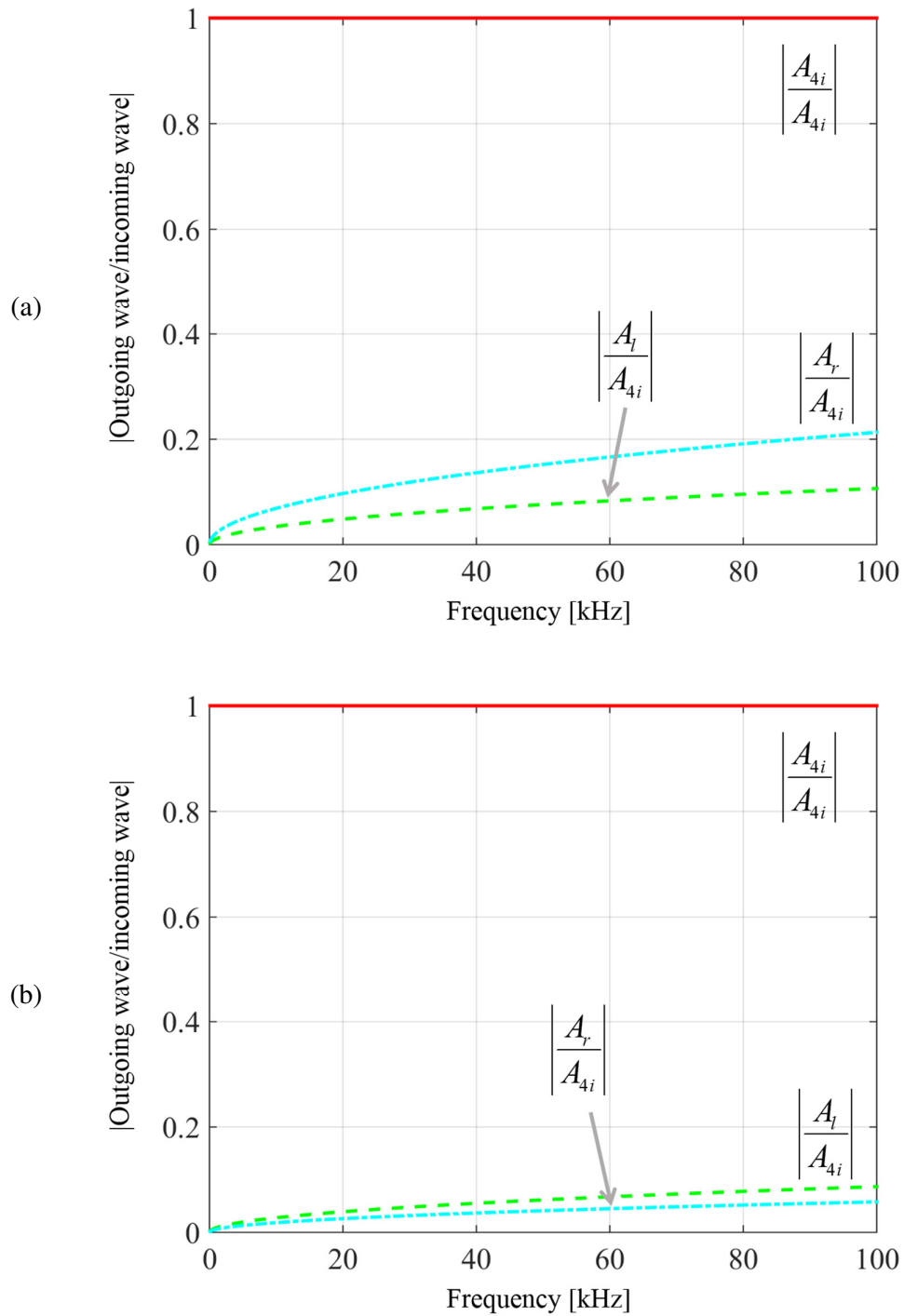
Source: Elaborated by author

And considering an incident right going propagating flexural waves the same studied (considering the properties of Table 3.1) can be seen on Figure 74 and Figure 75.

Observing the Figure 74 is possible to not that the longitudinal waves (reflected and transmitted) increase with the frequency.

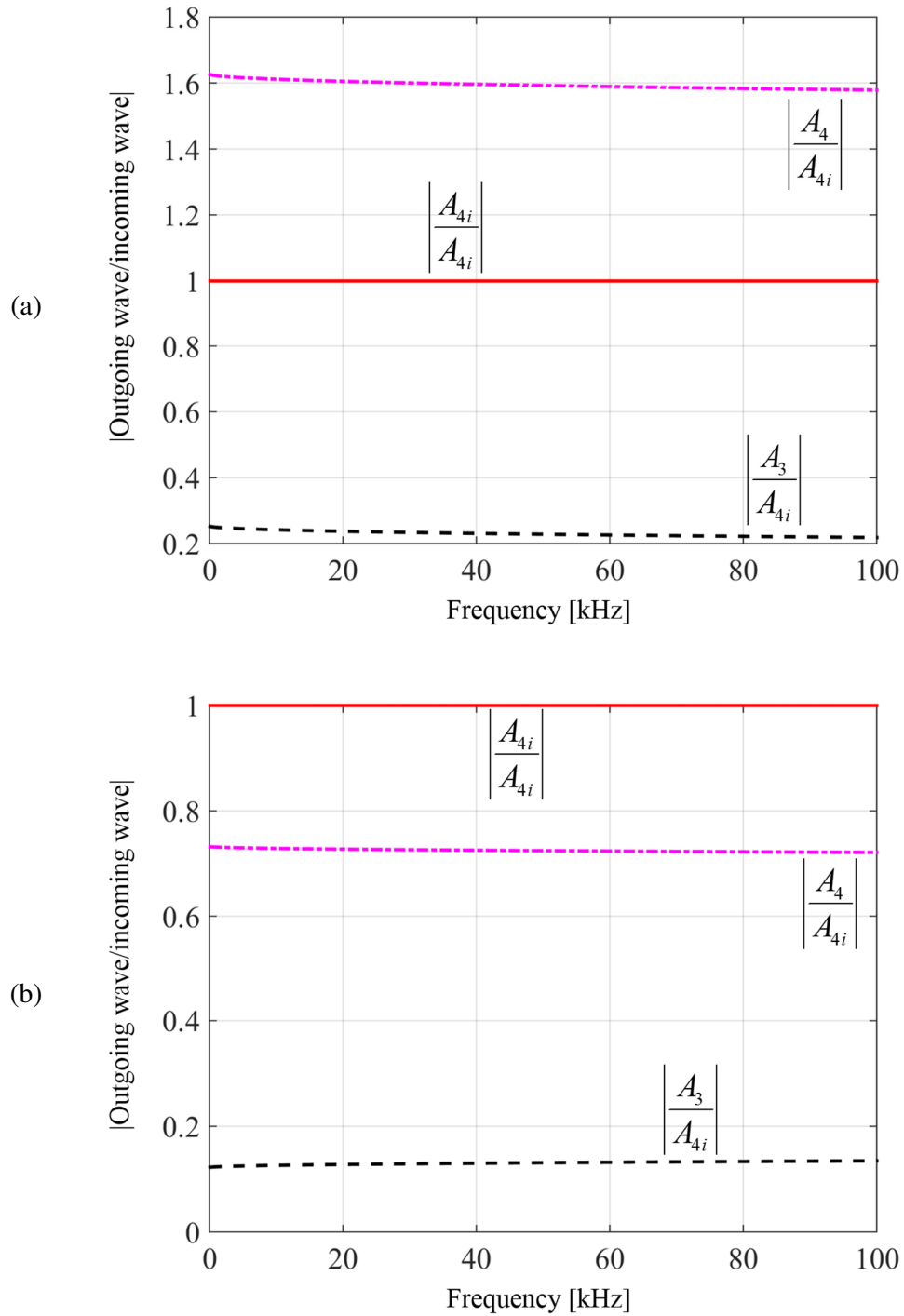
The behavior observed on Figure 75 are very close the waves behavior observed on Figure 71. However, a highlight point is for flexural reflected waves on the case of amplifying the cross-sectional area: it is very small, that means there is almost no reflected wave.

Figure 74: Amplitude of longitudinal scattering waves by asymmetric change of cross sectional area considering an incident flexural wave; (a) Reducing 50% and; (b) Amplifying 50%.



Source: Elaborated by author

Figure 75: Amplitude of flexural scattering waves by asymmetric change of cross sectional area considering an incident flexural wave; (a) Reducing 50% and; (b) Amplifying 50%.



Source: Elaborated by author

A.1.3 Conclusions

This Appendix presented the models for single change of cross sectional area. They are for symmetric and asymmetric reduction and amplification of area. The models were used to obtain the coefficients of reflection and transmission for each case.

For symmetric change of cross sectional area the coefficients were presented analytically. In the case of longitudinal waves they are in function of the ratio of cross sectional area (r). Working with flexural waves these coefficients can be write in function of the thickness ratio (h).

The asymmetric case is more complicated to write theses equations because there are coupling between the waves modes. For this case the equation were presented just in the matrix form.

When Longitudinal or Flexural waves impinges in an asymmetric single discontinuity the scattered waves are predominately in the same wave mode of incident one.

This Appendix provides additional information to support the comprehension of the physical phenomenon of wave's interaction into symmetric and asymmetric damages and is the background to understand the Appendix A.2.

A.2 PHYSICAL ASPECTS OF A LONGITUDINAL WAVE INTERACTING WITH SYMMETRIC DAMAGE

The symmetric and asymmetric discontinuities can be considered as simplifications of corrosion faults. However, the simplest problem to start is a symmetric discontinuity.

This appendix presents an analytical method in frequency domain to find the scattering waves (reflected and transmitted) by a symmetric discontinuity considering a longitudinal incident wave. Some physical aspects of the interaction of the incident wave with the damage are formulated and discussed.

A.2.1 Objectives

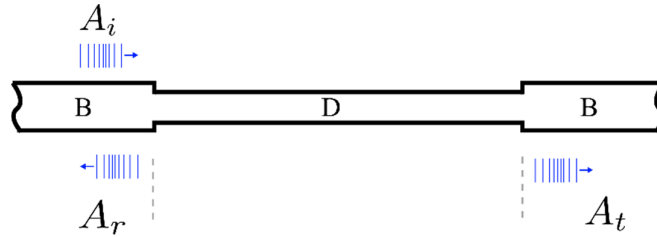
The objectives of this appendix are:

- Present and discuss a frequency domain approach used by Brennan (1994) to model the longitudinal waves interaction into a symmetric damage;
- Find the infinite waves packet of reflected and transmitted waves by a symmetric discontinuity considering a longitudinal incident wave;
- Show how many packets are necessary to be considered to obtain a good estimation of the total amplitudes of waves;
- Analyze the sensitivity of reflected and transmitted waves to detect the damage considering the optimum frequencies to excite the waves.

A.2.2 Methodology

The Figure 76 shows the problem of interesting in this study. It is an infinite beam with a symmetric discontinuity. The aim is to obtain the expression for reflected and transmitted waves from the damage.

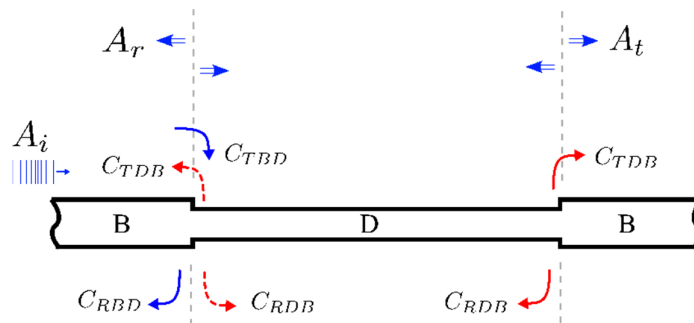
Figure 76: Scattering waves by a symmetric damage for an incident longitudinal wave.



Source: Elaborated by author

To solve this problem is adopted the modelling of finite beams showed by Brennan (1994). It means that the damage section is considered as a finite beam with boundary effects in the extremities. For the problem presented herein, the boundary effects are the cross sectional area changes and the reflection and transmission coefficients are illustrate in Figure 77.

Figure 77: Illustration of reflection and transmission coefficient.



Source: Elaborated by author

In Figure 77, C_{TDB} and C_{RDB} are respectively the transmission and reflection coefficients from damage to the beam, C_{TBD} and C_{RBD} are respectively the transmission and reflection coefficients from beam to the damage. These coefficients are given by the modelling of the symmetric cross sectional change presented in the Section A1.1.

$$C_{TDB} = \frac{2}{1 + s^{-1}} \quad (128)$$

$$C_{RDB} = \frac{1 - s^{-1}}{1 + s^{-1}} \quad (129)$$

$$C_{RBD} = -C_{RDB} = \frac{1-s}{1+s} \quad (130)$$

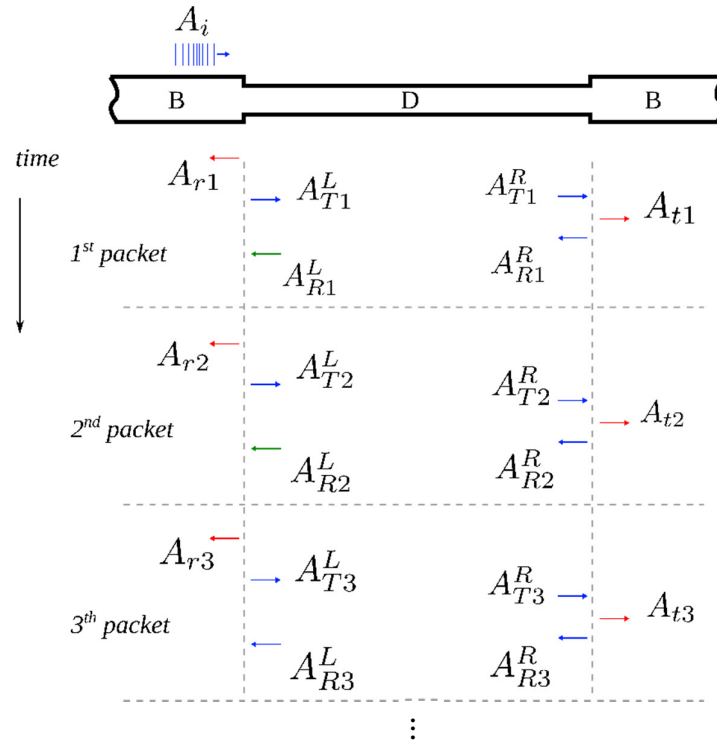
$$C_{TBD} = \frac{1}{s} \cdot C_{TDB} = \frac{2}{1+s} \quad (131)$$

where $s = S_D/S_B$ is the ratio of cross sectional area, S_D is the cross sectional area of the damaged segment (or discontinuity) and S_B is the cross sectional area of the beam.

Figure 78 presents the behavior of waves considering a time line (vertical direction). Three first packets are illustrated. Explaining the first packet when the incident longitudinal (A_i) waves impinges in the symmetric reduction of area part of this wave is reflected (A_{r1}) and part is transmitted (A_{t1}^L). The part reflected is the first packet of reflected waves (A_r). The wave designed A_{t1}^L is the transmitted waves in the left side of damage segment. This waves propagated to the right side (A_{t1}^R) and impinges in the symmetric amplification of area. As before, part of this waves is reflected (A_{r1}^R) and part is transmitted (A_{t1}). The wave A_{t1} is the first packet of transmitted waves (A_t). And the reflected wave in the right side of the damage segment, A_{r1}^R , propagates to the left side and became the A_{r1}^L .

The second packets starts to be generated when the waves A_{t1}^L achieves the symmetric amplification of area. Part of this wave is transmitted (A_{t2}) and part is reflected (A_{t2}^L) and this phenomenon still happens infinitely or until the waves dissipation.

Figure 78: Illustration of the waves behavior considering a vertical time line.



Source: Elaborated by author

In the following section is presented the formulation for the reflected wave (A_r) and after it similarly to the transmitted wave (A_t).

A.2.2.1 Reflected Wave

The first packet of the A_r is given by

$$\frac{A_{r1}}{A_i} = C_{RBD} = \frac{1-s}{1+s} \quad (132)$$

The second packet

$$\frac{A_{r2}}{A_i} = \frac{A_{r2}}{A_{R1}^L} \frac{A_{R1}^L}{A_{R1}^R} \frac{A_{R1}^R}{A_{T1}^R} \frac{A_{T1}^R}{A_{T1}^L} \frac{A_{T1}^L}{A_i} \quad (133)$$

or

$$\frac{A_{r2}}{A_i} = C_{TDB} T^- C_{RDB} T^+ C_{TBD} \quad (134)$$

where $T^+ = e^{-jkl_D} = e^{-j2\pi\frac{l_D}{\lambda}}$ and $T^- = e^{+jk(-l_D)} = e^{-j2\pi\frac{l_D}{\lambda}}$. These terms are related to the waves propagation between the extremities of damage segment. The equation (134) can also be write as

$$\frac{A_{r2}}{A_i} = \left(\frac{2}{1+s^{-1}}\right) T^- \left(\frac{1-s^{-1}}{1+s^{-1}}\right) T^+ \left(\frac{2}{1+s}\right) \quad (135)$$

Third packet is given by

$$\frac{A_{r3}}{A_i} = \frac{A_{r3}}{A_{R2}^L} \frac{A_{R2}^L}{A_{R2}^R} \frac{A_{R2}^R}{A_{T2}^R} \frac{A_{T2}^R}{A_{T2}^L} \frac{A_{T2}^L}{A_{R1}^L} \frac{A_{R1}^L}{A_i} \quad (136)$$

or

$$\frac{A_{r3}}{A_i} = C_{TDB} T^- C_{RDB} T^+ C_{RDB} \left[T^- C_{RDB} T^+ C_{TBD} \right] \quad (137)$$

and substituting the coefficients

$$\frac{A_{r3}}{A_i} = \left(\frac{2}{1+s^{-1}}\right) T^- \left(\frac{1-s^{-1}}{1+s^{-1}}\right) T^+ \left(\frac{1-s^{-1}}{1+s^{-1}}\right) \left[T^- \left(\frac{1-s^{-1}}{1+s^{-1}}\right) T^+ \left(\frac{2}{1+s}\right) \right] \quad (138)$$

Is possible to observe a pattern of repetition as follows:

$$\frac{A_{r3}}{A_i} = C_{TDB} \left(T^- C_{RDB} T^+ \right)^2 C_{RDB} C_{TBD} \quad (139)$$

The fourth packet is

$$\frac{A_{r4}}{A_i} = \frac{A_{r4}}{A_{R3}^L} \frac{A_{R3}^L}{A_{R3}^R} \frac{A_{R3}^R}{A_{T3}^R} \frac{A_{T3}^R}{A_{T3}^L} \frac{A_{T3}^L}{A_{R2}^L} \frac{A_{R2}^L}{A_i} \quad (140)$$

or

$$\frac{A_{r4}}{A_i} = C_{TDB} \left(T^- C_{RDB} T^+ \right)^3 C_{RDB}^2 C_{TBD} \quad (141)$$

The fifth packet is

$$\frac{A_{r5}}{A_i} = \frac{A_{r5}}{A_{R4}^L} \frac{A_{R4}^L}{A_{R4}^R} \frac{A_{R4}^R}{A_{T4}^R} \frac{A_{T4}^R}{A_{T4}^L} \frac{A_{T4}^L}{A_{R3}^L} \frac{A_{R3}^L}{A_i} \quad (142)$$

or

$$\frac{A_{r5}}{A_i} = C_{TDB} (T^- C_{RDB} T^+)^4 C_{RDB}^3 C_{TBD} \quad (143)$$

Then a general case can be formulated as:

$$\frac{A_{r(n)}}{A_i} = C_{TDB} (T^- T^+)^{n+1} (C_{RDB})^{2n-3} C_{TBD}, \text{ where } n \in [2, +\infty[\quad (144)$$

or

$$\frac{A_{r(n+2)}}{A_i} = C_{TDB} C_{TBD} (T^- T^+)^{n+1} (C_{RDB})^{2n+1}, \text{ where } n \in \mathbb{N} \quad (145)$$

Summing the total reflected wave amplitude:

$$\frac{A_r}{A_i} = \frac{A_{r1}}{A_i} + \sum_{n=0}^{+\infty} \frac{A_{r(n+2)}}{A_i} \quad (146)$$

or

$$\frac{A_r}{A_i} = \frac{A_{r1}}{A_i} + \sum_{n=0}^{+\infty} \left[C_{TDB} C_{TBD} (T^- T^+)^{n+1} (C_{RDB})^{2n+1} \right] \quad (147)$$

Rearranging for

$$\frac{A_r}{A_i} = \frac{A_{r1}}{A_i} + C_{TDB} C_{TBD} \sum_{n=0}^{+\infty} \left[(T^- T^+)^{n+1} (C_{RDB})^{2n+1} \right] \quad (148)$$

If $T^- T^+ = e^{-2jkl_D}$ the last equation can be rewritten by

$$\frac{A_r}{A_i} = \frac{A_{r1}}{A_i} + C_{TDB} C_{TBD} \sum_{n=0}^{+\infty} \left[(e^{-2jkl_D})^{n+1} (C_{RDB})^{2n+1} \right] \quad (149)$$

This is an expression in frequency domain to obtain the reflected wave of a symmetric discontinuity. An equivalent form

$$\frac{A_r}{A_i} = \frac{A_{r1}}{A_i} + C_{TDB} C_{TBD} e^{-2jkl_D} C_{RDB} \left\{ \sum_{n=0}^{+\infty} \left[(e^{-2jkl_D}) (C_{RDB})^2 \right]^n \right\} \quad (150)$$

Since $\left| (e^{-2jkl_D}) (C_{RDB})^2 \right| < 1$, the summation of the geometric series is given by (Gao *et al.*, 2009)

$$\sum_{n=0}^{+\infty} \left[(e^{-2jkl_D}) (C_{RDB})^2 \right]^n = \frac{1}{1 - (e^{-2jkl_D}) (C_{RDB})^2} \quad (151)$$

Then Equation (146) can be

$$\frac{A_r}{A_i} = \frac{A_{r1}}{A_i} + C_{TDB} C_{TBD} C_{RDB} e^{-2jkl_D} \left\{ \frac{1}{1 - \left[(e^{-2jkl_D}) (C_{RDB})^2 \right]} \right\} \quad (152)$$

which is simplified to

$$\frac{A_r}{A_i} = \frac{(s^2 - 1)(1 - e^{2jkl_D})}{(s + 1)^2 e^{2jkl_D} - (s - 1)^2} \quad (153)$$

Working with Equation (153) is possible to check the waves behavior when the damage segment tents to a free condition ($s \ll 1$) and for a cantilever condition ($s \gg 1$).

$$\lim_{s \rightarrow 0} \frac{A_r}{A_i} = 1 \quad (154)$$

and

$$\lim_{s \rightarrow \infty} \frac{A_r}{A_i} = -1 \quad (155)$$

It means that for a free condition the reflected waves are equal the incident waves and in the same phase. In other hand, for the engaged condition the reflected wave has the same amplitude of incident waves but opposite phase.

Comparing Equation (150) with Equation (153) is possible to understand the portion of each wave packet in the resultant wave amplitude

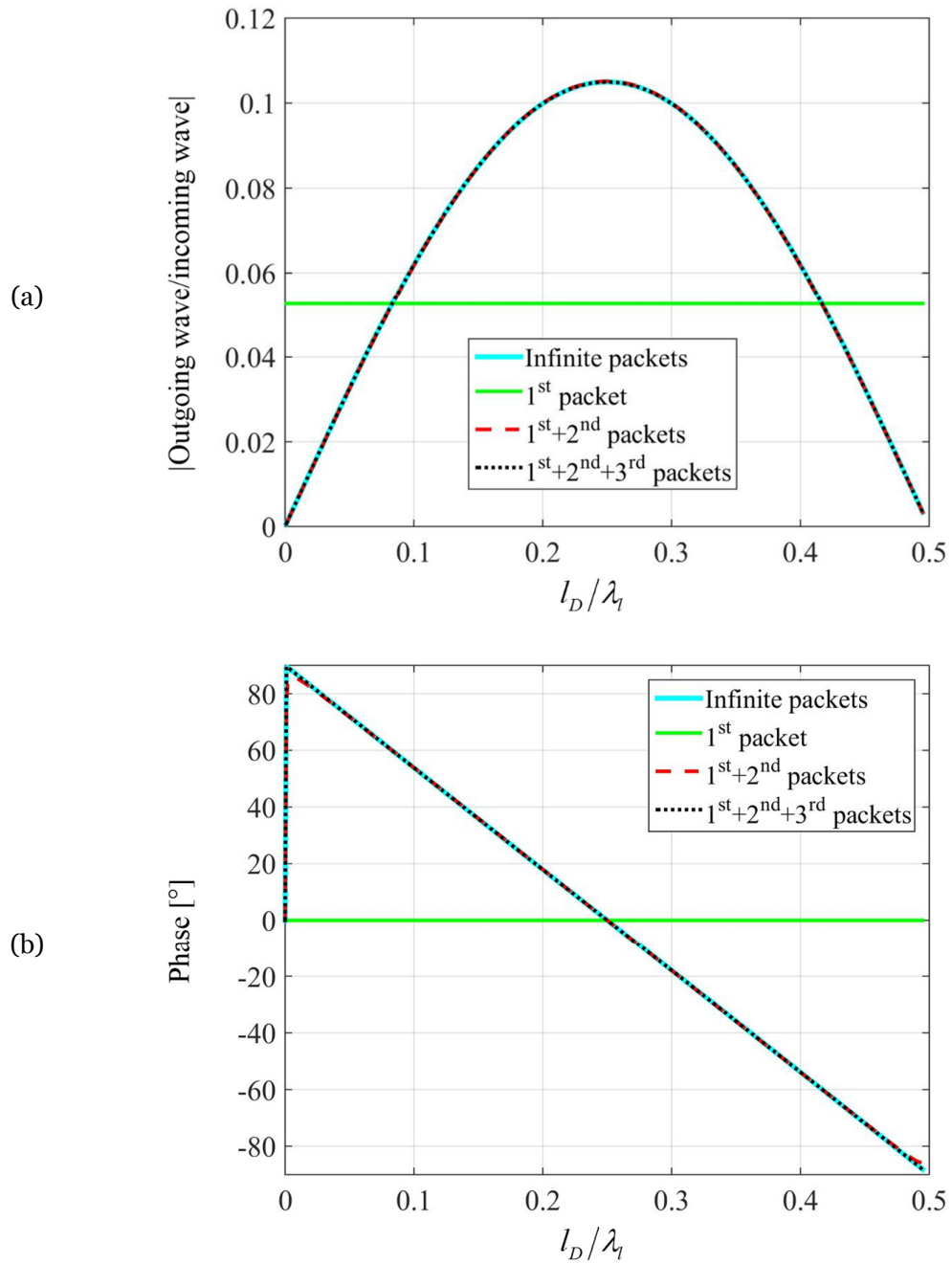
$$\frac{A_{r1}}{A_i} + C_{TDB} C_{TBD} e^{-2jkl_D} C_{RDB} \left\{ \sum_{n=0}^{+\infty} \left[(e^{-2jkl_D}) (C_{RDB})^2 \right]^n \right\} = \frac{(s^2 - 1)(1 - e^{2jkl_D})}{(s + 1)^2 e^{2jkl_D} - (s - 1)^2} \quad (156)$$

Infinite wave packets

Resultant wave

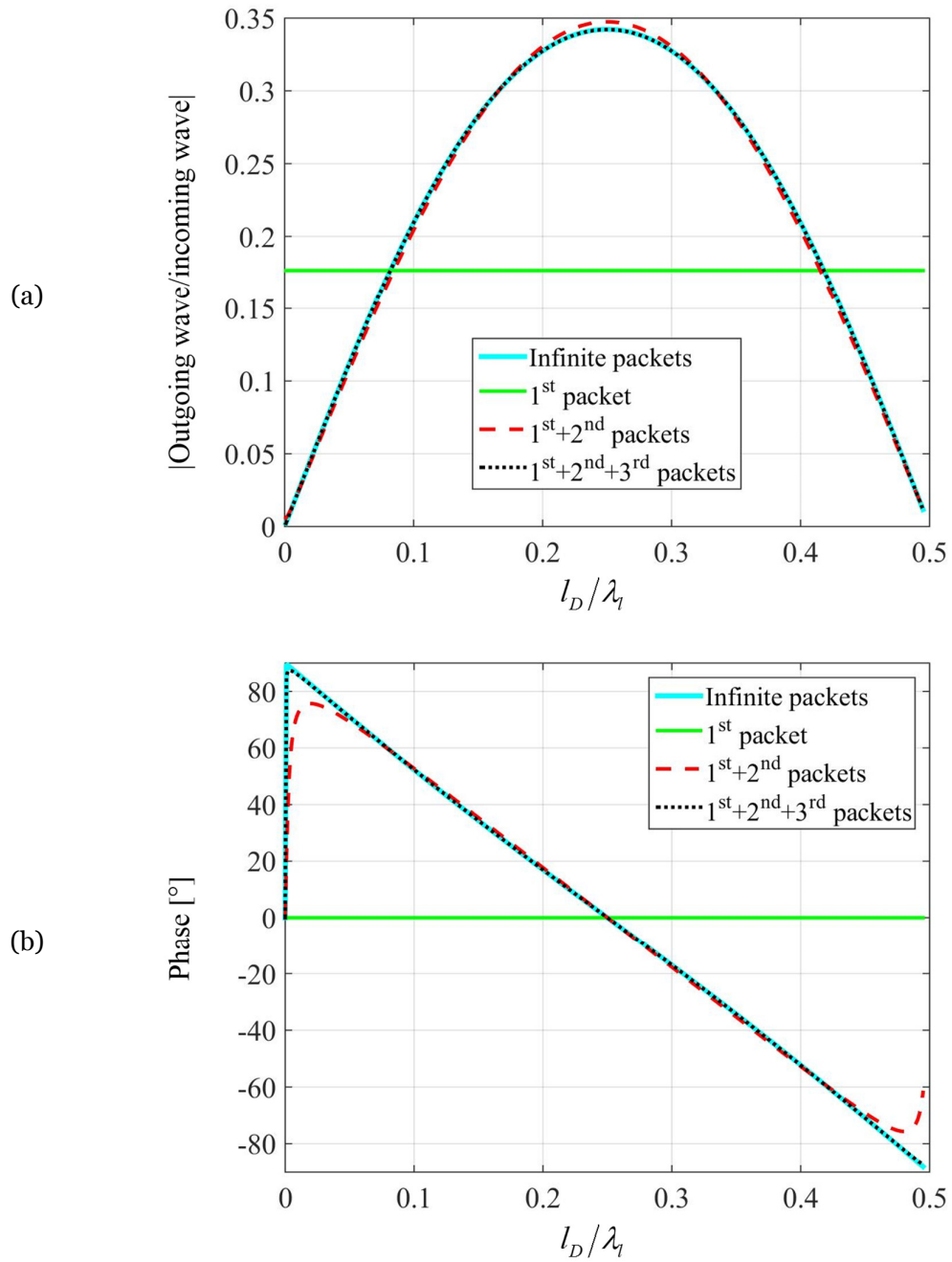
Figure 79 shows the both side of Equation (156) for a damage deep of 10%, Figure 80 shows the same for a damage deep of 30%. And Figure 81 for 50%.

Figure 79: Reflection coefficient in symmetric discontinuity for a damage deep of 10%; (a) Amplitude and (b) Phase.



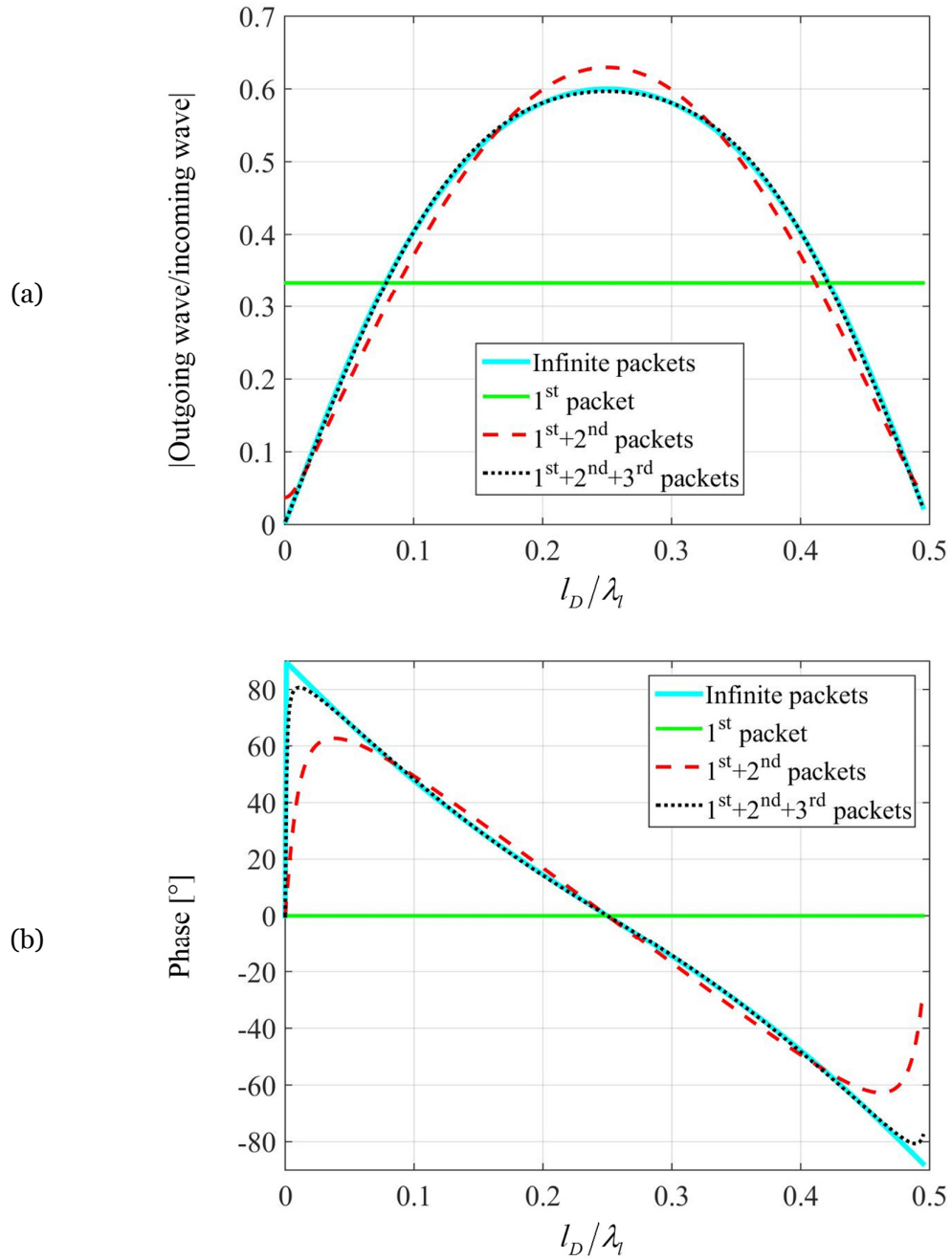
Source: Elaborated by author

Figure 80: Reflection coefficient in symmetric discontinuity for a damage deep of 30%; (a) Amplitude and (b) Phase.



Source: Elaborated by author

Figure 81: Reflection coefficient in symmetric discontinuity for a damage deep of 50%; (a) Amplitude and (b) Phase.



Source: Elaborated by author

As can be noted by the graphics above the number of packets necessary to obtain a good estimation of the total waves (considering infinite packets) depends of the damage depth. For

10% of damage (Figure 79) two packets are enough to have a good estimation of the reflected wave. For 30% (Figure 80) and 50% of damage (Figure 81) three packets showed a good estimation.

Is important to highlight the filtering effect of damage length. As can be noted in the figures above if the wavelength is $\lambda = 4l_D$ and by

$$\frac{l_D}{\lambda_i} = \frac{1+2n}{4}, n \in \mathbb{N} \quad (157)$$

and minimum when:

$$\frac{l_D}{\lambda_i} = \frac{1+n}{2}, n \in \mathbb{N} \quad (158)$$

where l_D is the length of damage segment and λ_i the longitudinal wavelength.

A.2.2.2 Transmitted Wave

The first packet of the A_i is given by

$$\frac{A_{i1}}{A_i} = \frac{A_{T1}}{A_{T1}^R} \frac{A_{T1}^L}{A_{T1}^L} \frac{A_{T1}^R}{A_i} \quad (159)$$

or

$$\frac{A_{i1}}{A_i} = C_{TBD} T^+ C_{TDB} \quad (160)$$

The second packet

$$\frac{A_{i2}}{A_i} = \frac{A_{T2}}{A_{T2}^R} \frac{A_{T2}^L}{A_{T2}^L} \frac{A_{R1}^L}{A_{R1}^R} \frac{A_{R1}^R}{A_{R1}^R} \frac{A_{T1}^R}{A_{T1}^L} \frac{A_{T1}^L}{A_i} \quad (161)$$

or

$$\frac{A_{i2}}{A_i} = C_{TBD} T^+ C_{RDB} T^- C_{RDB} T^+ C_{TDB} = C_{TBD} (T^+ C_{RDB})^2 T^- C_{TDB} \quad (162)$$

The third packet

$$\frac{A_{t3}}{A_i} = \frac{A_{t3}}{A_{T3}^R} \frac{A_{T3}^R}{A_{T3}^L} \frac{A_{T3}^L}{A_{R2}^L} \frac{A_{R2}^L}{A_{R2}^R} \frac{A_{R2}^R}{A_{T2}^R} \frac{A_{T2}^R}{A_{T2}^L} \frac{A_{T2}^L}{A_{R1}^L} \frac{A_{R1}^L}{A_{R1}^R} \frac{A_{R1}^R}{A_{T1}^R} \frac{A_{T1}^R}{A_{T1}^L} \frac{A_{T1}^L}{A_i} \quad (163)$$

or

$$\frac{A_{t3}}{A_i} = C_{TBD} (C_{RDB})^4 (T^+)^3 (T^-)^2 C_{TDB} \quad (164)$$

The forth packet

$$\frac{A_{t4}}{A_i} = \frac{A_{t4}}{A_{T4}^R} \frac{A_{T4}^R}{A_{T4}^L} \frac{A_{T4}^L}{A_{R3}^L} \frac{A_{R3}^L}{A_{R3}^R} \frac{A_{R3}^R}{A_{T3}^R} \frac{A_{T3}^R}{A_i} \quad (165)$$

or

$$\frac{A_{t4}}{A_i} = C_{TBD} (C_{RDB})^6 (T^+)^4 (T^-)^3 C_{TDB} \quad (166)$$

Let $n = 0, 1, 2, \dots$, the $(n + 2)$ packet can be computed by

$$\frac{A_{t(n+2)}}{A_i} = C_{TDB} (T^+)^{n+2} (T^-)^{n+1} (C_{RDB})^{2n+2} C_{TDB} \text{ where } n \in \mathbb{N} \quad (167)$$

In this case, the total transmitted longitudinal wave is given by

$$\frac{A_t}{A_i} = \frac{A_{t1}}{A_i} + C_{TDB} C_{TBD} \sum_{n=0}^{+\infty} \left[(T^+)^{n+2} (T^-)^{n+1} (C_{RDB})^{2n+2} \right] \quad (168)$$

where $T^+ = e^{-jkl_D}$ and $T^- = e^{+jk(-l_D)}$

$$\frac{A_t}{A_i} = \frac{A_{t1}}{A_i} + C_{TDB} C_{TBD} \sum_{n=0}^{+\infty} \left[(e^{-jkl_D})^{2n+3} (C_{RDB})^{2n+2} \right] \quad (169)$$

or

$$\frac{A_t}{A_i} = \frac{A_{t1}}{A_i} + C_{TDB} C_{TBD} (C_{RDB})^2 e^{-3jkl_D} \sum_{n=0}^{+\infty} \left[(e^{-jkl_D})^{2n} (C_{RDB})^{2n} \right] \quad (170)$$

Since $\left| \left[(e^{-2jkl_D}) (C_{RDB})^2 \right]^n \right| < 1$, the summation is replaced such that (Gao *et al.*, 2009)

$$\frac{A_t}{A_i} = \frac{A_{t1}}{A_i} + C_{TDB} C_{TBD} (C_{RDB})^2 e^{-3jkl_D} \left\{ \frac{1}{1 - \left[(e^{-2jkl_D}) (C_{RDB})^2 \right]} \right\} \quad (171)$$

which is simplified to

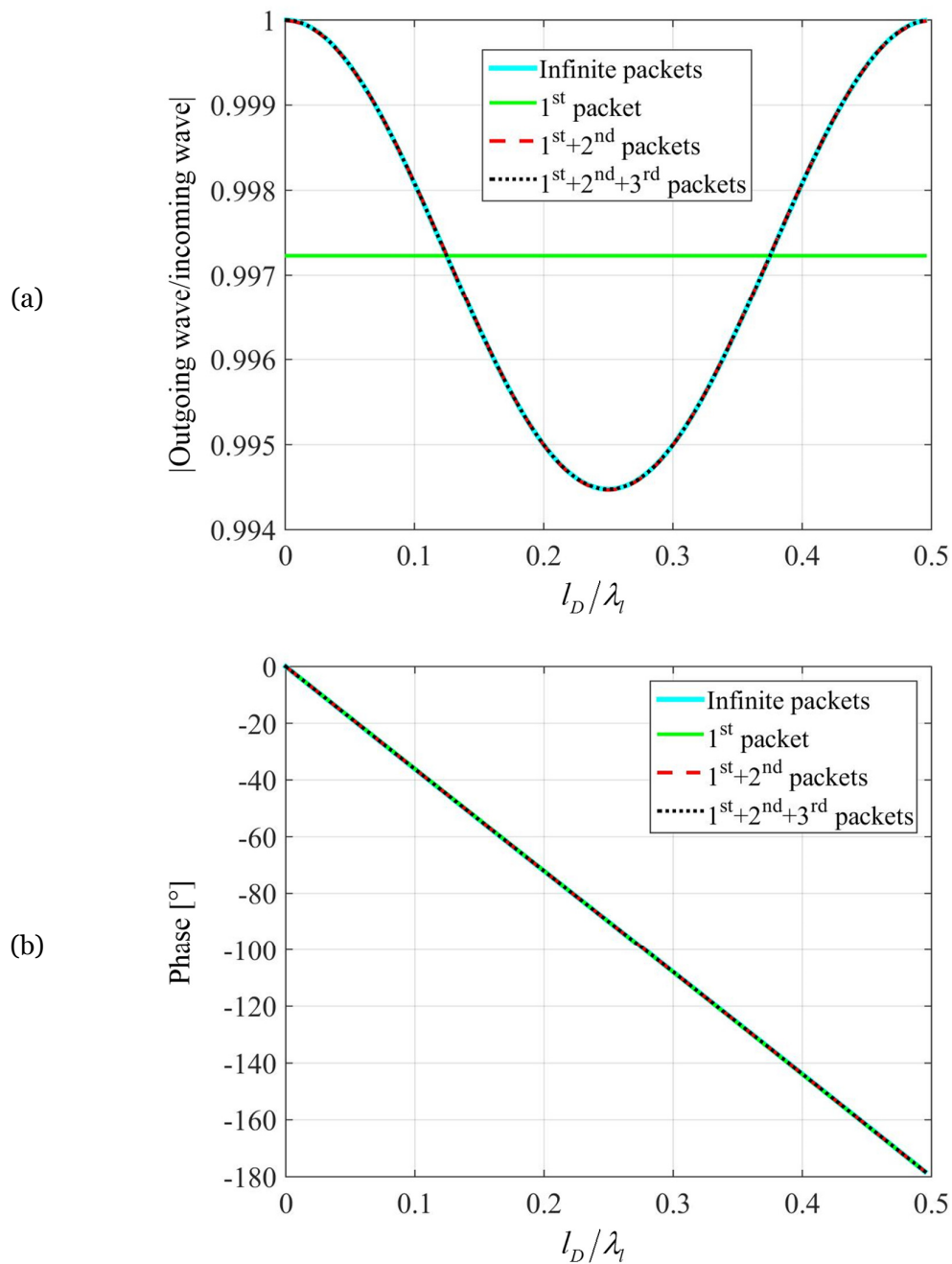
$$\frac{A_t}{A_i} = \frac{4se^{jkl_D}}{e^{2jkl_D} (s+1)^2 - (s-1)^2} \quad (172)$$

Comparing Equation (170) with Equation (172) is possible to understand the portion of each wave packet in the resultant wave amplitude

$$\underbrace{\frac{A_{t1}}{A_i} + C_{TDB} C_{TBD} (C_{RDB})^2 e^{-3jkl_D} \sum_{n=0}^{+\infty} \left[(e^{-jkl_D})^{2n} (C_{RDB})^{2n} \right]}_{\text{Infinite wave packets}} = \underbrace{\frac{4se^{jkl_D}}{e^{2jkl_D} (s+1)^2 - (s-1)^2}}_{\text{Resultant wave}} \quad (173)$$

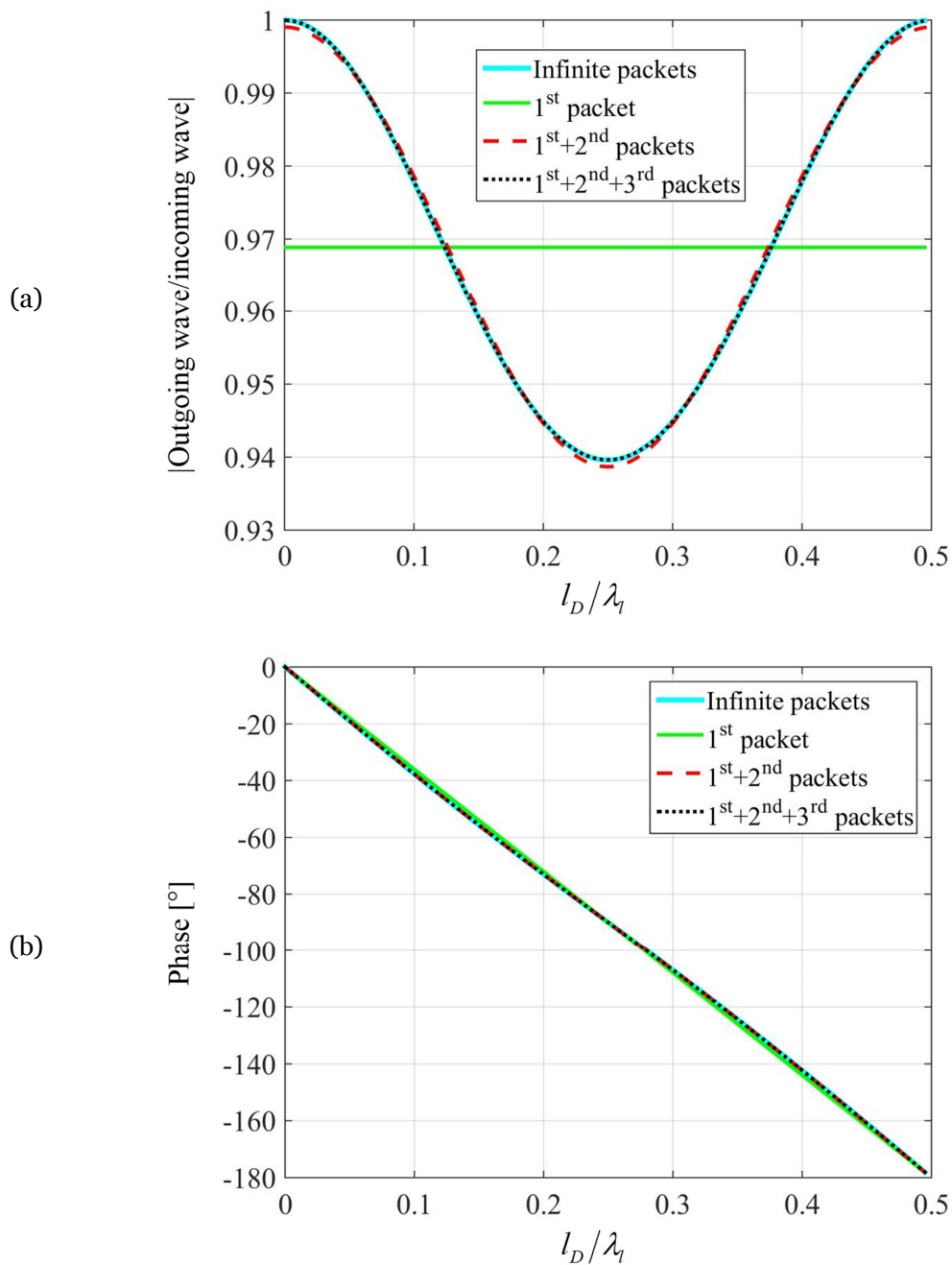
Figure 82 shows the both side of Equation (173) for a damage deep of 10%, Figure 83 shows the same for a damage deep of 30%. And Figure 84 for 50%.

Figure 82: Transmission coefficient in symmetric discontinuity for a damage deep of 10%; (a) Amplitude and (b) Phase.



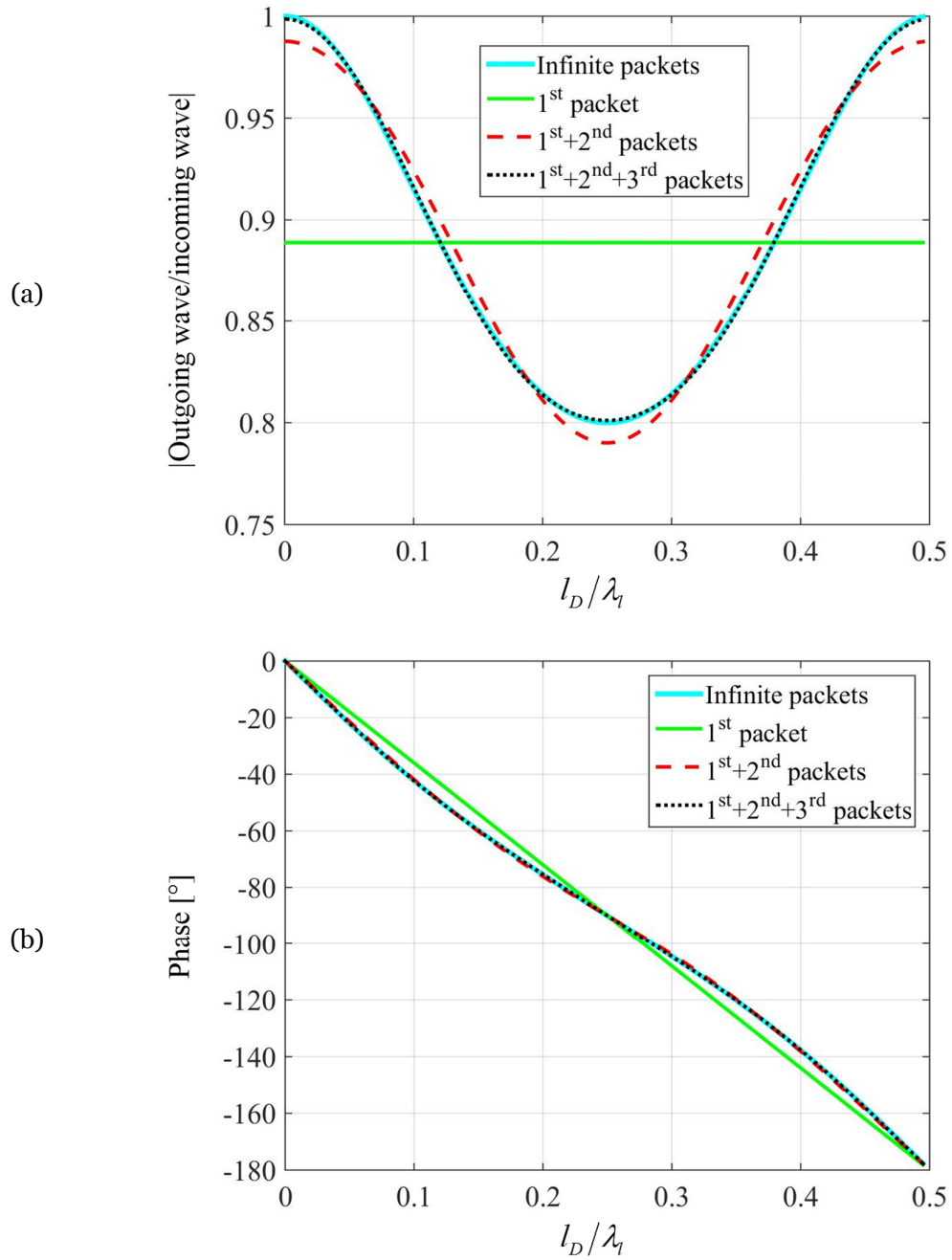
Source: Elaborated by author

Figure 83: Transmission coefficient in symmetric discontinuity for a damage deep of 30%; (a) Amplitude and (b) Phase.



Source: Elaborated by author

Figure 84: Transmission coefficient in symmetric discontinuity for a damage deep of 50%; (a) Amplitude and (b) Phase.



Source: Elaborated by author

A.2.3 In the Optimum Frequency

The frequency that the reflection coefficient is maximum is the same frequency that the transmission coefficient assumes its minimum value. It means that at this frequency the damage implies more modifications in the incident wave.

Considering the condition with maximum amplitude of reflected wave, i.e., $\lambda = 4l_D$, the exponential term of the Equation (153) is equal to -1 . In this case, the equation for the maximum amplitude is

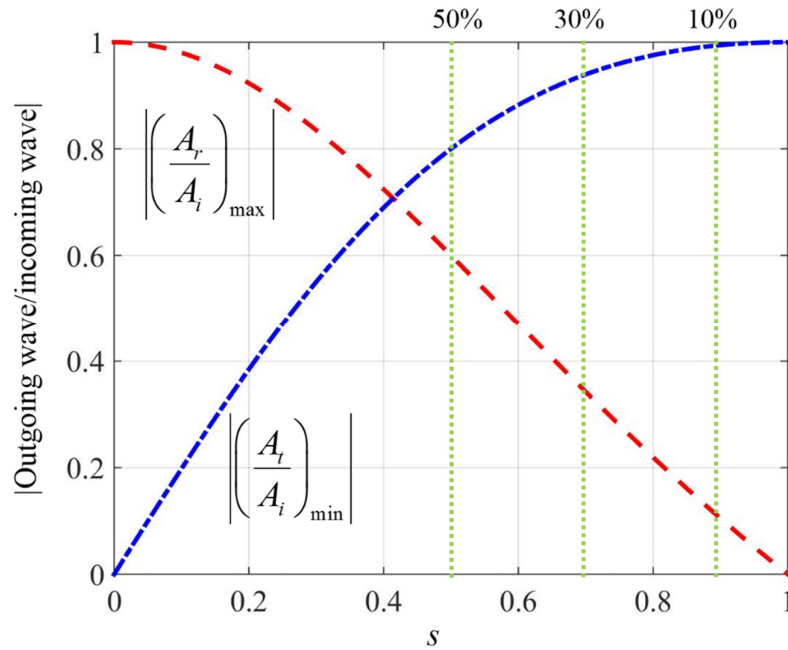
$$\left(\frac{A_r}{A_i}\right)_{\max} = \frac{s^2 - 1}{-s^2 - 1} \quad (174)$$

Similarly to the reflected wave, considering the condition for the maximum amplitude over frequency, i.e., $\lambda = 4l_D$, using the Equation (35) the minimum amplitude for the transmitted waves is given by

$$\left(\frac{A_t}{A_i}\right)_{\min} = \frac{-2js}{(1+s^2)} \quad (175)$$

Figure 85 shows the maximum reflection coefficient and the minimum transmission coefficient varying with the damage deep

Figure 85: Minimum transmission coefficient and maximum reflection coefficient for a symmetric discontinuities varying with the damage deep.



If $\left| \frac{A_r}{A_i} \right| = \left| \frac{A_t}{A_i} \right|$, it is obtained the equation $s^2 + 2s - 1 = 0$, and considering the range of s , it is found $s = 0.4142$. In this case, both amplitudes relations are the same, 0.7071, which indicates 50% of energy for each wave (i.e., the reflected and transmitted waves).

Is clear to note the higher sensitivity of reflected waves than transmitted waves for $s > 0.4142$. In this damage deep range is also possible to note the almost linear relation of reflected waves with the damage severity. Because that for the case studied here, the pulse-echo sensor configuration is better to detect and quantify the damage compared to a pitch-catch configuration.

A.2.4 Conclusions

Some physical aspects of a longitudinal wave interaction with symmetric corrosion-type fault on a beam has been studied and explained in frequency domain.

A model of the system has been formulated in the frequency domain and the wave resultant is obtained from the infinite packets sum using a geometric series solution.

The model has been used to demonstrate how many packets are necessary to be considered in the sum to obtain a good representation of the physical phenomena for reflected and transmitted waves. As showed this amount of packets is depend of the damage depth. But until to 50% of damage the sum of three first packets are enough to obtain a good estimation of the reflected wave.

The model also showed the wave filtering effects of damage. The investigation has shown that, in order to detect the damage there are thus good and bad frequency ranges to apply the structural excitation.

A general conclusion for the system studied is that a pulse-echo sensor configuration in better to detect and quantify the damage compared to a pitch-catch configuration.